Growth of Intermetallic Phases at Low Temperature

by

Cheryl Ann Klepser

S. B. Massachusetts Institute of Technology, 1991
S. M. Massachusetts Institute of Technology, 1992

Submitted to the Department of
Materials Science and Engineering
in Partial Fulfillment of the Requirements
for the Degree of

Doctorate of Science
in Materials Engineering

at the

Massachusetts Institute of Technology

February 1996

Signature of Author ....
Department of Materials Science and Engineering
January 12,1996

Certified by ....
Thomas W. Eagar
Department of Materials Science and Engineering
Thesis Supervisor

Accepted by ....
Michael F. Rubner
TDK Professor of Materials Science and Engineering
Chair, Departmental Committee on Graduate Students

Growth of Intermetallic Phases
at Low Temperature

by

Cheryl Ann Klepser

Submitted to the Department of Materials Science and Engineering
on January 12, 1996 in partial fulfillment of the requirements for the
Degree of Doctorate of Science in Materials Engineering

Abstract

The growth of intermetallic is important in many applications from solder joints in computer chips to superalloy strength in aircraft engine components. Understanding the growth rate of intermetallic phases, then, is a basic step in improving many products and processes. Because diffusion through the intermetallic is a necessary occurrence for growth, in this work, factors which affect diffusion through the intermetallic are evaluated. These factors are divided into two categories: chemical and physical. Chemical factors include bond character and chemical potential gradient. Physical factors are related to the structure of the material; crystal structure, grain boundary structure, and interface structure. These factors are used to rationalize the rapid diffusion seen in some intermetallic phases, but one unifying theory cannot be developed until the interactions of these factors are better understood.

Two models of intermetallic growth are evaluated. A diffusion-based, moving boundary model for the copper-tin system is reviewed. The diffusion-based model produces unstable results. It is concluded that the diffusion-based model is inadequate for modeling intermetallic growth in the copper-tin system because growth in this system is not controlled purely by diffusion. Thus, a model which includes both diffusion and interface control is presented. Both the copper-tin system and the nickel-tin system are analyzed with this model. Model results are consistent with observations of selective phase growth in these systems. Neither model is found to be complete or advanced enough to predict intermetallic layer thickness for practical applications. Currently, the best methods for predicting intermetallic layer thickness are empirical.

Thesis Supervisor: Prof. Thomas W. Eagar
Title: Head of the Department of Materials Science and Engineering

Table of Contents

List of Figures

List of Tables

List of Symbols

a = lattice parameter (Å)
a = grain boundary width (cm)
a_i = activity of species i
α = jump distance (cm)
b = lattice parameter (Å)
b = constant used in linear fit of activity
β = angle in lattice (°)
c = lattice parameter (Å)
$c_{\alpha L}$ = concentration at the liquidus
$c_{\alpha s}$ = concentration at the solidus
c_o, c_i = concentration
d = grain size (cm)
D, D_i = diffusion coefficient, diffusion coefficient of species i ($\mathrm{cm^2/s}$)
f = weighting factor for contribution of grain boundary diffusion
g_i = dimensionless interface position parameter
Γ = jump frequency (1/s)
G_m = activation energy for migration (J/mole)
G_v = activation energy for formation of a vacancy (J/mole)
$\Delta\mathrm{H_f}$ = heat of formation (J/mole)
J_i = flux of species i ($\mathrm{g/cm^2\ s}$)
k_i = interface reaction constant of reaction i
k_i = thickening constant of layer i ($\mathrm{cm/s^{1/2}}$)
$\mathrm{K_{IC}}$ = fracture toughness ($\mathrm{MPa\sqrt{m}}$)
λ = interface position parameter ($\mathrm{cm/s^{1/2}}$)
m = constant used in linear fit of activity
μ_i = chemical potential of species i (J/mole)
M_i = mobility coefficient of species i (flux per unit force)
n = growth exponent
ν_D = Debye frequency (1/s)
p_v = probability of a vacancy
r_{ij} = ratio of diffusion coefficients = D_i/D_j
R = gas constant, 8.314 J/mole K
R_i = resistance of an individual resistor i, (Ω)
R_T = total resistance (Ω)

R^2 = correlation coefficient

t = time (s)

T = temperature (˚C or K)

T_m = melting point temperature (˚C or K)

w = layer thickness (cm)

ω = frequency of successful jumps (1/s)

x = distance, position (cm)

ζ_{ij} = interface position (cm)

Z = coordination number

Acknowledgements

I am grateful to Professor Thomas W. Eagar for his guidance and support of the work that became this thesis.

I wish to thank my thesis committee members, Professors Kenneth C. Russell and Samuel M. Allen for their comments which have significantly improved this thesis.

I gratefully acknowledge the National Science Foundation both for the grant, DMR-9301444, which supported this research and for the fellowship I received from 1991-1994.

I thank my parents, William and Eleanore Klepser, and the rest of my family for their early guidance in my life and their support during my many years in college.

I also thank Darren Castro for encouraging me and believing in me when my spirit and drive flagged. His friendship has been a key factor in my survival and success.

I would like to thank the Welding and Joining Lab graduate students and staff for their friendship and help: Weidong "Mike" Zhang, Tadashi Imai, Jeff Nystrom, Ren-kae Shiue, Vivek Davé, Bryan Blackwell, John Matz, and Denise Wilsey.

I would like to acknowledge Professor Regis Pelloux who was the first person to encourage me to get a doctorate.

I would also like to acknowledge the numerous other friends and MIT staff members who have supported me in both my educational and recreational pursuits.

1. Introduction

1.1 The importance of intermetallic formation

Intermetallics are compounds comprised of two or more metals. Intermetallics form in many different situations. Sometimes their formation is beneficial as in the precipitation of fine nickel aluminide particles in nickel superalloys. The intermetallic particles dispersion strengthen the superalloy and help it maintain its strength at high temperature.[1,2] In other cases, the formation of intermetallic phases is not so advantageous. For example, the intermetallic layers that form between copper and tin can degrade the solderability of pre-tinned contacts.[3,4]

Intermetallic formation is a leading issue in the field of joining. In a joint, two materials are brought into contact. In practice, more and more frequently, the two materials being joined are different from each other. If the materials tend to form intermetallic compounds, coupling them is often all that is required to initiate intermetallic formation. Another opportunity for intermetallic formation in joining arises in applications such as brazing and transient liquid phase bonding, both of which employ interlayers to join parts. Intermetallic phases can form between the interlayer metal and the base metal.

Since joints between dissimilar materials are increasingly being incorporated into parts, opportunities for intermetallic formation are also becoming more numerous. For instance, one common practice is to use an advanced material only at the specific site its special properties are required and to use a more common material for the rest of the part. Large drill bits are made in this manner. Typically, a high-speed steel body is attached to a structural steel shank. Then, a cast nonferrous or carbide material is attached to the body for the cutting edges.[5] Thus, two interfaces which could be sites for intermetallic formation have been created in this drill bit.

A consideration when intermetallics form is the mechanical properties of the joint. Often, joints are at the site of stress concentrations or, as in the case of the drill bit, have to withstand high stresses. Intermetallic phases are brittle. The formation of such a brittle layer along the bond line can be deleterious to the mechanical integrity of the part. Additionally, at elevated temperatures, the intermetallic layers thicken more rapidly. The combination of high temperatures and stresses can weaken the bonded interface through intermetallic formation. Failure of such a weakened bond can have catastrophic consequences if it occurs in a critical application like the bond between a turbine blade and disk in an aircraft engine.

The formation of a layer of intermetallic can also be a problem in computer chip packaging or other soldered electrical connections. There is currently a major push to make chips smaller and to run them hotter. As chips get smaller, the joints between the chip and package get smaller as well. Higher temperature operation stimulates additional growth of the intermetallic layer. Therefore, the resulting intermetallic layer takes up proportionately more of the joint, and the joint is made more sensitive to fatigue from thermal cycling. Additionally, as shown by the data in Table 1.1, an intermetallic is usually not as good an electrical or thermal conductor as a metal so the electrical and thermal conductivity of a joint can be decreased by intermetallic formation.

Table 1.1: Thermal and electrical conductivities of several metals[6] and intermetallics[7]

Material	Thermal conductivity $\left(\frac{\text{watts}}{\text{cm deg.}}\right)$	Electrical conductivity $\left(\frac{1}{\text{m}\Omega\ \text{cm}}\right)$
Nickel	0.92	0.146
Copper	3.94	0.600
Tin	0.63	0.091
Cu_3Sn	0.70	0.112
Cu_6Sn_5	0.34	0.057
Ni_3Sn_4	0.20	0.035

Brazing and other processes in which a liquid and solid are in contact are susceptible to rapid intermetallic formation. Diffusion is enhanced in the solid at high temperatures, and diffusion in the liquid phase is inherently fast. Furthermore, in the copper-tin system, the morphology of the intermetallic formed at a liquid-solid interface differs from the morphology of the intermetallic formed at a solid-solid interface.[3,8] The difference in morphology may be related to the rate of formation of the intermetallic. The rate of intermetallic formation seems to be faster at solid-liquid interfaces than at solid-solid interfaces, even more so than can be explained by the fact that diffusion in liquid is faster than diffusion in solid.

Intermetallic growth is not only an issue in joining, however. Nickel-based superalloys are precipitation strengthened by a fine dispersion of $Ni_3(Al,Ti)$ particles. These alloys owe their high temperature strength to this dispersion of intermetallic particles. The degree of strengthening is dependent on several factors, but the key factor is particle size. The heat treatment of the alloy controls the particle size so the heat treatment must be tailored to produce the optimum particle size for strengthening. To determine the best heat treatment, an understanding of how the intermetallic particles grow is necessary.[1]

Coarsening of these intermetallic particles is another reason intermetallic formation in superalloys needs to be understood. These alloys experience high temperatures in service. The intermetallic particles grow more rapidly at these elevated temperatures. Since the strength of the alloys is dependent on the particle size and distribution, monitoring any changes in the particle size and distribution is vital.[2] If the particles become too large, they will no longer strengthen the material.

Because of the detrimental effects intermetallic growth can have on materials properties, formation of intermetallic phases needs to be considered when selecting materials and processing parameters. When mechanical integrity or electrical connection must be maintained, the formation of intermetallic phases must be prevented or controlled. One method to prevent intermetallic formation is to select materials that do not form intermetallic phases. However, this requirement greatly limits the choice of materials and can cause major changes to be necessary in the standard processing parameters. The other route, controlling intermetallic formation, requires understanding how intermetallic phases form. The relationships among variables such as temperature, time, and intermetallic thickness have to be established first. Then, processing parameters which optimize intermetallic formation can be determined based on these relationships. The most productive approach is one which combines theoretical work with experimental observations to evaluate practical applications.

The examples in this thesis are mostly drawn from the field of joining. However, the relationship among the variables affecting intermetallic formation and the insight into the mechanism of intermetallic formation can be applied in other fields such as alloy development and superalloy processing.

1.2 Areas to be explored in intermetallic formation

The goal of this work is to characterize the diffusional growth of intermetallic phases. Rapid advances in understanding intermetallic formation can be made and applied to real situations with a combination of theoretical research on intermetallic formation and modeling which incorporates experimental observations. Here, theoretical research focuses on diffusion in the intermetallic layer, while modeling efforts combine experimental data with diffusion equations to estimate diffusion coefficients and evaluate rate controlling steps.

Several aspects of diffusion in intermetallics can be evaluated theoretically. These aspects fall into two categories: chemical factors and physical factors. Chemical factors include bonding and chemical potential gradients. The driving force for diffusion is the chemical potential gradient. Intermetallic layers can have significant gradients in chemical potential even though they may have small composition gradients. Physical factors that affect diffusion are crystal structure, grain boundaries, and interface structure. Intermetallics have ordered structures that differ from the structures of the metals from which they form. These chemical and physical characteristics affect the diffusion coefficient in the intermetallic by influencing the mobility and jump frequencies of atoms. These issues are explored in Chapter 3.

Utilizing some experimental data allows for more practical applications than possible with theoretical evaluation alone. The experimental data can be used to calibrate a model, which can then predict the results of further tests without complete theoretical characterization of diffusion in the intermetallic. Intermetallic layer growth rates can be calculated and related to the necessary processing parameters for controlling intermetallic growth. Additionally, comparison of the model predictions with the theoretical data and with actual results can provide more insight into intermetallic formation than any single approach would by itself. With this in mind, a diffusion-based model of intermetallic growth is presented and evaluated in Chapter 4, and an intermetallic growth model which includes both diffusion and interface control is discussed in Chapter 5. A summary of the experimental work and the conclusions drawn from this work are presented in Chapter 6. Several recommendations for future work are discussed in Chapter 7.

2. Background

2.1 Definition of an intermetallic

The Metals Handbook[6] defines an intermetallic compound:

> **intermetallic compound.** An intermediate phase in an alloy system, having a narrow range of homogeneity and relatively simple stoichiometric proportions, in which the nature of the atomic bonding can vary from metallic to ionic.

This definition aptly defines the broad range of intermetallic compounds but leaves room for interpretation. The narrowness of the range of homogeneity is not specified. An intermetallic is distinct from a solid solution in terms of the range of homogeneity. As typified by the intermetallic phases in the nickel-tin phase diagram in Figure 2.1, the range of homogeneity of an intermetallic is usually less than ten atomic percent.

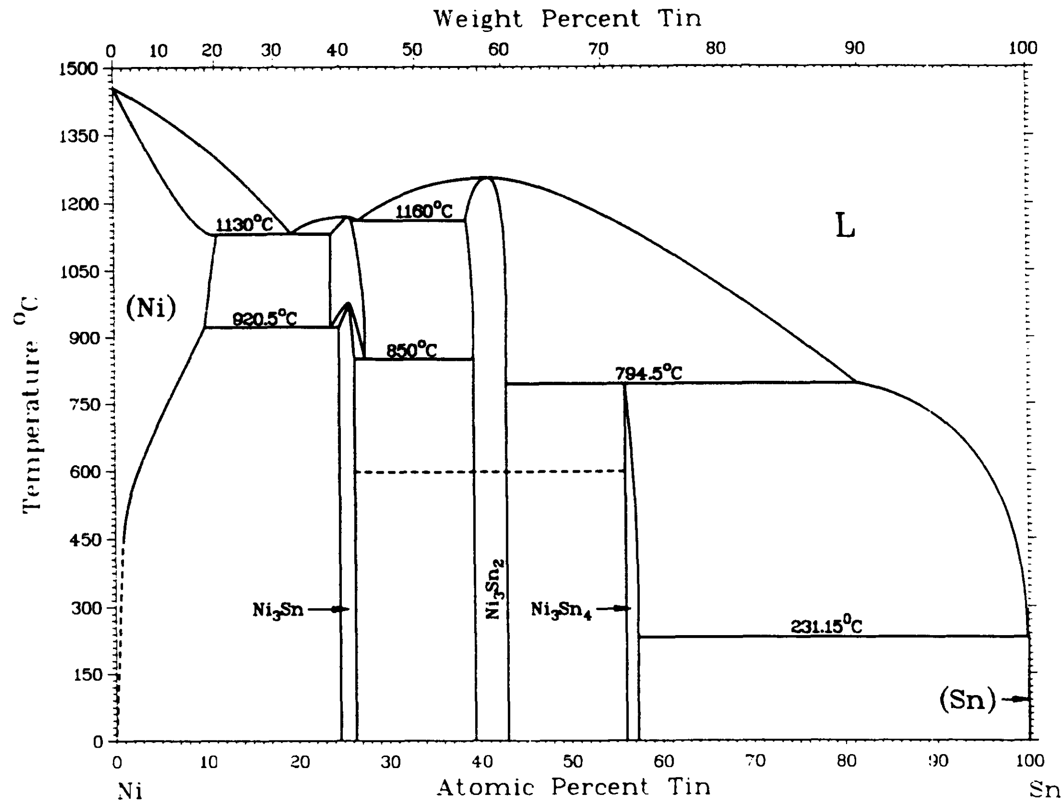

Figure 2.1: Nickel-tin phase diagram.[9] The three intermetallic phases, Ni_3Sn, Ni_3Sn_2, and Ni_3Sn_4, are representative of intermetallic phases in general in that they have a narrow range of homogeneity and are described by simple stoichiometric formulas.

The nickel-tin intermetallics, Ni_3Sn, Ni_3Sn_2, and Ni_3Sn_4, also illustrate that intermetallic phases can be described by simple formulas. A solid solution is differentiated from an intermetallic in that it has a much wider range of homogeneity and is not characterized by a simple formula as shown by alloy phases β and γ in the indium-tin phase diagram shown in Figure 2.2.

The definition allows for any type of bonding in the intermetallic phase because a wide variety of bonding is exhibited by intermetallic phases. A general indication of bond character is the heat of formation, ΔH_f. Small values of ΔH_f, numerically smaller than -30 kJ/mole, correspond to metallic bonding. Large negative values of ΔH_f, -40 to -170 kJ/mole, correspond to ionic bonding.[10] Intermetallics have values for $\Delta H_{f,\ 298K}$ ranging from -2.10 kJ/mole for Au_2Pb [11] and -3.14 kJ/mole for AgZn [12] to -109.6 kJ/mole for Al_2Cu_3 [11] and -138 kJ/mole for Ni_3Ti.[11] Bonding in intermetallic phases is primarily metallic in nature, but these data illustrate the broad range of bond character in intermetallic phases.

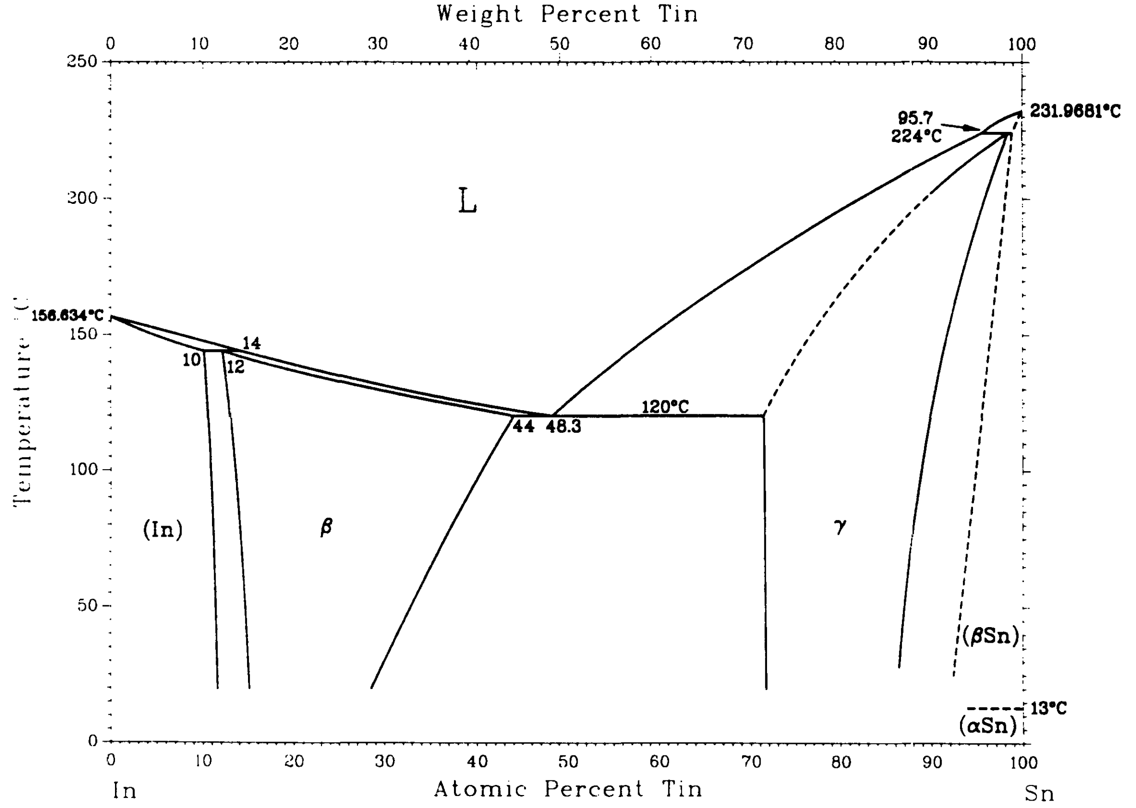

Figure 2.2: Indium-tin phase diagram.[9] The alloy phases, β and γ, have broad ranges of homogeneity and can not easily be described by a particular ratio of atoms.

A defining characteristic of intermetallic compounds that is missing from the above definition is long-range order. Intermetallic structures have long-range ordered arrangements of the constituent atoms, forming a superalttice.[13] Consequences of the complex structures created by the ordering are the brittleness and high hardness common to intermetallics. Table 2.1 compares the fracture toughnesses of some intermetallics to some typical alloy classes. The toughnesses of the alloys are one to two orders of magnitude greater than the those of the intermetallics.

Table 2.1: Room temperature fracture toughness, K_{IC}, of several alloys[14] and intermetallics.[7]

Material:	Cu_6Sn_5	Cu_3Sn	Ni_3Sn	Al alloys	Ti alloys	Steels
Toughness: (MPa√m)	1.4	1.7	1.2	~30	~100	~50-100

Intermetallic compounds form because the atoms of the different metals have a great affinity for each other. Correspondingly, metals that form intermetallic phases tend to wet each other well, as do copper and tin, and intermetallic phases usually have higher melting points relative to the metals from which they are formed. For instance, as shown in Figure 2.1, Ni_3Sn_2 melts at a temperature above 1200°C despite the large amount of tin, which melts at 232°C.

Rhines refers to congruently melting intermediate phases that behave as components in the alloy system as intermetallic compounds.[15] Intermetallic phases do often melt congruently, as does Ni_3Sn_2 (refer to Figure 2.1), because they tend to exhibit high melting points. However, Rhines' definition of an intermetallic compound is too limited for practical discussion because only a small subset of phases that fit the other characteristics of intermetallics melt congruently.

For this work, intermetallic phases possess the following defining characteristics:

1) intermediate phases comprised of two or more metal species
2) range of homogeneity less than ten atomic percent
3) can be described by a simple ratio of atoms
4) long-range order
5) bond character can vary from metallic to covalent to ionic.

2.2 Observation of fast isothermal solidification

During experiments to test the remelt temperature of transient liquid phase (TLP) bonds, Roman[16] found that isothermal solidification occurred more rapidly than predicted by the accepted model of TLP when intermetallics formed in the system. The current work on intermetallic formation grew out of Roman's initial observations on TLP bonding. This work is more generally applicable to intermetallic formation at any interface, not just at a TLP joint. However, to understand the observation of fast isothermal solidification, the mechanism of TLP bonding must first be understood.

2.2.1 Transient liquid phase bonding

Transient liquid phase bonding is a mixture of brazing and diffusion bonding. Initially, the process resembles brazing; an interlayer is placed between the two parts to be joined and the assembly is heated to a bonding temperature at which the interlayer liquefies. In a braze, once the interlayer is liquid, the assembly would be cooled, and the joint would be complete. For a TLP bond, the assembly is held at the bonding temperature and allowed to isothermally solidify by diffusion of the interlayer material into the parts being joined. This portion of the process is similar to diffusion bonding. The resulting TLP joint can have near base material properties and can maintain its strength at temperatures above the original bonding temperature.[17]

The choice of the interlayer is critical to the process. The interlayer needs to be chosen such that it will melt at a lower temperature than the base metal and such that the base metal has some solubility for the interlayer material. Other process parameters include bonding temperature, pressure, and time. The relationship between interlayer selection and bonding time is determined by the thermodynamics and kinetics of the system as well as by the bond thickness. Applying pressure to the joint during bonding influences the bond thickness by squeezing out some of the liquid layer. The extrusion of the interlayer reduces the amount of material that needs to be diffused into the base material and so shortens the bonding time. Large pressures are not required for the formation of the TLP bond. This is an advantage over conventional diffusion bonding which requires very large pressures to complete a joint in a reasonable amount of time.

Current applications of TLP focus on bonding nickel-based superalloys[18-22] and titanium alloys[23,24] for aircraft engine parts and on bonding metal matrix composites such as boron-aluminum.[25] The process is also of interest in integrated chip packaging as an improvement on soldering processes.[26,27]

The mechanism of TLP bonding has been studied by several researchers and models have been developed to describe the process.[28-31] The TLP process can be divided into stages, each of which can be modeled independently. The stages of TLP are shown in Figure 2.3 with accompanying diagrams depicting the bond status.

An in-depth analysis of the techniques and mathematics used to model each stage is given by MacDonald.[31] The basic result is that in most cases stages 0, I, and II take place rapidly compared to stages III and IV, isothermal solidification and homogenization. Since the joint is effectively complete after isothermal solidification, the isothermal solidification stage, stage III, is focused on as the rate limiting step. The degree of homogenization required can vary, or homogenization may not be necessary at all.

Isothermal solidification is controlled by diffusion of the interlayer into the base metal. If the two materials being joined are the same, the diffusion is symmetric. The diffusion in a joint between dissimilar materials is more complicated.

A moving boundary analysis with error function solutions for the concentration profiles effectively predicts the bonding time for eutectic systems such as the copper-silver system.[31] When intermetallic layers form, the analysis of the diffusion profiles becomes more complicated because of the additional boundaries created and the additional data needed on the diffusion coefficients in the intermetallic layers. However, the time required for isothermal solidification should still be controlled by solid-state diffusion of the interlayer material.

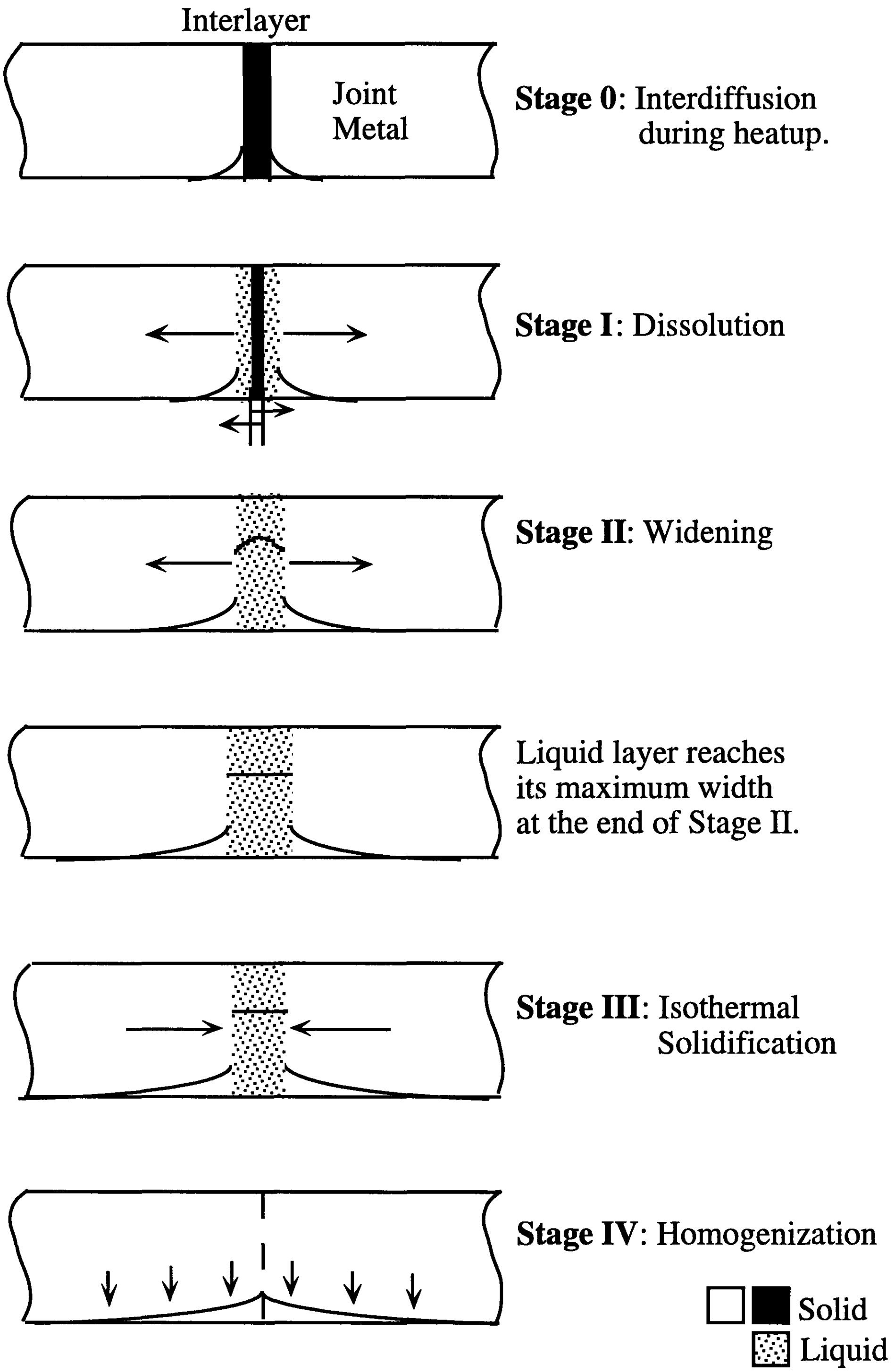

Figure 2.3: The stages of TLP bonding. The arrows in Stage I, II, and III indicate the direction of motion of the solid/liquid interface. The concentration profile of the interlayer material is shown for each stage. In Stage IV, the arrows indicate the flattening of the concentration profile during homogenization. Adapted from ref. 31.

2.2.2 Meaning of "fast"

The observation of fast isothermal solidification is based on the theory that solidification time is controlled by solid-state diffusion. Roman[16] recorded a solidification time of one hour for an interlayer of 52% indium, 48% tin on copper. The joint was approximately 50 μm thick. Estimating the diffusion coefficient by

$$D \approx x^2/t \tag{2.1}$$

an apparent diffusion coefficient of 10^{-8} cm^2/s can be calculated for this case. The bonding temperature was 130°C. At temperatures this low, 10^{-8} cm^2/s is too fast to represent solid-state substitutional diffusion. For comparison, the diffusion coefficient for tin in copper at this temperature is on the order of 10^{-24} cm^2/s.[32]

Both indium and tin form intermetallic compounds with copper in the binary systems as shown by the phase diagrams given in Figures 2.4 and 2.5. Roman was testing the remelt temperatures of the TLP bonds. For the Cu-In/Sn bond, the remelt temperature was about 600°C which was also the limit of the testing method. This result indicates that the bond was complete; no indium-tin solder, which would have melted at a much lower temperature (refer to the indium-tin phase diagram in Figure 2.2), remained in the joint. The remelt temperature also corresponds to the approximate melting temperatures of the binary intermetallic phases that are predicted to form at 130°C, the bonding temperature of the joint (refer to the phase diagrams in Figures 2.4 and 2.5). A more accurate assessment would require the ternary phase diagram for this system. However, since the ternary diagram has not yet been determined, the binary systems can be used for a general evaluation.

The obvious conclusion is that the formation of the intermetallic layers somehow sped up the solidification. However, diffusion through intermetallic compounds is generally taken to be slower than diffusion through metals. Formation of an intermetallic layer should create a barrier to further diffusion of the interlayer material out of the joint and slow down solidification. Instead, the opposite effect is seen. A better understanding of intermetallic formation is necessary to determine how intermetallic layer formation affects the solidification.

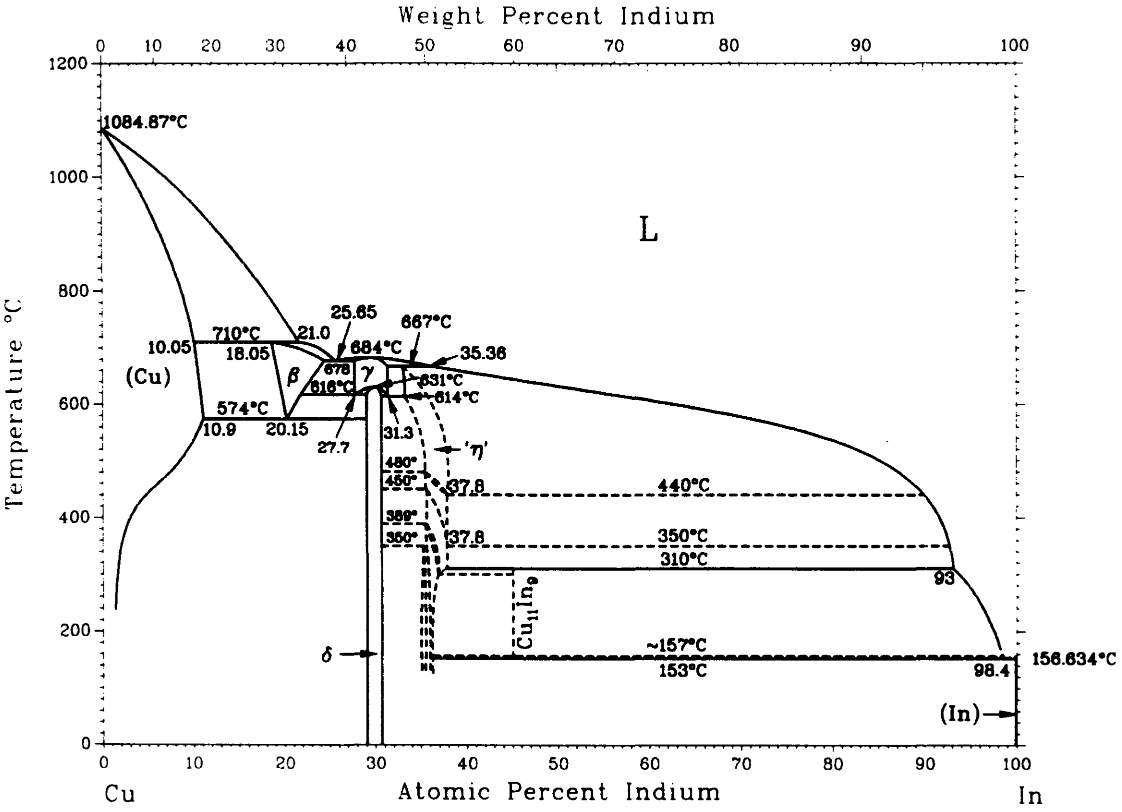

Figure 2.4: Copper-indium phase diagram.[9] At 130°C, the δ (Cu_7In_3) phase forms between copper and indium. This phase decomposes at 631°C but does not completely melt until 684°C.

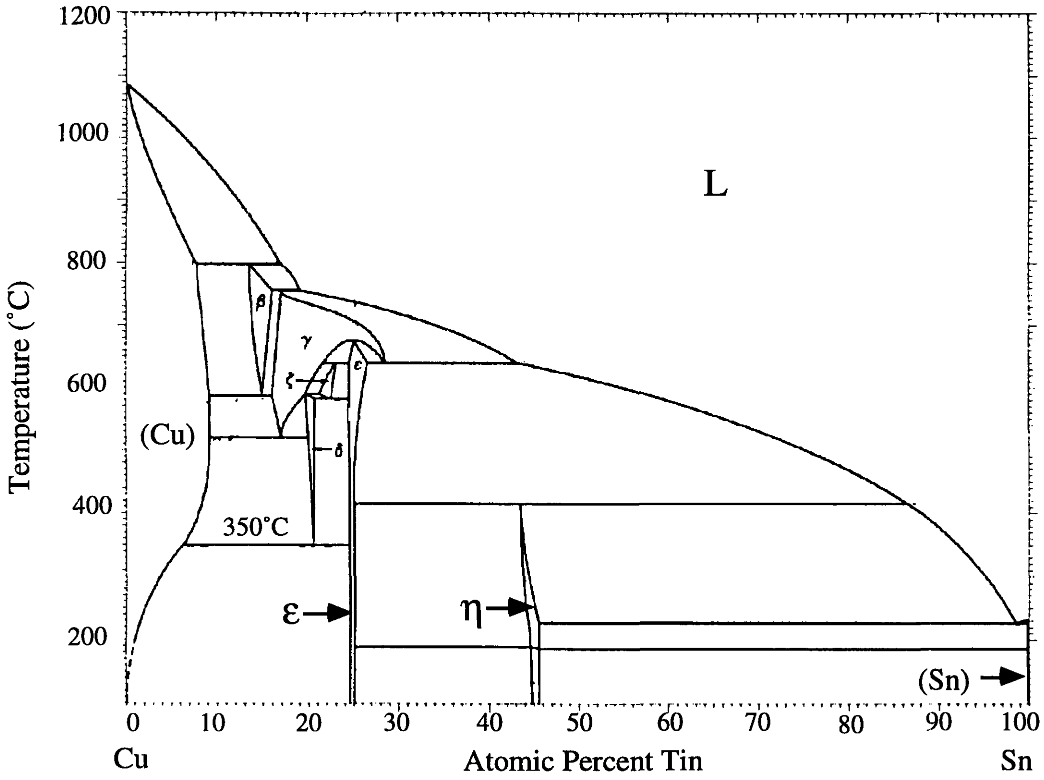

Figure 2.5: Copper-tin phase diagram.[9] At 130°C both the ε (Cu_3Sn) and the η (Cu_6Sn_5) phases form between copper and tin. Both phases melt at temperatures significantly higher that 130°C.

2.3 Comparison of systems with and without intermetallics

To better understand how intermetallic formation affects isothermal solidification, a TLP bond in a system which contains intermetallics is compared to a bond in a system in which intermetallics do not form. The copper-tin system, which contains intermetallic phases, and the copper-silver system, a eutectic system, are chosen for this comparison because the phase diagrams are well known and are relatively simple. Additionally, much research has been published on both systems. Several efforts to model TLP bonding have focused on the copper-silver system.[28,31] The copper-tin system has been extensively studied because of its wide range of applications in soldering.

In the following analysis, the concentration profiles of TLP joints in each of these systems are calculated. Comparison of the diffusion distances in the two cases starts to explain why isothermal solidification in systems that contain intermetallics is fast. The diffusion distance in the copper-tin system, which contains intermetallics, is much shorter than the diffusion distance in the copper-silver system, which does not contain intermetallics. However, diffusion across the intermetallic layers is still necessary. Factors that affect diffusion across the intermetallic layers will be explored in Chapter 3.

2.3.1 Calculation of concentration profiles

The concentration profiles are calculated for the minimum bonding time, defined as the time at which the joint no longer contains any liquid. This point in time corresponds to the end of the isothermal solidification stage of TLP and the beginning of homogenization. The copper-silver profile is based on a moving boundary analysis developed by MacDonald.[31] The copper-tin profile is calculated by extrapolation of results from a more complicated moving boundary analysis which requires some experimental data to be solved.[32]

2.3.1.1 Copper-silver system

The phase diagram for the copper-silver system is shown in Figure 2.6. The initial state is a 100 μm interlayer of pure silver between two pieces of pure copper. The copper pieces are assumed to be semi-infinite. The thickness of the copper necessary to satisfy this assumption is checked at the end of the calculation. The bonding temperature is 820°C. This temperature is necessarily above the eutectic temperature and below the melting point of copper. As the assembly is raised to the bonding temperature, the silver and copper interdiffuse. The change in composition and phase can be thought of as following an isothermal line across the phase diagram. Liquid will first appear at the interface between the copper and silver and then will consume the entire interlayer. As the silver continues to diffuse into the copper, the liquid layer will narrow until it disappears. The progression of the copper-silver TLP bond is accurately described by the stages of TLP bonding illustrated in Figure 2.3.

MacDonald[31] developed a complete moving boundary model to predict a solidification time and concentration profiles for a TLP bond in the copper-silver system. A brief overview of his approach and results are presented here to explain how the concentration profile for the copper-silver joint is generated.

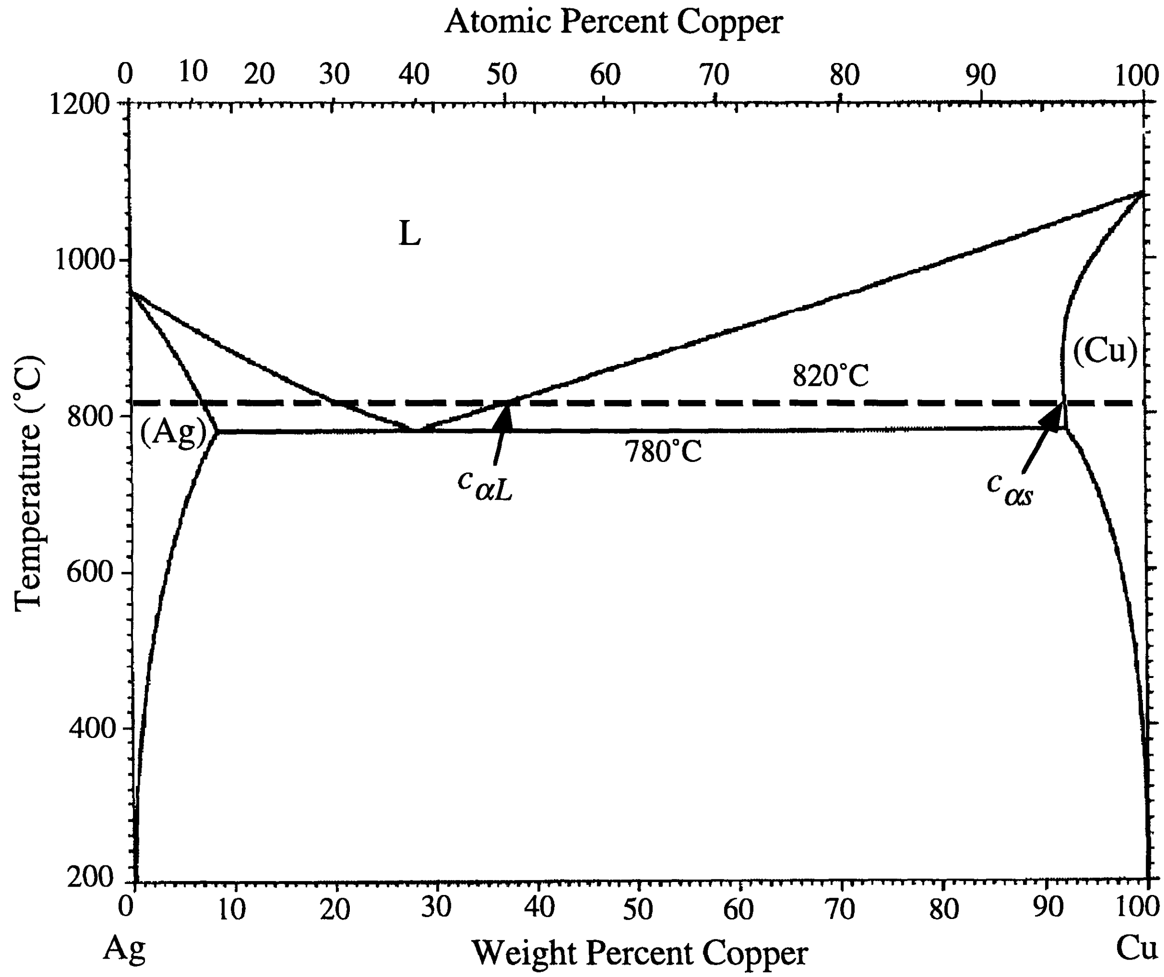

Figure 2.6: The copper-silver phase diagram.[9] The bonding temperature of 820°C is indicated by the dashed line. $c_{\alpha L}$ and $c_{\alpha s}$ are the equilibrium concentrations in the liquid and the solid phases, respectively, in the liquid-copper solid solution two phase region.

MacDonald's moving boundary analysis covers only the isothermal solidification stage (stage III). Since isothermal solidification is the most time-consuming step, ignoring homogenization, the solidification time is effectively the bonding time. Several assumptions are made to simplify the analysis. Diffusion during heat-up, dissolution, and widening (stages 0, I and II of TLP bonding) is neglected. This assumption is valid since most of the region into which the interlayer diffuses during heat-up is melted during dissolution. Diffusion in the liquid is much faster than diffusion in the solid state so the concentration in the liquid is assumed to be both uniform and constant. Equilibrium at the interface is also assumed. Figure 2.7(a) shows the state of the system at the start of isothermal solidification with the above assumptions included. Figure 2.7(b) shows the state of the system midway through solidification.

MacDonald's analysis combines error function solutions for the concentration profiles, the mass balance at the moving interface, and the constraint on the flux at the original interface to determine equations for the bonding time and concentration profiles. For a 100 μm interlayer at 820°C, the bonding time is calculated to be 1780 hours.[31] The penetration depth of the silver is calculated from

$$x_{\max} \approx 4\sqrt{Dt} \tag{2.2}$$

to be 0.17 cm.

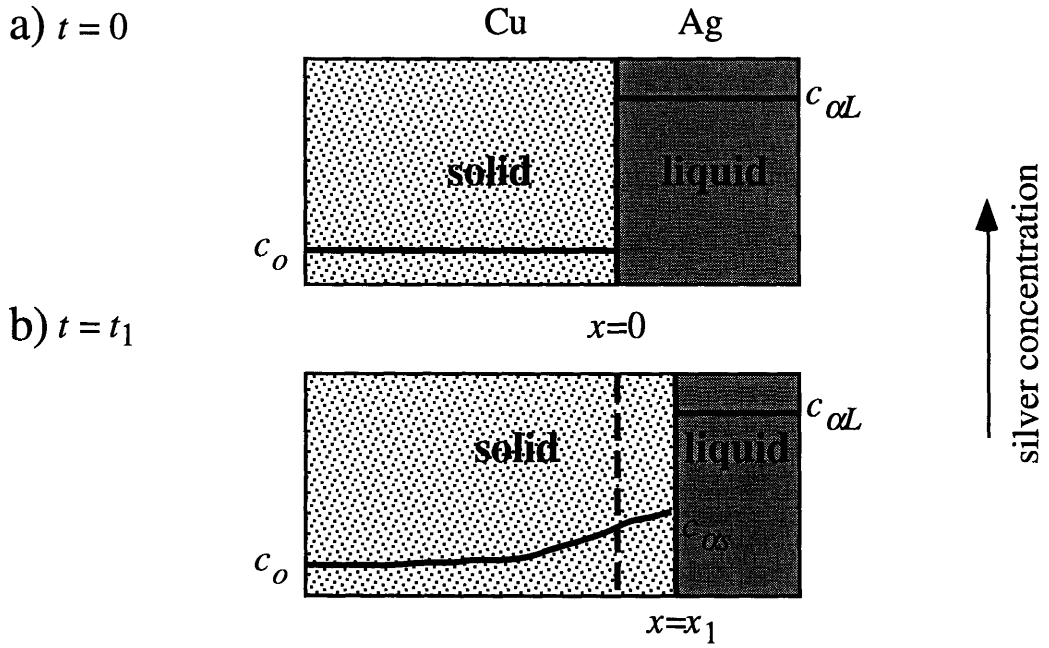

Figure 2.7: The progress of a TLP bond in the copper-silver system at (a) the beginning of isothermal solidification and (b) a time, t_1, into solidification. Interdiffusion prior to the start of isothermal solidification is ignored.

2.3.1.2 Copper-tin system

The phase diagram for the copper-tin system is shown in Figure 2.5. The initial set-up for the copper-tin joint is the same as that for the copper-silver case; a 100 μm interlayer of pure tin is placed between two semi-infinite pieces of copper. Figure 2.8 illustrates schematically the bonding process for a TLP bond in the copper-tin system. The bonding temperature is 300°C. When the assembly is heated to the bonding temperature, the tin layer melts and dissolves some of the copper. Additionally, the intermetallic phases, ε (Cu_3Sn) and η (Cu_6Sn_5), form at the liquid-solid interface. The intermetallic layers thicken, consuming the tin from the interlayer. The joint will be completely solid when the last of the tin interlayer has been converted to intermetallic.

The concentration profile cannot be calculated with an analysis as basic as the one done above for the copper-silver case. Instead, a more complicated formulation which includes several moving boundaries must be solved. Mei *et al.*[32] used such a multiple boundary analysis to calculate the diffusion coefficients from experimental data on intermetallic layer thickness as a function of time. This model will be discussed in-depth in Chapter 4. Here, however, the results from Mei's work with this model can be extrapolated to predict the concentration profile at solidification.

Mei *et al.*[32] calculate an interface position parameter, λ, for each of the three interfaces in the system: the interface between the copper solid solution and the ε phase, $x_{\text{Cu-}\varepsilon}$; the interface between the ε and the η phase, $x_{\varepsilon-\eta}$; and the interface between the η phase and tin solid solution, $x_{\eta\text{-Sn}}$. The interface position parameters give the position of the interface for a given time from the equation

$$\Delta x = \lambda t^{1/2} \tag{2.3}$$

where Δx equals the distance the interface has moved in time t and λ is the interface position parameter. The temperature dependence of interface position parameter can be fit to an Arrhenius type equation

$$\lambda = \lambda_o \exp\left[\frac{A}{T}\right] \tag{2.4}$$

where λ_o and A are constants and T is temperature in Kelvin. The constants, λ_o and A, are determined by fitting Mei's *et al.*[32] data for 190-220°C to Equation 2.4. Then, the values of λ for each interface can be calculated for 300°C. Table 2.2 shows the constants, λ_o and A, and the calculated values of λ for 300°C.

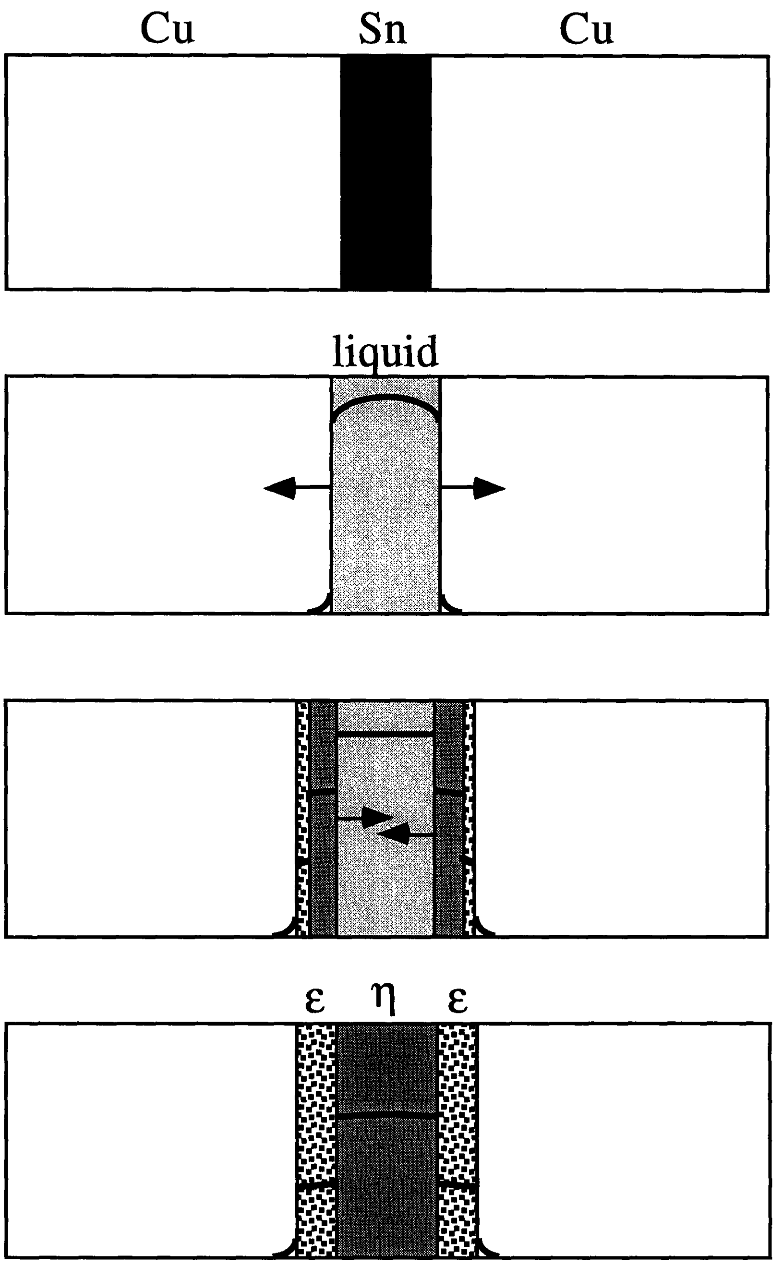

Figure 2.8: Schematic illustration of the TLP bonding process at 300°C for copper with a tin interlayer. The intermetallic phases, ε and η form in the joint. The arrows indicate the direction of motion of the solid-liquid interfaces. The curves show the tin concentration profiles.

Table 2.2: Interface position parameter data

Interface	λ_o (cm/s$^{1/2}$)	A (1/K)	$\lambda_{300^\circ C}$ (cm/s$^{1/2}$)
Cu-ε	-1.59 x 10^{-3}	-3434	-3.97 x 10^{-6}
ε–η	-1.66 x 10^{-4}	-2757	-1.35 x 10^{-6}
η-Sn	8.74 x 10^{-4}	-3461	2.08 x 10^{-6}

The values of $\lambda_{300^\circ C}$ can be used to determine the interface positions at the completion of the TLP bond. For the joint to completely solidify, the η-Sn interface must move 50 μm, half the thickness of the interlayer. This value of $x_{\eta\text{-Sn}}$ is used in Equation 2.3 to calculate the time to solidify the joint. The calculated solidification time is 5.8 x 10^6 s. In turn, this time is used to calculate the position of the other two interfaces using Equation 2.3 and the interface position parameter corresponding to the particular interface. The sketch in Figure 2.9 shows the results of the interface position calculations.

The solidification time calculated above, 5.8 x 10^6 s, is 1600 times longer than the typical solidification time observed experimentally in TLP bonds containing intermetallics.[16] One reason could be that Mei's *et al.* data were collected at a temperature below the melting point of tin (232°C). As the bonding temperature here is 300°C, the tin is liquid. The solidification of the joint is assumed to be diffusion controlled. Diffusion through the solid intermetallic or the solid copper is slower than diffusion in the liquid tin. Thus, the solid state diffusion should still be the rate limiting step, and the fact that the tin is liquid should not affect the results. Instead, the calculated time may be incorrect because the entire analysis is based on the assumption that the intermetallic formation is diffusion controlled.

There is much data that supports diffusion control for the solid state formation of intermetallics.[33-37] However, some researchers have found non-parabolic behavior for solid state intermetallic growth,[8,38] and there is little information about intermetallic formation at liquid-solid interfaces. It is known that the intermetallic that forms at a liquid-solid interface has a more rounded morphology while the intermetallic that forms at a solid-solid interface has an angular morphology.[3,8] This difference seen in the morphology of the intermetallic formed at the liquid-solid interface as compared to the intermetallic formed from solid state diffusion indicates the possibility of another mechanism. The controlling mechanism for intermetallic growth in the copper-tin system will be explored in greater detail in Section 4.2 when Mei's model is critiqued. In any case, the calculation above should give a general sense of the intermetallic layer thicknesses, and that is all that is necessary for the order of magnitude comparisons in the analysis which follows.

2.3.2 Interpretation of profiles

The calculated profiles for the copper-silver joint and the copper-tin joint are overlaid in Figure 2.10. The copper-silver profile is calculated from MacDonald's model, and the copper-tin profile is based on the data shown in Figure 2.9. The characteristic distance that the interlayer material has to diffuse to solidify the joint is very different for the two base metals.

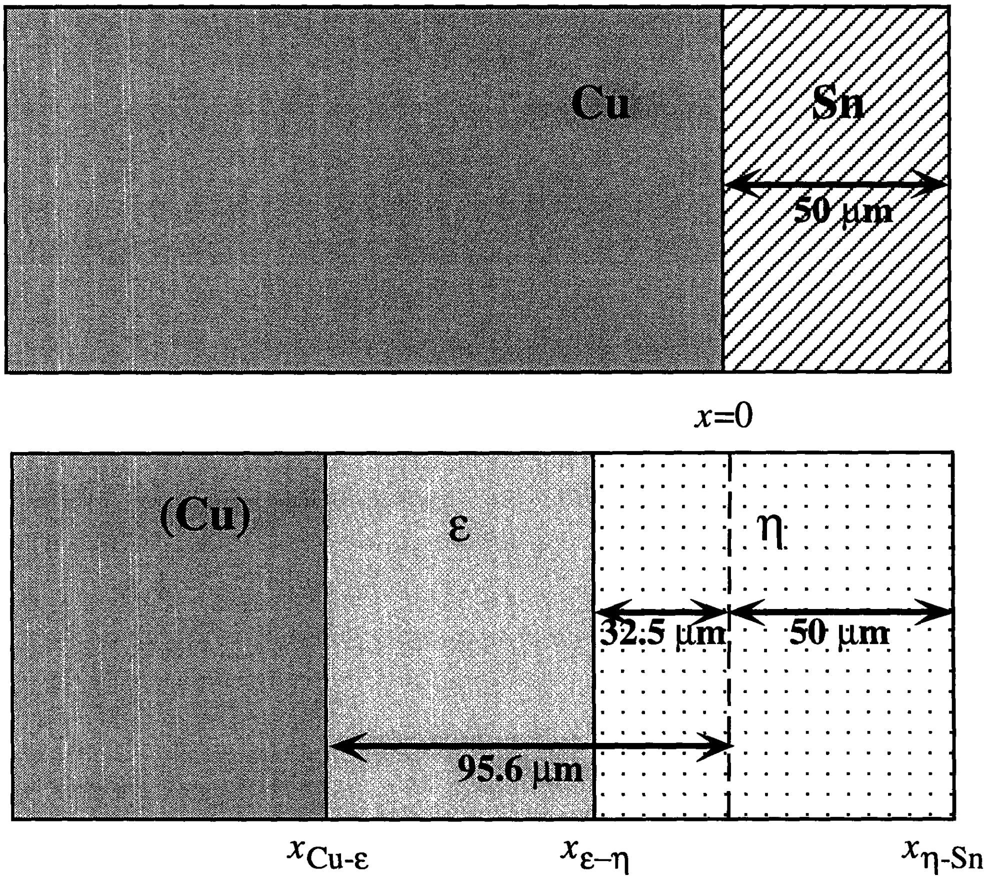

Figure 2.9: Positions of the interfaces at the completion of a TLP bond at 300°C in copper with a 100 μm tin interlayer. Only half of the joint is shown.

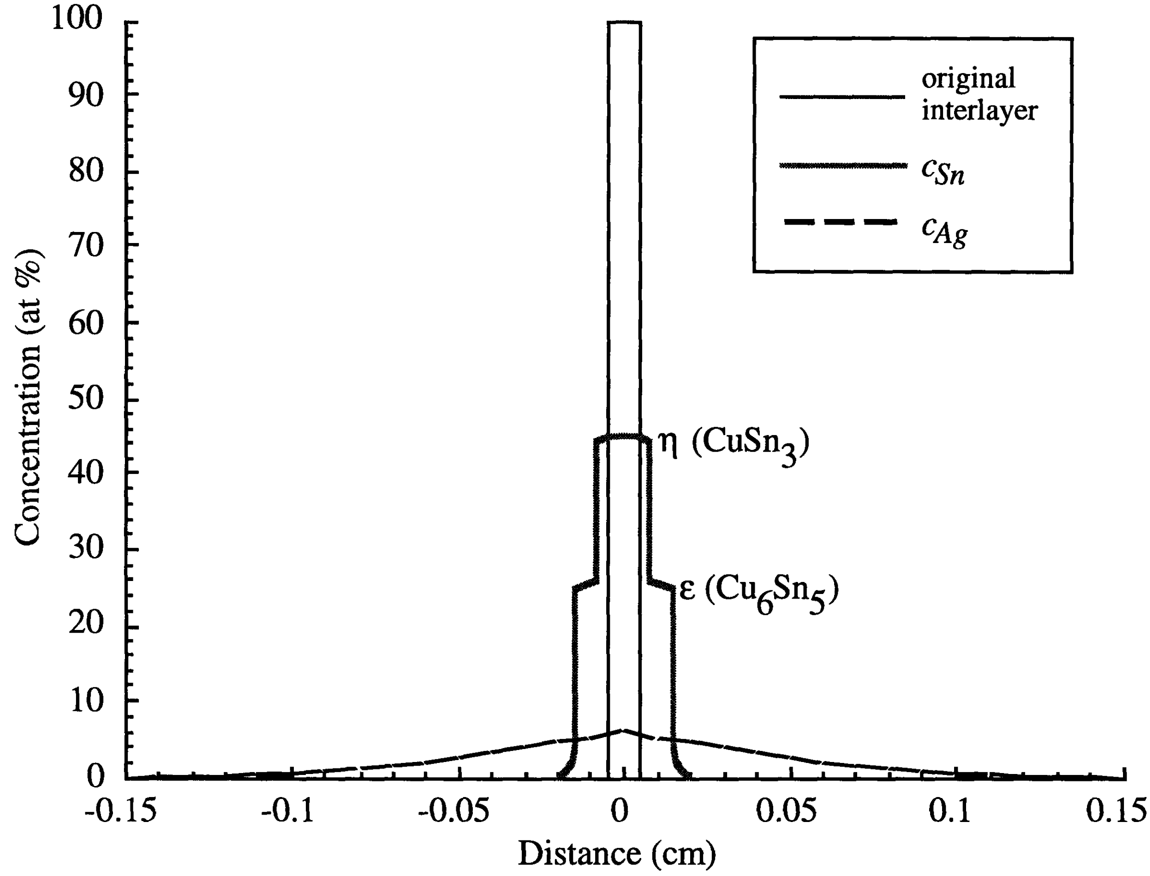

Figure 2.10: Concentration profiles at the end of the isothermal solidification stage for a TLP joint in copper with a tin interlayer at a bonding temperature of 300°C, and with a silver interlayer at a bonding temperature of 820°C. Intermetallic phases form in the copper-tin joint.

The silver travels a much greater distance to solidify the joint than does the tin. The characteristic diffusion distance for the silver is on the order of 0.2 cm while the distance for the tin is on the order of 0.02 cm. Considering

$$t \approx x^2/D \tag{2.5}$$

the order of magnitude difference in the diffusion distance translates into a two order of magnitude difference in the time since the diffusion coefficients are comparable: $D_{\text{Cu-Ag, 820°C}} = 2.9 \times 10^{-10}$ cm^2/s [31] and $D_{\text{Cu-Sn, 300°C}} \approx 10^{-10}$ cm^2/s.[32] This difference in time may start to explain why the bonding time for the copper-silver system is on the order of 1000 hours while the bonding time observed experimentally for a copper joint containing intermetallics is on the order of 1 hour.

However, a diffusion coefficient of 10^{-10} cm^2/s is considered fast, especially for an intermetallic compound not near its melting point. The diffusion coefficients in the copper-tin intermetallics are well established.[8,32,34,39] The data in the literature are consistent as shown by Table 2.3 and in Figure 2.11.

If diffusion across an intermetallic layer is slow, then the shorter diffusion distance in the base material will not matter. Instead, the intermetallic layer will act as a barrier, and diffusion through the layer will be the rate-limiting step. Examining the factors that govern the amount of diffusion possible through the intermetallic layer, or more precisely the amount of flux possible through the intermetallic layer, should give more insight into the effect of the intermetallic formation on solidification.

This thesis explores intermetallic formation in an effort to understand its mechanism and kinetics. Since diffusion through the intermetallic plays a key role in intermetallic growth, diffusion through intermetallic phases is examined from a theoretical standpoint in Chapter 3. On a more practical note, a diffusion-based model for intermetallic layer formation is evaluated and critiqued in Chapter 4. Since the diffusion-based model in found to be lacking, another model which combines diffusion and interface reaction rates is assessed in Chapter 5.

Table 2.3: Experimentally measured diffusion coefficients in the copper-tin intermetallics

Temperature (°C)	D_ε (cm^2/s)	D_η (cm^2/s)	Reference
180	4.3×10^{-12}	2.7×10^{-12}	Starke and Wever[39]
190	5.8×10^{-12}	1.86×10^{-11}	Mei *et al.*[32]
200	7.94×10^{-12}	2.39×10^{-11}	Mei *et al.*[32]
	9.0×10^{-12}	3.1×10^{-11}	Lubyovà *et al.*[34]
210	1.19×10^{-11}	3.1×10^{-11}	Mei *et al.*[32]
	3.7×10^{-11}	2.2×10^{-11}	Starke and Wever[39]
220	1.5×10^{-11}	4.35×10^{-11}	Mei *et al.*[32]
	1×10^{-11}	3×10^{-11}	Cogan *et al.*[8]
300	3.5×10^{-9}	3.0×10^{-9}	Lubyovà *et al.*[34]
400	1.2×10^{-8}	2.0×10^{-8}	Lubyovà *et al.*[34]
450	3.8×10^{-8}		Lubyovà *et al.*[34]

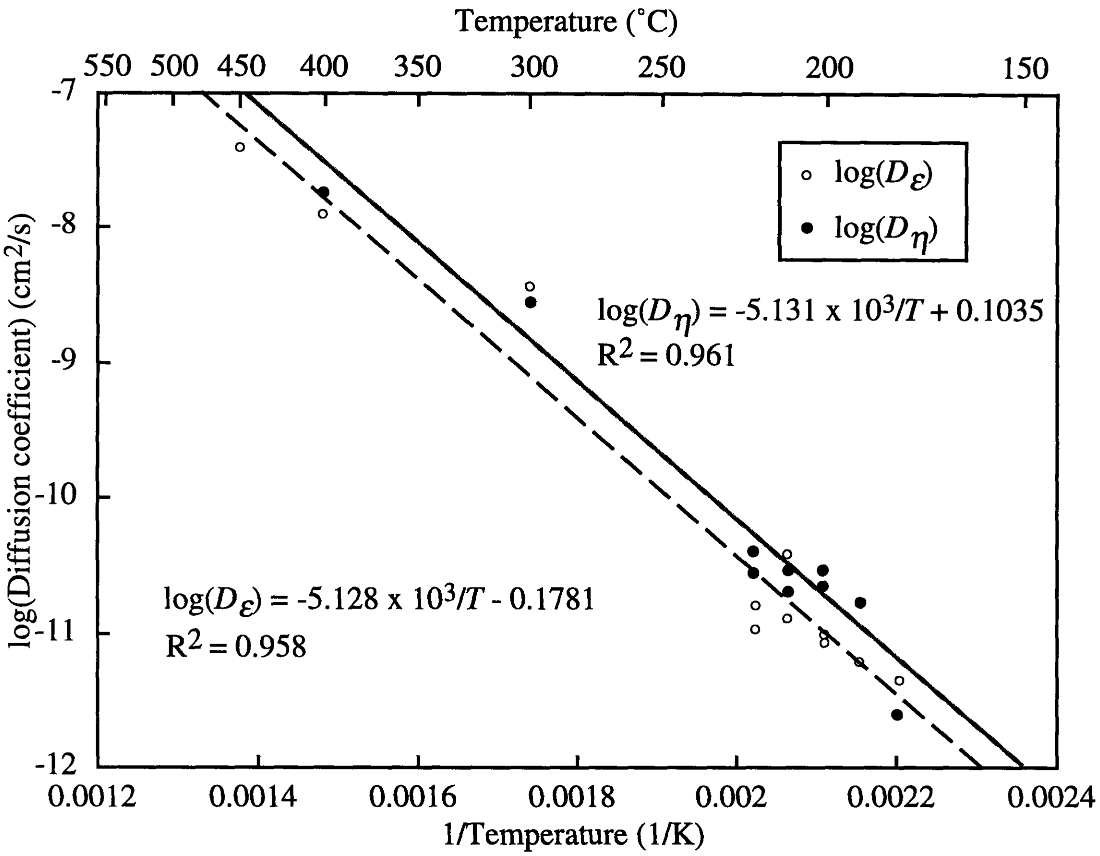

Figure 2.11: Plot of all the experimentally measured diffusion coefficients from Table 2.3. Even though the data comes from many different sources and experiments,[8,32,34,39] it is reasonably consistent. There is a lack of data at the higher temperatures though.

3. Fast diffusion in intermetallic phases

A central issue in growth of intermetallic layers is the flux through the intermetallic. The amount of material that can be transported through the existing intermetallic layer determines the growth rate. This concept is at the heart of diffusion control of layer growth. If diffusion through the intermetallic is slow, then the intermetallic layer acts as a barrier to further intermetallic growth. If diffusion through the intermetallic layer is fast, the intermetallic layer will continue to grow.

Some intermetallic phases have high diffusivities. For instance, the diffusion coefficient in the copper-tin intermetallics is about 10^{-10} cm^2/s at 300°C.[32] At 500°C, the diffusion coefficient of copper in the intermetallic CuZn is 1.7 x 10^{-8} cm^2/s and that of zinc is 6.6 x 10^{-9} cm^2/s.[40] In the intermetallic AgZn, the diffusion coefficient for silver is 1.8 x 10^{-8} cm^2/s, and for zinc it is 3.2 x 10^{-9} cm^2/s at 350°C.[40] Figure 3.1 compares the diffusion rates seen in the copper-zinc intermetallic and the silver-zinc intermetallics with those typical of metals. The diffusion rates in these intermetallics are much faster than those seen in metals. Additionally, the observations of fast isothermal solidification discussed in the previous chapter indicate that diffusion through an intermetallic phase can be fast. To understand how an intermetallic could support a high rate of diffusion, the underlying principles that govern the flux through a material need to be examined.

Flux through a material depends on many characteristics of the material. The flux, J, of species i is given by Fick's First Law:

$$J_i = -D_i \frac{\partial c_i}{\partial x} \qquad (3.1)$$

where D_i is the diffusion coefficient and $\partial c_i / \partial x$ is the concentration gradient. It is through the diffusion coefficient that the characteristics of the material influence the flux.

Einstein offers a more fundamental equation to describe the flux through a material:[41,42]

$$J_i = -M_i \frac{\partial \mu_i}{\partial x} \qquad (3.2)$$

where M_i is a positive mobility coefficient and $\partial \mu_i / \partial x$ is the spatial gradient of chemical potential. Here, the driving force for diffusion is clearly and correctly identified as the chemical potential gradient.

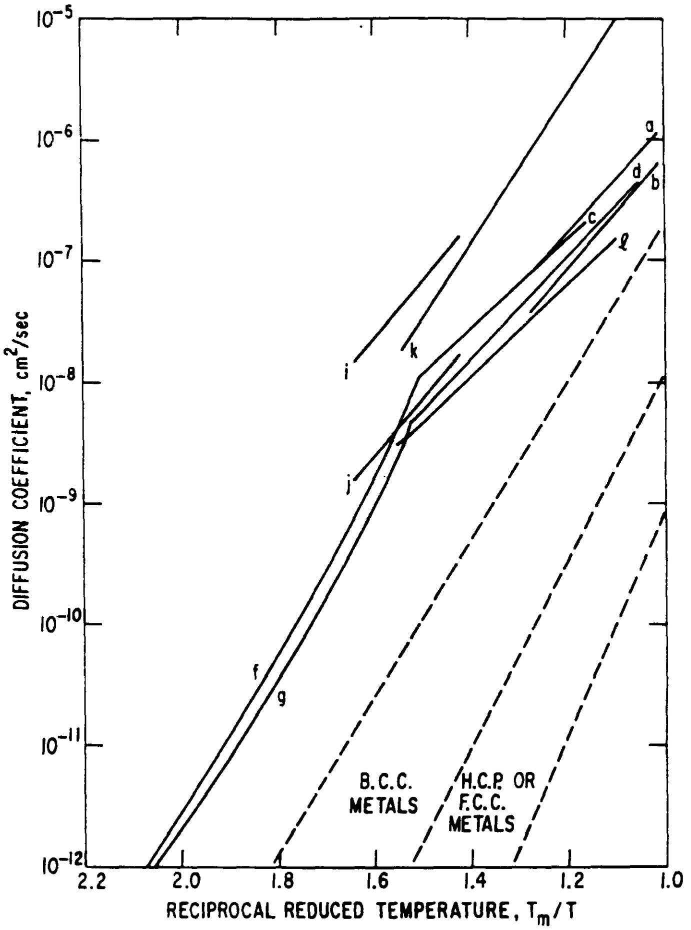

Key	Intermetallic	Diffusing atom
a	β-CuZn	^{65}Zn
b	β-CuZn	^{64}Cu
c	β-CuZn	^{65}Zn
d	β-CuZn	^{64}Cu
f	β'-CuZn	^{65}Zn
g	β'-CuZn	^{64}Cu
i	γ-Cu$_5$Zn$_8$	Zn
j	γ-Cu$_5$Zn$_8$	Cu
k	β-AgZn	^{65}Zn
ℓ	β-AgZn	^{110}Ag

Figure 3.1: Intrinsic diffusion coefficients for β-CuZn, γ-Cu$_5$Zn$_8$, and β-AgZn compared with the diffusion coefficients typical of metals. Reprinted with permission from ref. 40.

Comparing Equations 3.1 and 3.2 it can be seen that

$$D_i = M_i \frac{\partial \mu_i}{\partial c_i} \qquad (3.3)$$

This equation emphasizes the relationship between the diffusion coefficient and the chemical potential and is used to understand the "uphill" diffusion seen in spinodal decomposition where the diffusion coefficient is required to be negative. Since M_i is always positive by definition, the diffusion coefficient can be negative when the gradient of the chemical potential with respect to concentration is negative.

If diffusion is examined in terms of atomistics, another equation defining the diffusion coefficient can be developed:[42]

$$D = \frac{1}{6}\alpha^2\Gamma \tag{3.4}$$

where α is the jump distance and Γ is the jump frequency.

For substitutional diffusion, the jump frequency is proportional to the coordination number, Z, the probability of there being a vacancy, p_v, and the frequency with which the atom successfully jumps into that vacancy, ω:

$$\Gamma = Zp_v\omega \tag{3.5}$$

The probability of a vacancy is given by

$$p_v = \exp\left[\frac{-G_v}{RT}\right] \tag{3.6}$$

where G_v is the activation energy for forming a vacancy, R is the gas constant and T is temperature.

The frequency of successful jumps, ω, is related to the frequency at which the atom attempts to jump and to the probability that an attempt is successful. The mean vibrational frequency of an atom around its equilibrium site is an estimate of the frequency at which an atom tries to jump. This frequency can be taken to be the Debye frequency, ν_D, which is a characteristic of the material. The probability that an attempted jump is successful is quantified by the energy required to form the activated complex necessary for diffusion to take place. This energy is also referred to as the migration free energy, G_m, and is shown conceptually in Figure 3.2. Thus, ω is determined from

$$\omega = \nu_D \exp\left[\frac{-G_m}{RT}\right] \tag{3.7}$$

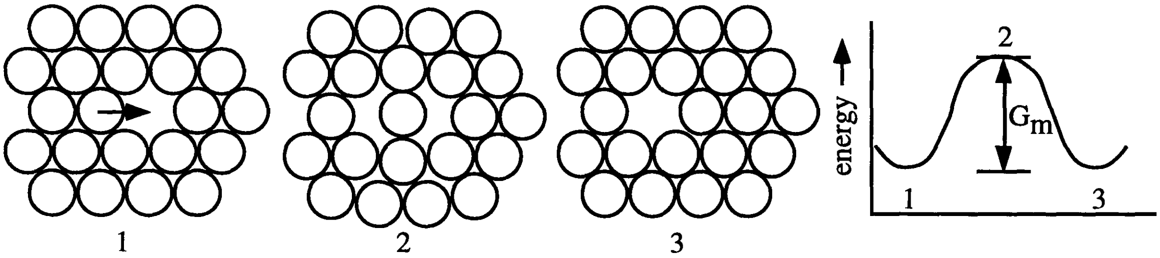

Figure 3.2: The activation energy for motion, G_m, of a atom in the lattice is the energy required to form the activated complex illustrated in state 2.

These relations for the jump frequency can be substituted into Equation 3.4 for the diffusion coefficient:

$$D = \frac{1}{6}\alpha^2 Z \nu_D \exp\left[\frac{-(G_v + G_m)}{RT}\right] \qquad (3.8)$$

For most materials, α is on the order of 5 x 10^{-8} cm, Z is 4 to 12, and the Debye frequency is about $10^{13}s^{-1}$. Large differences in diffusion coefficients, then, must result from variation in the exponential term. For instance, one reason interstitial diffusion is generally much faster than substitutional diffusion is that G_v for interstitial diffusion is zero. G_v represents the probability that a site for the atom to jump into exists. For substitutional diffusion, a jump requires a vacant site, but sites for interstitial diffusion are always plentiful.

G_m is the energy required for an atom to overcome the barriers to motion. This energy has both chemical and physical components. The chemical component relates to the bonding of the atom. Bonding can be ionic, covalent, metallic or a mixture of types. An additional chemical factor is the chemical potential gradient which is the driving force for diffusion. The physical component is based on structural considerations which include both the lattice structure and the grain structure of the material.

The observations of fast diffusion in intermetallics can be rationalized through consideration of these chemical and physical factors. However, the interactions of these factors are complex and not well understood. A single factor can not be separated from all the other factors affecting diffusion and alone be used to predict diffusion rates. Thus, it is difficult to develop hypotheses that are encompassing. Warburton and Turnbull[43] propose a complex interstitial mechanism as an explanation of fast diffusion in certain systems. However, their hypothesis is not unique in explaining fast diffusion.

In Section 3.1, the chemical influences on diffusion in intermetallics are discussed. The effects of both bonding and chemical potential gradient are explored. Warburton's and Turnbull's hypothesis for explaining fast diffusion is evaluated in terms of bond character. Section 3.2 explores the effect of structural considerations on diffusion. In Section 3.3, the factors that affect diffusion in intermetallics are summarized, and their applications are discussed.

3.1 Chemical factors

3.1.1 Bonding

There are three general types of bonding: metallic, covalent, and ionic. These three types of bonding are not independent but are a part of a continuous spectrum of bond character. Bonding in a particular compound is often not purely one type or another but a combination of types. Two main indicators of bond character are the heat of formation of a compound and the electronegativity difference between the components of the compound. Intermetallic compounds generally have metallic bonding. However, within the realm of metallic bonding, bonding in an intermetallic can have some degree of covalent, or even ionic, character.

Bonding affects diffusion by influencing the mobility of the atoms. If the bonds in a material are strong, the atoms will be less mobile; if the bonds in a material are weak or delocalized, the atoms will have more mobility. However, analyzing the effects of the different types of bonding on diffusion is more complicated than only looking at the strength of the bond. Different types of bonding have different diffusion characteristics. Metallic bonding is delocalized and requires that the atoms be about the same size. Thus, substitutional diffusion is favored. In covalent bonding, the electrons involved in the bond are shared by the atoms. This arrangement greatly restricts the mobility of the atoms. In ionic compounds, charge considerations are important in determining mobility. Impurity concentration can have a great effect on diffusion rates by adjusting the vacancy concentration which also affects the charge distribution. In general, diffusion in a material with metallic bonding is faster than diffusion in a covalently bonded material. Diffusion in an ionic compound varies systematically with the concentration of extrinsic vacancies. Thus, knowing the bond character in a material can supply some indication of the diffusion in that material.

3.1.1.1 Heat of formation and electronegativity

As discussed in Section 2.1, bond strength and character can be correlated with the heat of formation, ΔH_f. Ionic bonds have large negative values for ΔH_f. Metallic bonds have small values of ΔH_f. Along with ΔH_f, electronegativity difference also can indicate the bond character. Ionic compounds have large electronegativity differences while metallically bonded phases have very small differences. In a covalent compound, the electronegativity difference is larger than that for a metallic bond and smaller than that for an ionic bond. For example, using Pauling's electronegativity scale,[44] the electronegativity difference for NaCl, an ionic compound, is 2.23. For Ag_3Sn, which has metallic bonding, the difference in electronegativities is 0.03, and for the covalent compound, Si_3N_4, the electronegativity difference is 1.14.

In Figure 3.3, many intermetallic compounds are plotted along with several ionic and covalent compounds as a function of heat of formation and electronegativity difference on Pauling's scale. Three regions corresponding to the three main types of bonding are clearly defined. The compounds with metallic bonding, the intermetallics, are all clustered in the lower left corner with both small heats of formation and small electronegativity differences. The ionic compounds are found in the upper right corner with large heats of formation and large electronegativity differences. The covalent compounds are in the middle.

Robinson and Bever[10] developed a plot for intermetallic compounds which combines electronegativity difference, heat of formation, atomic or ionic radii, and the bond character. Their plot is shown in Figure 3.4. The electronegativity scale they use is the Gordy and Thomas scale,[45] and the radii are based on the Goldschmidt atomic diameters.[46] Bonding in intermetallic phases is primarily metallic. However, within metallic bonding there is a range of bond character. Robinson's and Bever's plot indicates the secondary character of the metallic bond in an intermetallic.

In Figure 3.5, Robinson's and Bever's figure is shown with some intermetallic compounds plotted on it along with two covalent compounds, Si_3N_4 and AlN, and two ionic compounds, NaCl and CsCl. The systems which contain intermetallic compounds mentioned at the start of this chapter as having fast diffusion all fall in the lower left corner indicating they have metallic or mixed ionic-covalent-metallic bonding: (f) copper-tin, (a) copper-zinc, and (b) silver-zinc. The indium containing systems (c, d and e) in which Roman[16] observed fast isothermal solidification, are also found in this corner.

Some correlation, then, seems to exist between metallic bonding and fast diffusion in intermetallics. A correlation between metallic bonding and fast diffusion is logical. Metallic bonding is characterized by delocalized electrons. This non-directional bonding allows the atoms more mobility than a covalent bond.

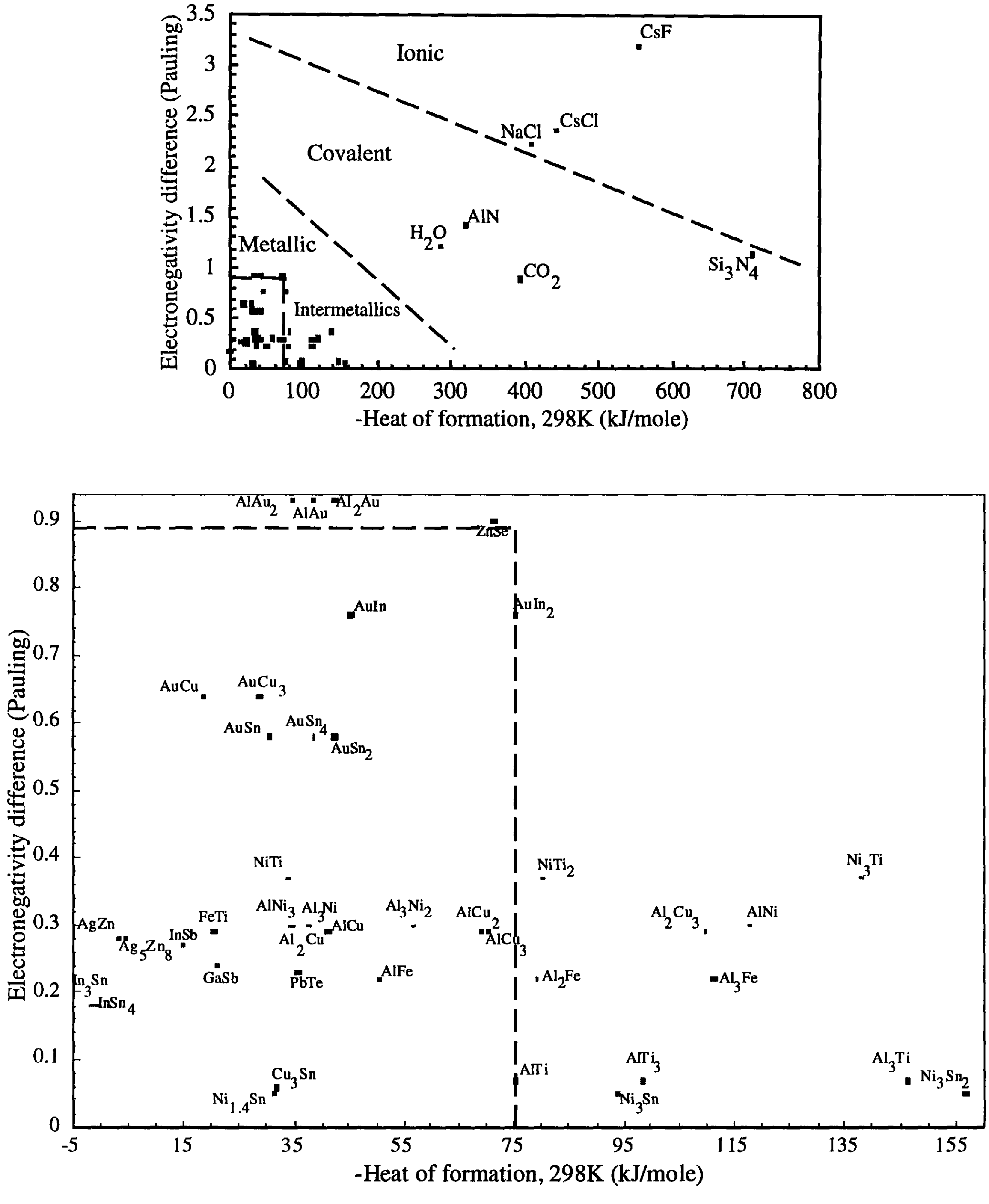

Figure 3.3: Compounds plotted as a function of heat of formation[10,11,47] and electronegativity difference.[44] Three regions corresponding to the three types of bonding are defined. All the intermetallic compounds are found in the metallic bonding region. The dashed box indicates the region in which Massalski and Pops[48] say the intermetallics exhibit metallic bonding.

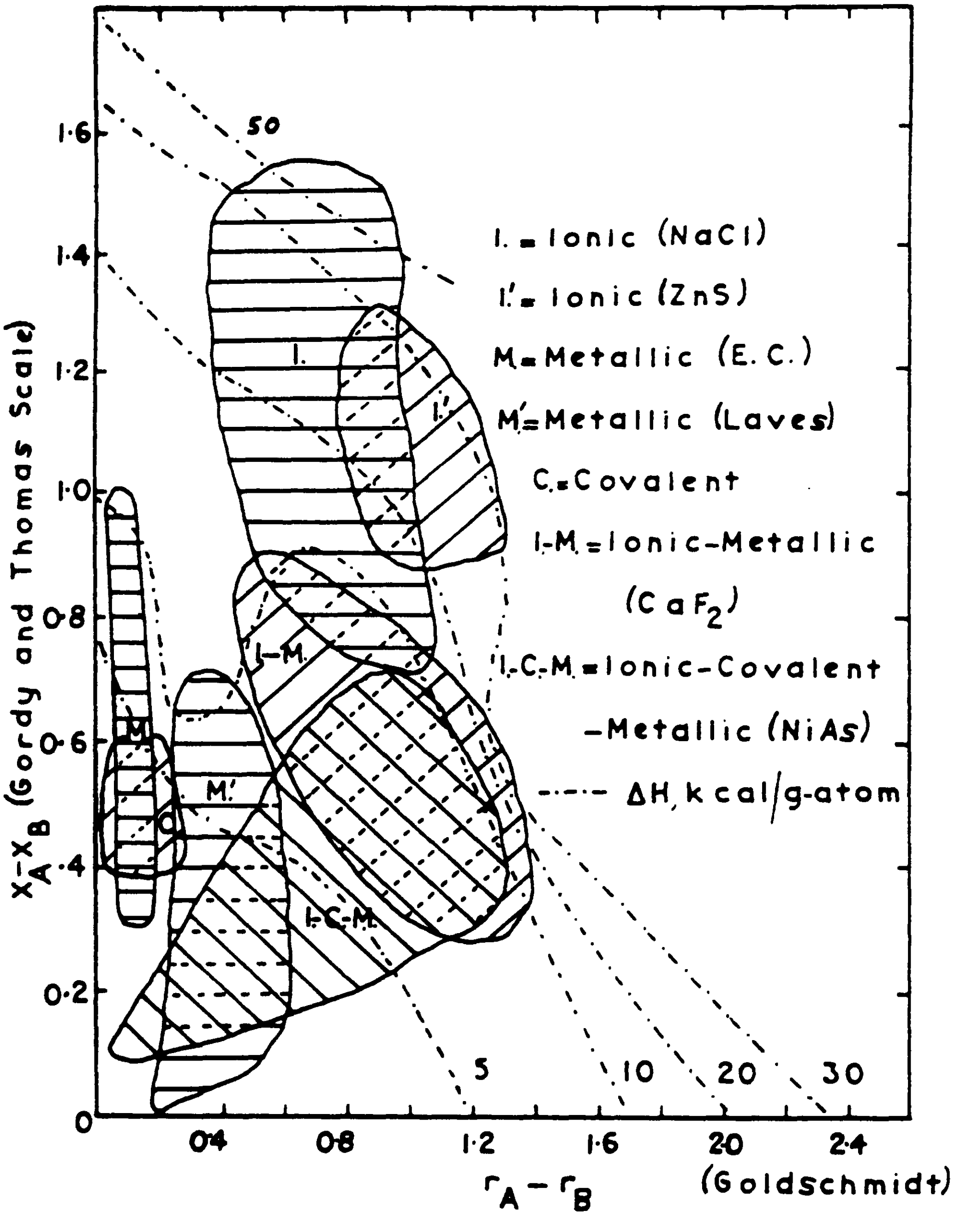

Figure 3.4: Robinson's and Bever's plot[10] of bond character in intermetallic compounds in terms of electronegativity difference and atomic or ionic radii. Used with permission.

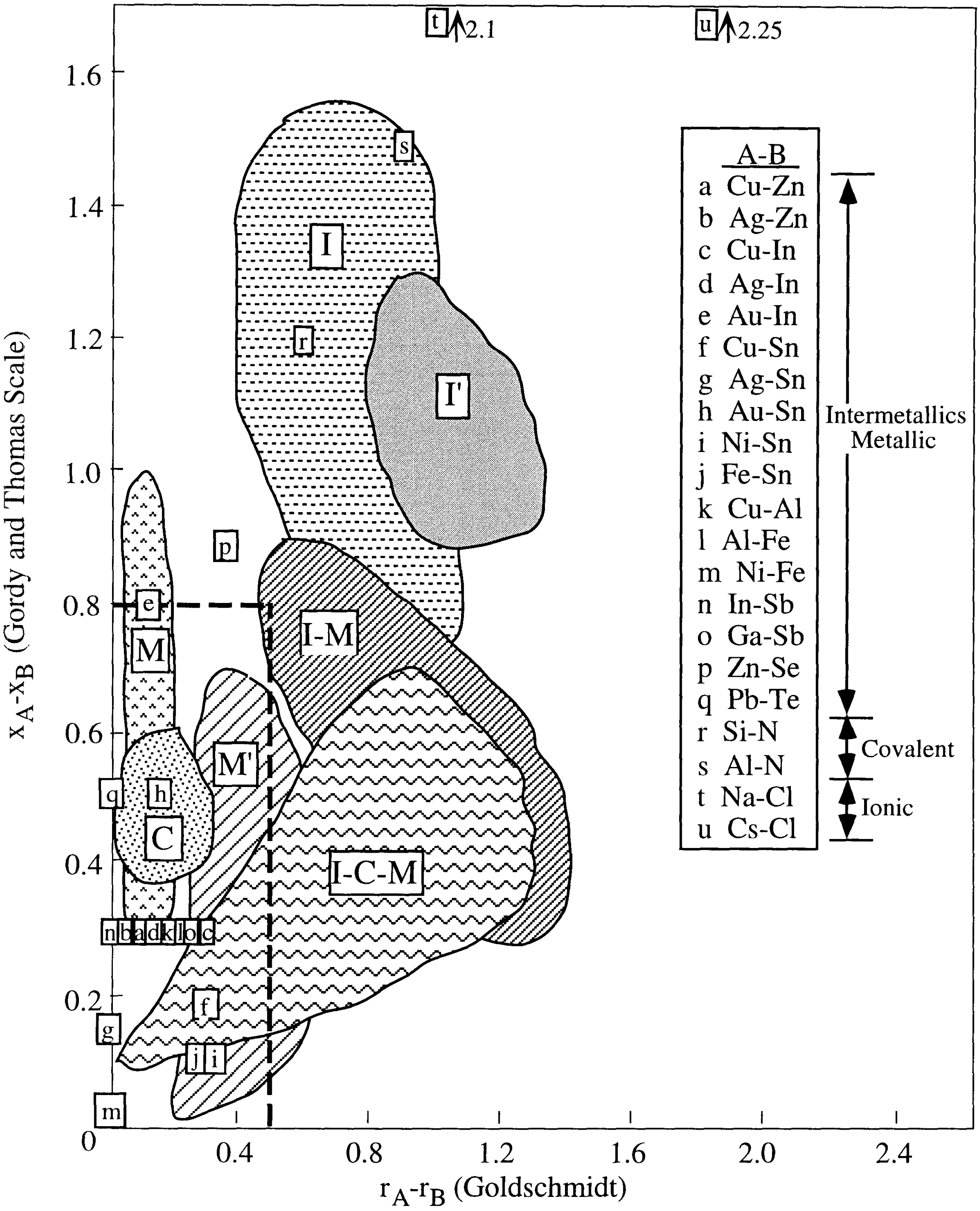

Figure 3.5: Robinson's and Bever's[10] plot of bond character in intermetallic compounds in terms of electronegativity difference and atomic or ionic radii with the location of several intermetallic compounds indicated. Two covalent, Si_3N_4 and AlN, and two ionic compounds, NaCl and CsCl, are included for reference. The dashed box indicates the region in which the intermetallics Massalski and Pops[48] say have metallic bonding would be found.

3.1.1.2 Warburton's and Turnbull's fast diffusion

An example of the degree to which bonding affects diffusion can be drawn from Warburton's and Turnbull's[43] work on fast diffusion. The fast diffusion that Warburton and Turnbull describe is characterized by diffusion of one metal into another at rates up to five orders of magnitude faster than self diffusion in that metal. Warburton and Turnbull develop a complex interstitial mechanism to explain these fast diffusion phenomena. The fast diffusion systems Warburton and Turnbull discuss are listed in Table 3.1. All the systems in which they try to explain the fast diffusion also appear in a table compiled by Massalski and Pops[48] listing systems in which the intermediate phases tend to have metallic bonding. Additionally, the system of germanium in silver, mentioned by Warburton and Turnbull as exhibiting fast diffusion but not fitting their interstitial hypothesis, also appears in the metallic bonding chart. Massalski's and Pops' compilation of systems exhibiting metallic interactions is shown in Table 3.2.

Table 3.1: The systems exhibiting fast diffusion, after Warburton and Turnbull[43]

Cu in Pb	Ag in In
Ag in Pb	Au in In
Au in Pb	Ag in Tl
Cu in Sn	Au in Tl
Ag in Sn	Ge in Ag
Au in Sn	

Table 3.2: Systems (A-B) with intermetallic compounds that have metallic bonding, after Massalski and Pops[48]

A	B			
Cu	Zn	Ga	Ge	As
Ag	Cd	In	Sn	Sb
Au	Hg	Tl	Pb	Te

Tables 3.3 and 3.4 list the Goldschmidt radii and the electronegativity on both the Pauling and the Gordy and Thomas scales for the elements in Massalski's and Pops' table. The largest size difference is 0.47 (Cu-Te) and the largest electronegativity difference on the Gordy and Thomas scale is 0.8 (Au-Zn, -Cd, -Ga, -In, or -Tl). These limits are indicated on Robinson's and Bever's plot in Figure 3.5 by the dashed box. All the systems would fall in the lower left corner where the bond character is mainly metallic. Thus, Massalski's and Pops' and Bever's and Robinson's conclusions on systems which exhibit purely metallic bonding are consistent.

Table 3.3: Goldschmidt radii[46] of the elements listed in Massalski's and Pops' table

A	B			
Cu 1.28	Zn 1.37	Ga 1.35	Ge 1.39	As ≈1.5
Ag 1.44	Cd 1.52	In 1.57	Sn 1.58	Sb 1.61
Au 1.44	Hg 1.55	Tl 1.71	Pb 1.75	Te ≈1.75

Table 3.4: Electronegativities on Pauling's scale[44] and on the Gordy and Thomas scale[45] (in parenthesis) of the elements listed in Massalski's and Pops' table.

A	B			
Cu 1.90 (2.0)	Zn 1.65 (1.5)	Ga 1.81 (1.5)	Ge 2.01 (1.8)	As 2.18 (2.0)
Ag 1.93 (1.8)	Cd 1.69 (1.5)	In 1.78 (1.5)	Sn 1.96 (1.8)	Sb 2.05 (1.8)
Au 2.54 (2.3)	Hg 2.00 (1.8)	Tl 2.05 (1.5)	Pb 2.33 (1.6)	Te 2.1 (2.1)

Tables 3.5 and 3.6 list the heats of formation of some of the intermetallic phases that form between the elements listed in Massalski's and Pops' table of systems which contain intermetallics with metallic bonding. The largest $-\Delta H_f$ is 75.4 kJ/mole ($AuIn_2$), and the second largest is 45.2 kJ/mole (AuIn). From Table 3.4, the largest electronegativity difference on the Pauling scale is 0.89 (Au-Zn). The range defined by these limits is well within the metallic corner of Figure 3.3 as shown by the dashed box on that figure. Thus, Massalski's and Pops' table of metallic systems is consistent with the data presented here.

Table 3.5: Heats of formation[10,11,47] of some of the intermetallic compounds formed between copper and the B elements in Massalski's and Pops' table.

A	**B:** Intermetallic, ΔH_f (kJ/mole)			
Cu	Zn	Ga	Ge	As Cu_3As: -11.7
	Cd Cu_2Cd_3: -23	In	Sn Cu_3Sn: -31.8	Sb Cu_2Sb: -11.7 Cu_3Sb: -8
	Hg	Tl	Pb	Te Cu_2Te: 20.9

Table 3.6: Heats of formation[10,11,47] of some of the intermetallic compounds formed between silver or gold and the B elements in Massalski's and Pops' table.

A	**B:** Intermetallic, ΔH_f (kJ/mole)			
	Zn	Ga	Ge	As
Ag	Cd AuCd: -38.9	In AuIn: -45.2 $AuIn_2$: -75.4	Sn AuSn: -30.5 $AuSn_2$: -42.5 $AuSn_4$: -38.7	Sb $AuSb_2$: -10.9
Au	Hg	Tl	Pb $AuPb_2$: -6.3	Te AgTe: -37.2

All the systems in which Warburton and Turnbull try to explain fast diffusion also have metallic bonding. Metallic bonding in a compound is indicated by a combination of low $-\Delta H_f$, small electronegativity difference, and small size difference. Perhaps the complex interstitial mechanism for fast diffusion that Warburton and Turnbull hypothesize is unnecessary. Fast diffusion can, instead, be related to these basic characteristics of the materials.

3.1.2 Chemical potential

Chemical potential is indirectly related to bonding in that they both deal with the chemical interactions of the atoms in a material. The chemical potential is the link between the thermodynamics and the kinetics of a material. The chemical potential gradient is the true driving force for diffusion. The diffusion coefficient is proportional to the derivative of the chemical potential with respect to concentration. Thus, analyzing this derivative of the chemical potential in intermetallics can help in understanding fast diffusion.

Specifically, this analysis enables the separation of the thermodynamic and the physical influences on diffusion. The thermodynamic influences are represented by the derivative of the chemical potential with respect to concentration, and the physical influences are contained in the mobility. Together, the derivative of the potential and the mobility make up the diffusion coefficient as shown in Equation 3.3.

In this section, the derivatives of the chemical potential with respect to concentration for intermetallic phases that exhibit fast diffusion, CuZn and Cu_5Zn_8, are compared to the derivative in an intermetallic that does not have fast diffusion, FeAl. Then, using published data on the diffusion coefficient in these three intermetallics, the mobility coefficient is calculated from the derivative of the chemical potential. As would be expected, the intermetallics with fast diffusion have higher mobilities than the intermetallic that does not show fast diffusion.

The chemical potential is related to the activity

$$\mu_i = \mu_o + RT\ln a_i \tag{3.9}$$

where μ_o is the chemical potential of the pure material, R is the gas constant, T is temperature, and a_i is the activity of the species i. Since μ_o is not a function of composition, the derivative of the chemical potential with respect to composition is a function of the activity and of temperature:

$$\frac{\partial\mu_i}{\partial c_i} = \frac{RT\partial(\ln a_i)}{\partial c_i} = \frac{RT}{a_i}\frac{\partial a_i}{\partial c_i} \tag{3.10}$$

Activity data is published in standard tables for some systems.[49] Often, the only data is for the phase boundaries. A relationship for the activity as a function of composition can be determined by assuming that the activity is linear with composition. Thus, a simple equation for a_i as a function of c_i can be determined, and $\partial a_i / \partial c_i$ is a constant:

$$\begin{gathered} a_i = mc_i + b \\ \frac{\partial a_i}{\partial c_i} = m \end{gathered} \tag{3.11}$$

For a given temperature, *m* and *b* are constants which are determined from fitting the activity versus composition data to Equation 3.11. Appendix A shows that this approximation is adequate for intermetallic phases.

Intermetallic layers have only small concentration gradients across them because they have a limited range of composition over which they are stable. However, large chemical potential gradients can exist. If the gradient of chemical potential is steep, a large diffusion coefficient and high flux are possible. The hypothetical phase diagram and chemical potential plot in Figure 3.6 illustrate a large difference in chemical potential across an intermetallic layer that has only a small variation in concentration.

Since the flux is proportional to the spatial gradient of the chemical potential, the thickness of the intermetallic layer is also important. Assuming equilibrium at the interfaces between the intermetallic and the base metal, the concentrations and the chemical potentials at the interfaces are fixed. The width of the intermetallic layers determines the steepness of the chemical potential gradient. A thin layer will have a steeper gradient, and thus faster diffusion, than a thick one.

Figures 3.7, 3.8 and 3.9 show the activity as a function of composition for three systems which contain intermetallic phases: the copper-zinc system, the aluminum-nickel system, and the iron-aluminum system. The derivative of the activity is proportional to the derivative of the chemical potential so some indication of the derivative of the chemical potential can be gleaned from these activity plots. Large changes in the activity are seen in several of the intermetallic phases. For instance, the activity of zinc varies from 0.107 to 0.585 in γ-Cu_5Zn_8. The activity of nickel goes from 0.000379 to 0.637 in AlNi, and the activity of aluminum drops from 0.712 to 0.145 in $FeAl_3$.[49]

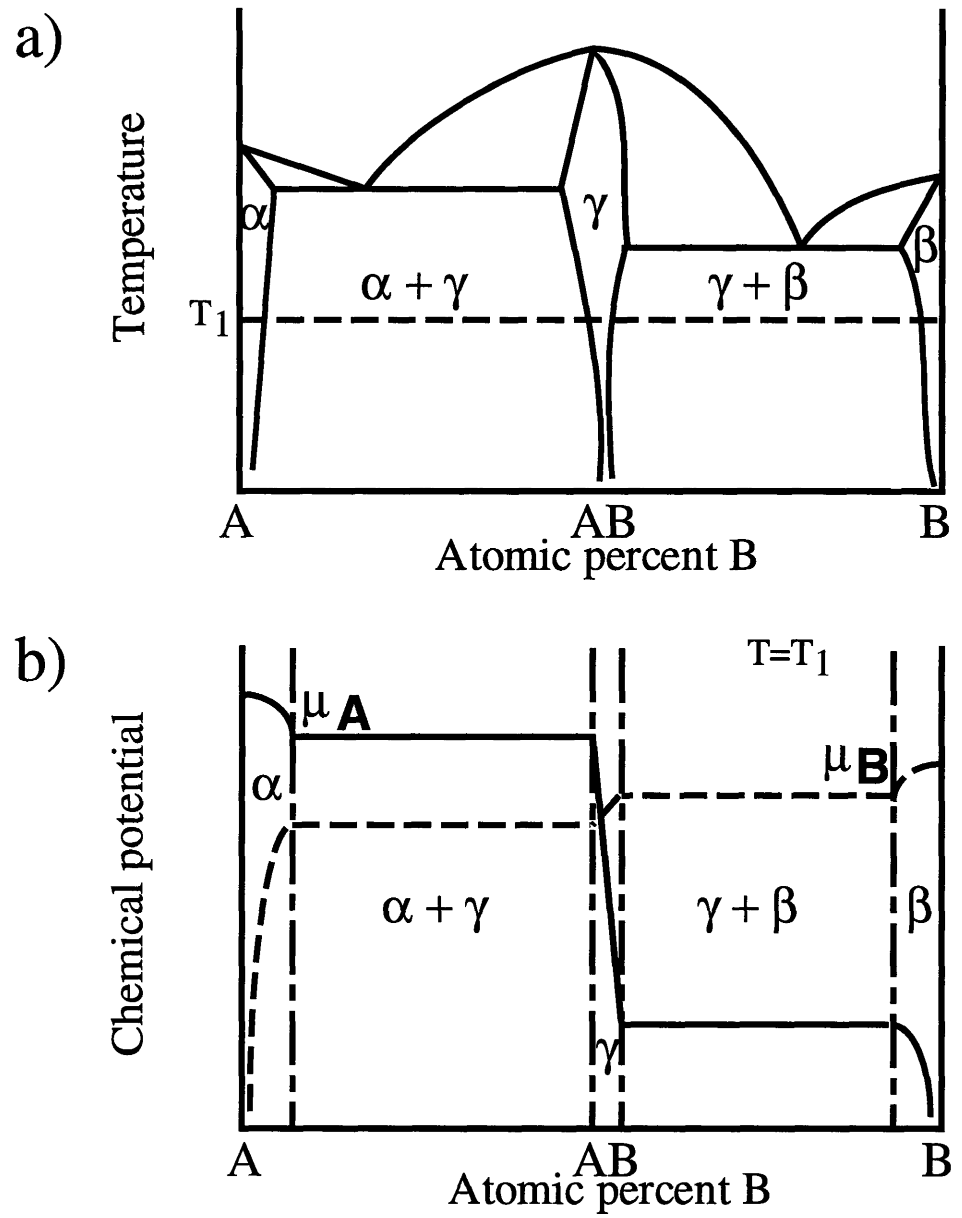

Figure 3.6: The difference in concentration across the intermetallic phase, γ, is small compared to the difference in the chemical potential. (a) Hypothetical phase diagram with an intermetallic phase, γ. The temperature T_1 is indicated with the dashed line. (b) Plot of the chemical potential as a function of composition for the system defined by the phase diagram in (a) at T_1.

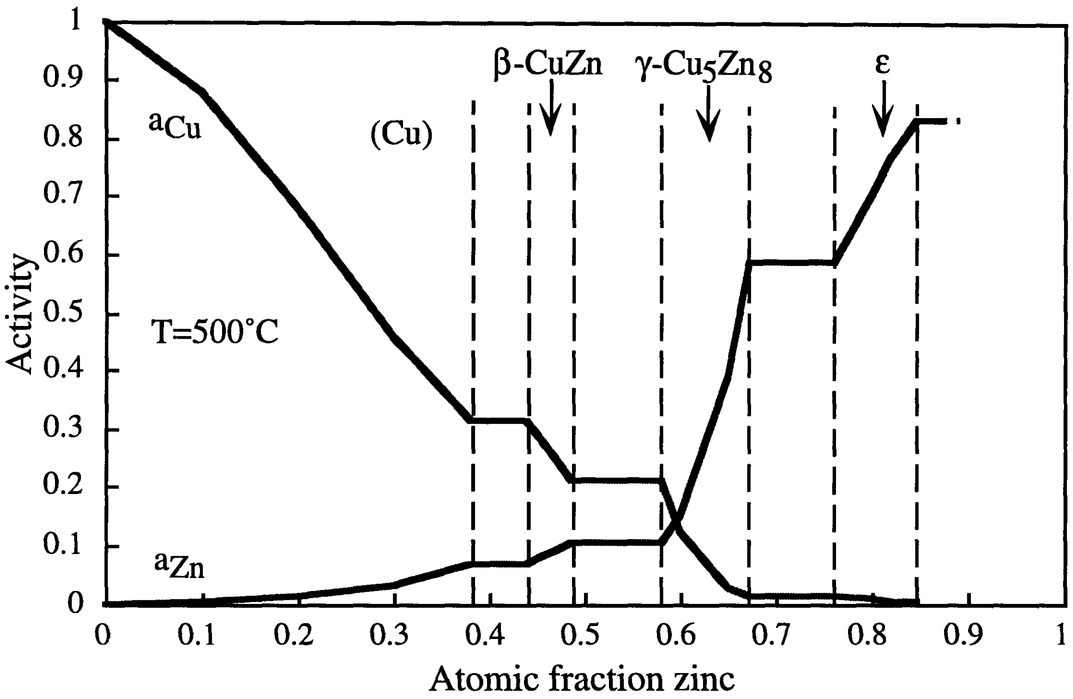

Figure 3.7: Activities of copper and zinc at 500°C as a function of atomic fraction of zinc.[49]

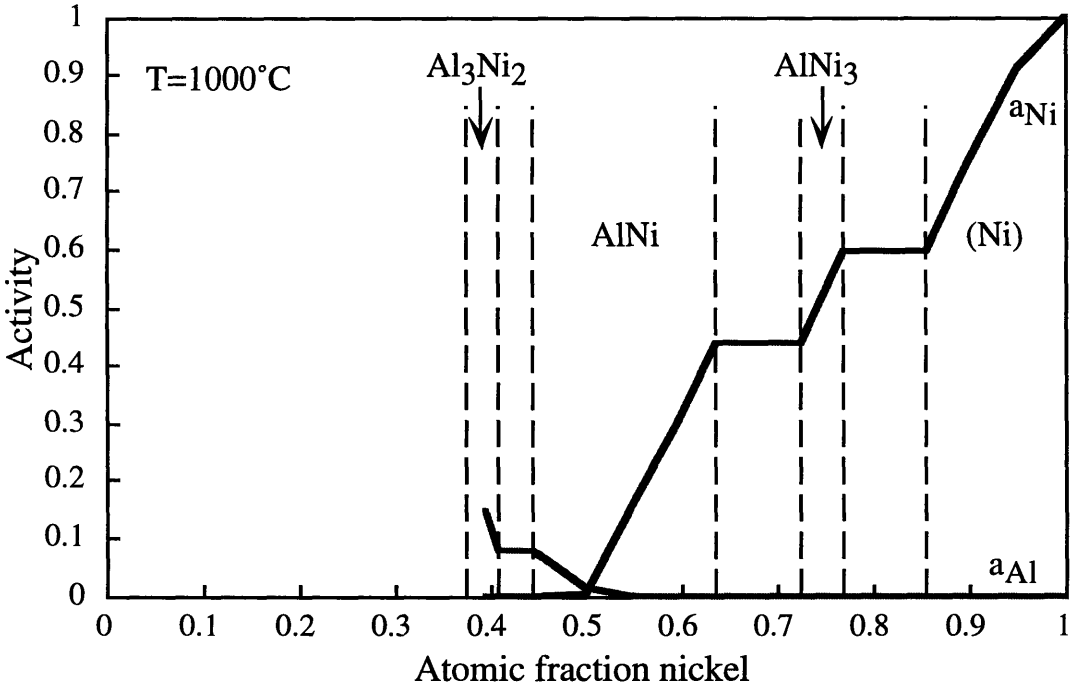

Figure 3.8: Activities of aluminum and nickel at 1000°C as a function of atomic fraction of nickel.[49]

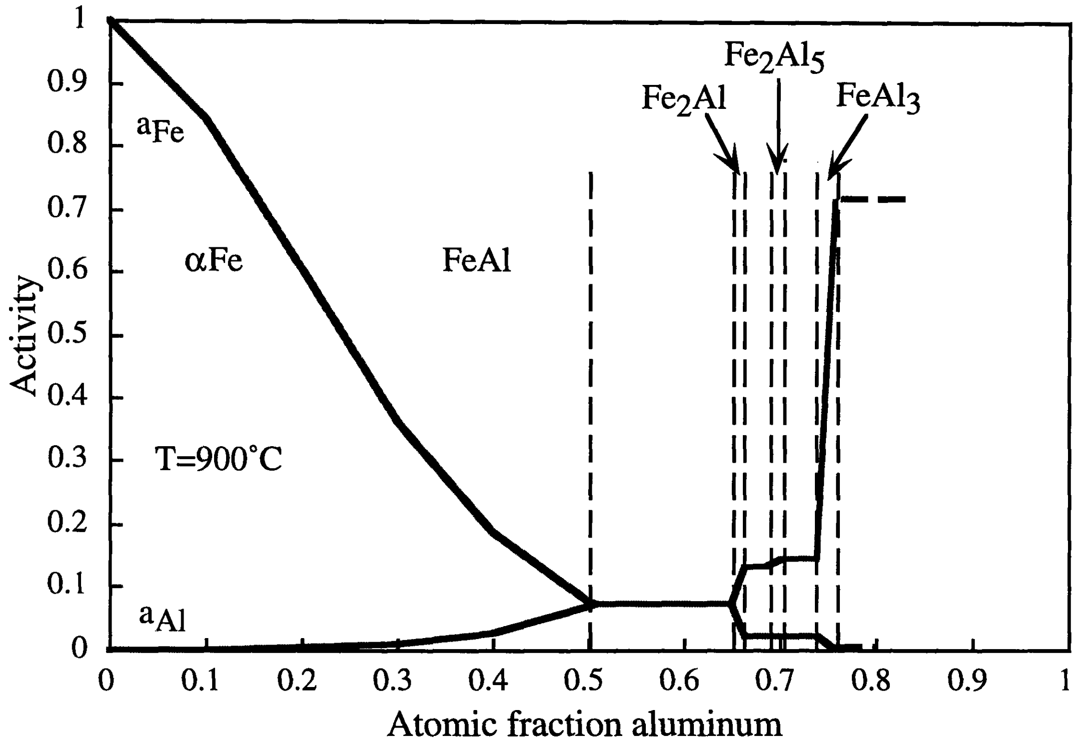

Figure 3.9: Activities of aluminum and iron at 900°C as a function of atomic fraction of aluminum.[49]

Based on the activity data shown in Figures 3.7-3.9, the derivative of the chemical potential with respect to composition can be calculated from Equation 3.10. Such a calculation was done for the β-CuZn, the γ-Cu_5Zn_8, and the β-FeAl intermetallic phases. These three phases were chosen because fast diffusion has been reported in the copper-zinc intermetallics but not in the iron-aluminum ones. The resulting equations for the derivative of chemical potential have the form

$$\frac{\partial \mu_i}{\partial c_i} = \frac{RTm}{mc_i + b} \tag{3.12}$$

based on the form of the activity as a function of composition given in Equation 3.11. The values of the constants for each intermetallic phase are given in Table 3.7. The chemical potential derivatives are plotted as a function of composition in Figure 3.10

Table 3.7: Constants for the equations for the derivatives of the chemical potential

Intermetallic	Temperature	Element, *i*	*m*	*b*
β-CuZn	500°C	Cu	0.0330	-0.863
		Zn	0.0124	-0.289
γ-Cu_5Zn_8	500°C	Cu	0.0340	-0.714
		Zn	0.0795	-2.95
β-FeAl	900°C	Fe	0.0301	-0.780

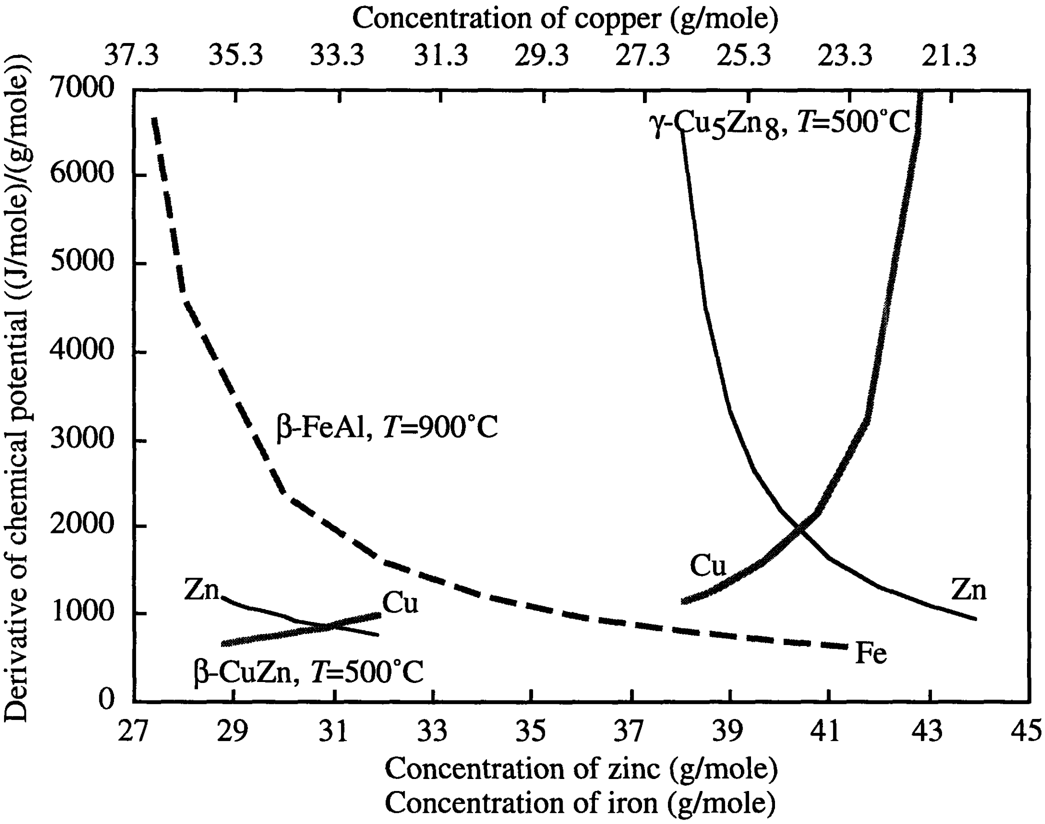

Figure 3.10: Derivative of the chemical potential with respect to concentration for zinc and copper in the β-CuZn and the γ-Cu_5Zn_8 intermetallic phases at 500°C and iron in the β -FeAl intermetallic at 900°C. From Equation 3.12 with data from Table 3.7.

The derivatives of the chemical potential are about the same order of magnitude for all three of these intermetallics. This indicates that the thermodynamic contribution to the diffusion coefficient is approximately equal in each intermetallic. However, the diffusion coefficients are not comparable. As shown by the data in Table 3.8, the copper-zinc intermetallics have much higher diffusion coefficients than the iron-aluminum intermetallic at similar reduced temperatures. Recall that the diffusion coefficient is a function of the derivative of the chemical potential and the mobility coefficient (Equation 3.3):

$$D_i = M_i \frac{\partial \mu_i}{\partial c_i}$$

Since the derivatives of the chemical potential are approximately equal, the differences in the diffusion coefficients must be in the mobilities.

If the derivative of the chemical potential and the diffusion coefficient is known for a phase, then the mobility coefficient can be calculated from Equation 3.3. For CuZn, Cu_5Zn_8, and FeAl, the chemical potential derivatives were calculated above, and the diffusion coefficients were found in the literature.[40] Thus, the mobility coefficient can be calculated from

$$M_i = D_i \frac{1}{\frac{\partial \mu_i}{\partial c_i}} = D_i \frac{mc_i + b}{RTm} \tag{3.13}$$

Table 3.8 summarizes the data used for the mobility calculations along with the data from Table 3.7. The mobility coefficients are graphed in Figures 3.11.

The mobility of iron in the FeAl intermetallic is two to three orders of magnitude smaller than the mobility of copper or zinc in the copper-zinc intermetallics. The large difference in the mobilities reflects the difference in the diffusion coefficients. However, the mobility does not include thermodynamic effects, represented by the derivative of the chemical potential, which are included in the diffusion coefficient.

Table 3.8: Data for the calculation of the mobility coefficients

Intermetallic	Temp.	T_m/T	Element, *i*	D (cm²/s)[40]
β-CuZn	500°C	1.49	Cu	1.7×10^{-8}
			Zn	6.6×10^{-9}
γ-Cu_5Zn_8	500°C	1.38	Cu	2.67×10^{-8}
			Zn	2.46×10^{-7}
β-FeAl	900°C	1.31	Fe	3.0×10^{-11}

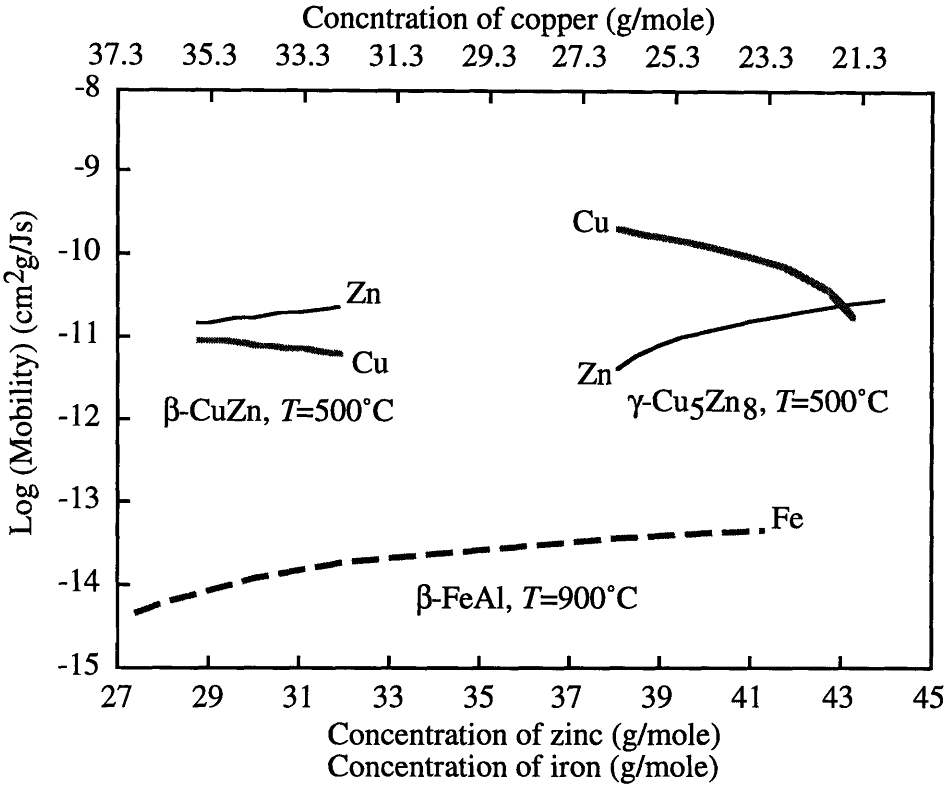

Figure 3.11: Mobility as a function of composition in β-CuZn and γ-Cu_5Zn_8 for 500°C and in β-FeAl for 900°C.

None of the chemical or physical factors discussed in this work would predict such a large difference in mobilities between the copper-zinc intermetallics and the iron-aluminum one. The electronegativity differences and the size differences for these two systems are about the same, as shown in Table 3.9, so the bonding argument does not provide any insight into this difference in mobilities. Structural considerations, which will be discussed in the next section, also are of no help in explaining the difference in the mobilities. The structures of all three of these intermetallic phases are derivatives of the body-centered cubic structure.[40] The inability to rationalize the difference in the mobilities shows the limits of analysis based on these factors and illustrates why an integrated hypothesis to explain rapid diffusion is difficult to develop.

Table 3.9: Comparison of the data on β-CuZn, γ-Cu_5Zn_8, and β-FeAl

Intermetallic	Electronegativity difference (Pauling)[44]	Goldschmidt radii[46] difference	Structure[40]
β-CuZn	0.25	0.099	BCC
γ-Cu_5Zn_8	0.25	0.099	BCC
β-FeAl	0.22	0.155	BCC

The three intermetallic phases analyzed above may not be representative of the majority of intermetallic phases. The temperature of the copper-zinc data is 500°C, which is above the critical temperature for β-CuZn, so this phase might be more similar to a disordered solid solution than an intermetallic at this temperature. FeAl and Cu_5Zn_8 have broader ranges of composition than the typical intermetallic compound. The effect of the width of composition range on chemical potential and activity is shown in Figure 3.12 in terms of the free energy curves.

The free energy curve for a intermetallic compound with a narrow range of composition has greater curvature than the curve for a compound with a broader range of stable compositions. The chemical potential is determined by the tangent to the free energy curve. The activity corresponds to the difference between this chemical potential and the chemical potential of the standard state. When the free energy curve is sharper, Figure 3.12(a), the tangent rotates more rapidly with changes in composition than when the free energy curve is flatter, Figure 3.12(b). Thus when the range of composition is wider, the chemical potential and activity are not as strong a function of the composition as they are for a narrow intermetallic. For a narrow intermetallic compound, the chemical potential and activity undergo large changes over a small range of concentration. This makes the chemical potential and activity difficult to measure and may be the reason little data on activity in intermetallic compounds exist.

For calculation of the mobility, both the activity data and the diffusion coefficients are necessary. These data tend to be rare for intermetallics so the full analysis can be done for only a few intermetallics. The activity data for an iron-aluminum intermetallic, $FeAl_3$, which has a narrow range of composition over which is it stable, is available although the diffusion coefficient is not. The composition of $FeAl_3$ varies less than two atomic percent from the stoichiometric formula. The copper-zinc intermetallics and FeAl vary from six to twenty-five atomic percent from their basic formula. The derivative of the chemical potential with respect to concentration is graphed in Figure 3.13. The derivatives range from 10^4 to 10^5 (J/mole)/(g/mole) for both aluminum and iron. The derivatives of the chemical potential for $FeAl_3$ are about an order of magnitude larger than those found for the other intermetallic compounds analyzed (Figure 3.10). These larger values for the derivatives may be related to the smaller range of composition of $FeAl_3$ as discussed in conjunction with Figure 3.12.

Values for the diffusion coefficients of iron or aluminum in $FeAl_3$ are not well-established. As a gross approximation, the diffusion coefficient can be taken to be about that in FeAl, $\approx 10^{-11}$ cm^2/s. Thus, the mobility in $FeAl_3$ would be 10^{-15} to 10^{-16} which is an order of magnitude lower than the mobility in FeAl. This difference is due to the increase in the derivative of the chemical potential since the diffusion coefficient was assumed to be the same for both intermetallics. In reality, the diffusion coefficient may be even lower than 10^{-11} cm^2/s because $FeAl_3$ is a more ordered phase than FeAl and because the reduced temperature for $FeAl_3$ is slightly lower. The reduced temperature for $FeAl_3$ at 900°C is 1.22, compared to 1.31 for FeAl. A lower diffusion coefficient would mean that the mobility would be even smaller.

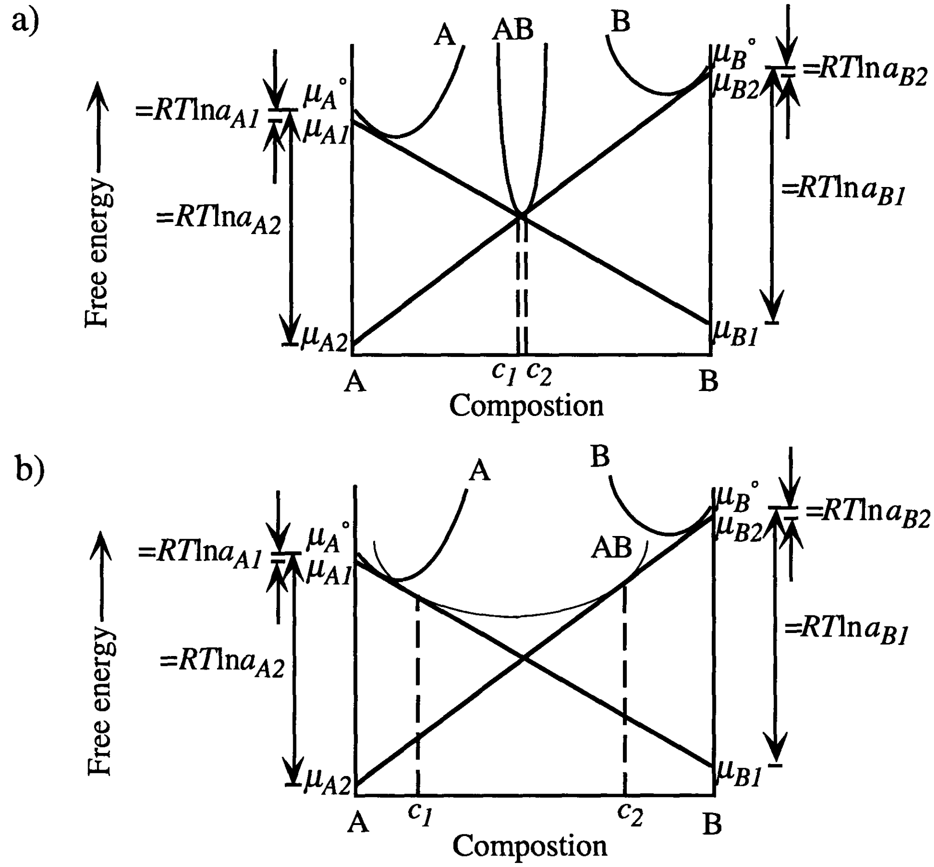

Figure 3.12: Comparison of the free energy curves for an intermetallic with (a) a narrow range of stable compositions and (b) a broad range of composition. The derivative of the chemical potential with respect to composition would be smaller for the intermetallic with the wider range of composition. The phases in this figure are taken from the hypothetical phase diagram in Figure 3.6.

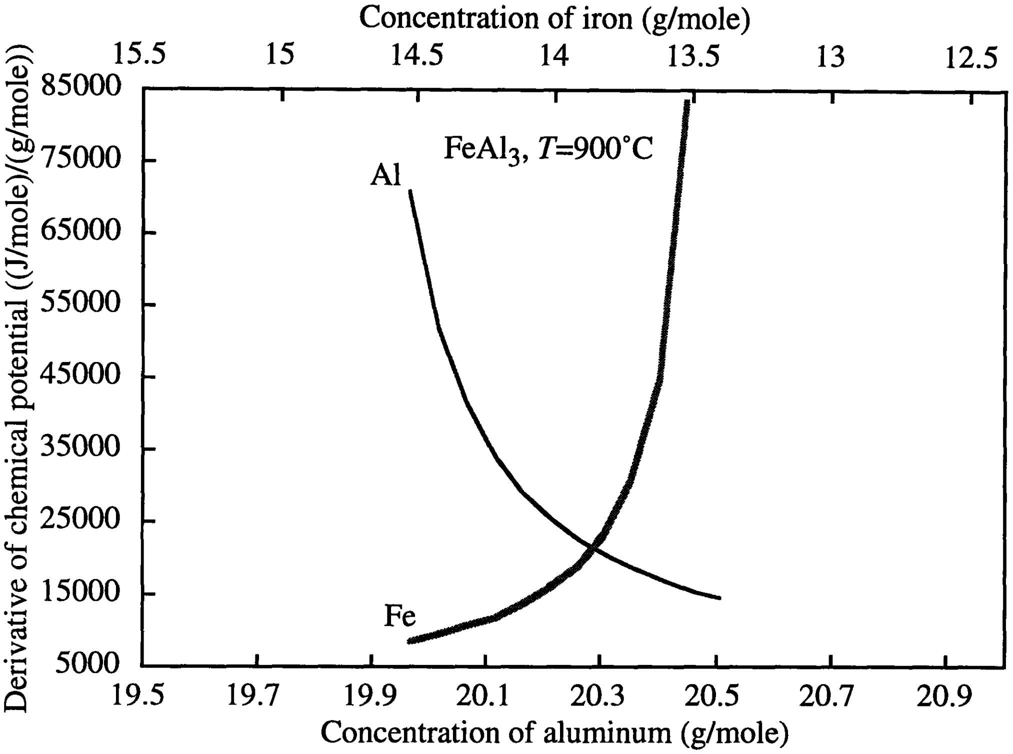

Figure 3.13: Derivative of the chemical potential with respect to concentration for iron and aluminum for the $FeAl_3$ intermetallic at 900°C. From Equation 3.12 with $m_{Fe} = 0.016$ and $b_{Fe} = -0.216$, and $m_{Al} = 1.051$ and $b_{Al} = -20.83$.

3.2 Physical factors

The physical factors that affect diffusion in intermetallics can be divided into three categories: crystal structure, grain boundaries, and interface structure. The crystal structure is a factor in determining the mobility of the atoms. The degree of stoichiometry and the concentration of defects are two other issues related to crystal structure which also affect diffusion. Grain boundaries provide low resistance paths for diffusion. Thus, grain boundaries can be an important factor in explaining fast diffusion in intermetallics. The structure of the interface between the intermetallic and the base metal affects the diffusion through the intermetallic layer. If the interface is rough, more area exists for exchange than if the interface is flat. Each of these influences is discussed in turn in this section.

3.2.1 Crystal structure

The crystal structures of intermetallics are often complex. This complexity tends to preclude close packing, leaving more free space in the lattice. As shown schematically in Figure 3.2, one of the contributions to the migration free energy has to do with moving the atom through the lattice pinch point. All other things being equal, if the atoms are farther apart, it is easier to move another atom through. Less energy would be required for the migration of the atom in a more open lattice, and the diffusion coefficient would be higher.

The defect structure is also important to diffusion. Generally, the more defects there are in a material, the higher the possible rate of diffusion. In intermetallics, the defect structure is often tied to the degree of stoichiometry of the material. Intermetallic phases are stable over a range of composition. Their structures have to accommodate this variation in composition. This accommodation is usually accomplished through defects; substitutional atoms, interstitials, or vacancies. These defects are built into the structure of the intermetallic. The examples that follow illustrate how these concepts relate to diffusion in intermetallics.

3.2.1.1 Copper-tin intermetallics

Copper and tin form two low temperature intermetallic phases, the ε (Cu_3Sn) and the η (Cu_6Sn_5) phases as shown in the phase diagram in Figure 2.5. Fast diffusion has been reported in both of these phases. The crystal structures of these intermetallics support the observations of fast diffusion because they are open and can have high concentrations of defects. These structures also illustrate how a lattice can adapt to fit a range of compositions.

The ε phase, Cu_3Sn, intermetallic has the Cu_3Ti-type lattice which has hexagonal close packing of the form AB,A....[50-53] The structure of the η phase, Cu_6Sn_5, intermetallic is based on the NiAs type lattice ($B8_1$) which is a modified close packed structure with ABAC,A... stacking. The tin is hexagonally close packed on the B and C sites, and the copper occupies the A sites which are the octahedral interstitials. The excess copper atoms are found on one tenth of the tetrahedral interstitial sites.[52-54] The information on the structures of both the ε and the η phases is summarized in Table 3.10.

Table 3.10: Structures of ε and η intermetallic phases

ε phase structure[50-53]	η phase structure[52-54]
a = 5.51 Å	a = 4.2 Å
b = 4.77 Å	b = a
c = 4.33 Å	c = 5.09 Å
Type: Cu_3Ti	Type: NiAs type with Cu on 1/10 of the tetrahedral interstitial sites
Structure symbol: -	Structure symbol: $B8_1$ (NiAs) with interstitials
Packing fraction: 0.78	Packing fraction: 0.61

The ε phase structure is a close packed structure which would indicate there is not much extra room for atom motion as is indicated by the packing fraction of 0.78. The packing fraction is the ratio of the volume of the atoms in the unit cell to the volume of the unit cell. The larger the packing fraction is, the less open space there is in the lattice. For hexagonal close packing of equal sized spheres, the packing fraction is 0.74. However, the copper atoms are 20% smaller than the tin atoms; the Goldschmidt radius of copper is 1.28 and of tin is 1.58. The lattice is close packed on the tin layers, but the copper layers have a reasonable amount of space between the atoms. This space is shown in the picture of the structure of Cu_3Sn in Figure 3.14. Additionally, there are open channels along the C sites in the close packing. The stacking sequence is AB,A... which leaves the C sites open in every layer.

Other considerations in the structure of the ε phase are the degree of stoichiometry and how variations in the stoichiometry are handled by the structure. The composition of this phase varies by about one atomic percent tin from the structure's standard 25 atomic percent tin. Since this phase has metallic bonding and a close packed structure, the composition is most likely maintained by the creation of vacancies or substitutional atoms rather than by the creation of interstitials. A one atomic percent variation in composition, from 25 atomic percent tin to 24 atomic percent tin, could translate into one vacancy for every 25 tin sites which is a high vacancy concentration. Recall that for substitutional diffusion, the probability a vacancy exists enters into the determination of the diffusion coefficient through the jump frequency (Equation 3.5). A high vacancy concentration would, then, serve to increase the diffusion coefficient.

Figure 3.14: Structure of the ε phase copper-tin intermetallic, Cu_3Sn. The lattice type is Cu_3Ti which has AB,A... hexagonal close packing. The yellow balls represent copper atoms, and the white ball are the tin atoms. The proper size ratio of copper to tin is maintained. Notice the space in the copper layer. Ni_3Sn also has this basic structure.

The η, Cu_6Sn_5, structure is based on the NiAs structure which has ABAC,A packing as shown in Figure 3.15. The tin layers are close packed on the B and C sites, but, as with Cu_3Sn, the copper layers on the A sites have some free space since the copper atoms are smaller than the tin atoms. This intermetallic has a low packing fraction, 0.61, which also indicates that there should be significant free space in this structure.

The basic NiAs structure does not account for the extra copper atoms in the formula Cu_6Sn_5. The excess copper atoms are placed on the tetrahedral interstitial sites. Putting the copper atoms on the interstitial sites expands the lattice. In Figure 3.15, the ordering of the copper and tin atoms in the NiAs structure is shown with the tetrahedral interstitial sites marked with small red balls. It can be seen how placing copper atoms (yellow balls) on the "red" sites would open up the lattice. Additionally, since the excess copper atoms occupy only one tenth of the tetrahedral interstitial sites, the other nine tenths of the sites would be available for diffusion.

Figure 3.15: Structure of the η phase copper-tin intermetallic, Cu_6Sn_5. The copper (yellow) and the tin (white) atoms are shown in the NiAs structure. The excess copper atoms would be located on one tenth of the tetrahedral interstitial sites indicated with the small red balls. The proper size ratio for copper to tin is used. Both Ni_3Sn_2 and FeSn also have structures based on NiAs.

The strain energy cost of putting a copper atom on an interstitial site is high. Thus, it is likely that the variation in composition of this intermetallic phase is accommodated by fewer copper interstitials for the case of excess tin and by tin vacancies or copper substitution on the tin sites for the case of excess copper. The phase diagram (Figure 2.5) indicates that the composition of the η phase tends to have excess copper rather than excess tin. An excess of copper would favor tin vacancies and the placing of copper atoms on tin sites. Thus, the defect concentration in the η phase intermetallic depends on composition.

The η phase intermetallic also illustrates how bonding and structure can be interrelated. In the NiAs structure, which is the basis for the Cu_6Sn_5 structure, an excess of the transition metal indicates primarily metallic interactions.[10] The η phase has an excess of copper, the transition metal, so, based on the structural argument, the bonding should be metallic. Metallic bonding in this system was indicated in the previous section as determined by chemical factors.

3.2.1.2 Nickel-tin intermetallics

The nickel-tin system has three low temperature intermetallic phases, Ni_3Sn, Ni_3Sn_2, and Ni_3Sn_4, as shown in the phase diagram in Figure 2.1. Table 3.11 summarizes the structures of the three low temperature nickel-tin intermetallics.

The structure of Ni_3Sn is hexagonal close packed with AB,A... stacking.[50,55,56] This structure is similar to that of Cu_3Sn. Since nickel atoms are about the same size as the copper atoms, the Cu_3Sn structure shown in Figure 3.14 can be used to describe this structure. Instead of the yellow balls representing copper atoms, they now represent nickel atoms. Free space exists in the nickel packing planes in Ni_3Sn just as it does in the copper packed planes in Cu_3Sn. The channels along the C sites can also be found in the Ni_3Sn structure. Ni_3Sn is stable over a slightly wider composition range than is Cu_3Sn so more vacancies or substitutional atoms could be induced by composition variations in Ni_3Sn as compared to Cu_3Sn.

Ni_3Sn_2 has the NiAs type structure[10] with excess nickel atoms. The structure of this nickel-tin intermetallic is very similar to that of Cu_6Sn_5. Thus, the Cu_6Sn_5 structure shown in Figure 3.15 can be used to visualize the structure of Ni_3Sn_2 with the white balls still representing tin, the yellow balls representing nickel, and one quarter of the "red" interstitial sites occupied by the excess nickel atoms. More of the interstitial sites are occupied in Ni_3Sn_2 than in Cu_6Sn_5 so the Ni_3Sn_2 lattice should be more distorted than the Cu_6Sn_5 one. Comparison of the packing fractions of these two intermetallics indicates that the increased lattice distortion in Ni_3Sn_2 leads to denser packing; the packing fraction for Ni_3Sn_2 is 0.76, while for Cu_6Sn_5 the packing fraction is 0.61.

The Ni_3Sn_4 intermetallic has the most complicated structure of the three nickel-tin intermetallics. It is monoclinic with the C2/m space group.[55,57] The structure is shown in Figure 3.16. The c axis is 5.18 Å long. The atomic radius of nickel is 1.25 Å. Thus, there is 2.68 Å between the nickel atoms along this axis. Similarly, along the b axis which is 4.05 Å long, there is 1.55 Å between the nickel atoms. These measurements indicate that there is some free space in this structure as confirmed by the packing fraction of 0.71.

Table 3.11: Structures of the low temperature nickel-tin intermetallics[55-57]

Ni_3Sn	Ni_3Sn_2	Ni_3Sn_4
a = 5.28 Å	a = 4.14 Å	a = 12.2 Å
b = a	b = a	b = 4.05 Å
c = 4.23 Å	c = 5.20 Å	c = 5.18 Å
Type: $D0_{19}$, AB,A...	Type: $B8_1$ (NiAs) with	Type: monoclinic
stacking	interstitials	β = 103°
	ABAC,A... stacking	
Space group: $P6_3/mmc$ (194)	Space group: Pnma (62)	Space group: C2/m (12)
Packing fraction: 0.70	Packing fraction: 0.76	Packing fraction: 0.71

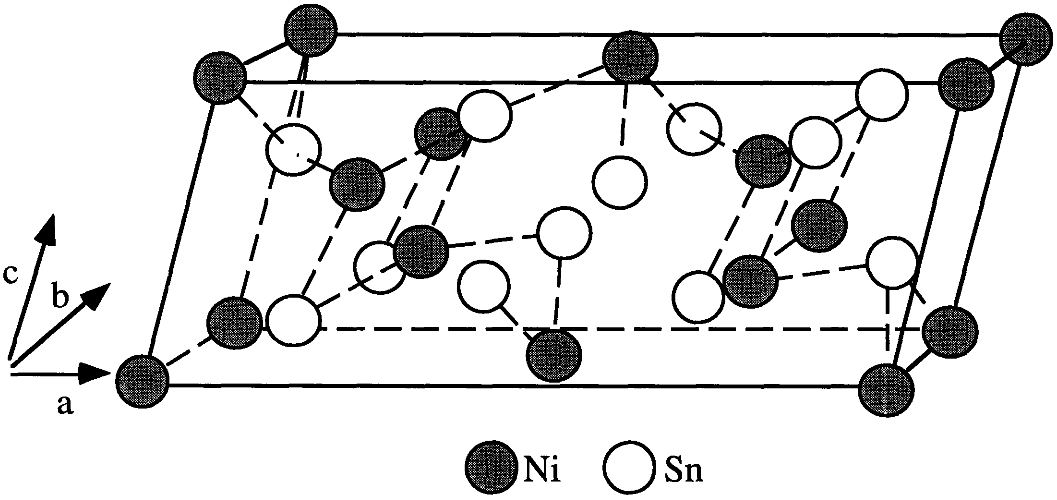

Figure 3.16: The structure of Ni_3Sn_4,[57] the intermetallic with the most complicated structure of the three low temperature nickel-tin intermetallics. This structure is monoclinic with the space group C2/m.

more mobility at the grain boundary due to the more open structure at the grain boundary so the rate of diffusion is higher.[60]

Grain boundary diffusion dominates at low temperatures. Grain boundary diffusion has a much lower activation energy than lattice diffusion because the grain boundary has a more open structure. Because the lattice diffusion has a higher activation energy, it is more sensitive to temperature. At high temperatures, volume diffusion overwhelms the grain boundary diffusion, and the apparent diffusion coefficient is determined by the volume diffusion coefficient. At low temperatures, volume diffusion diminishes leaving grain boundary diffusion to dictate the observed diffusion coefficient.[60]

The contribution of the faster grain boundary diffusion can be accounted for in the diffusion coefficient :[61]

$$D_{obs} = D_{vol} + fD_{gb} \tag{3.14}$$

where D_{obs} is the observed diffusion coefficient, D_{vol} is the volume, or lattice, diffusion coefficient, D_{gb} is the grain boundary diffusion coefficient, and f is a weighting factor. f is a function of the grain boundary width, a, and the grain size, d:

$$f = \frac{a}{d} \tag{3.15}$$

Grain boundaries can be abundant in the growing intermetallic layer as can be seen in Figure 3.17. The intermetallic layers usually form in fine columnar grains[53,62] oriented in the direction of diffusion. This grain structure results in a great number of grain boundaries also aligned in the direction of diffusion.

Figure 3.17: Micrograph of fractured intermetallic layers between copper and lead70-tin30 solder. The solder layer was selectively removed by chemical etching. Used with permission from ref. 63. (2500X)

An estimate of whether grain boundary contributions to diffusion are significant in intermetallics can be made by comparing D_{vol} and fD_{gb} with D_{obs}. To calculate f, the grain boundary width and grain size are needed. Grain boundaries are typically 5 x 10^{-8} cm in width. Estimates of the grain size can be based on micrographs from the literature. The grain size of the intermetallic formed between copper and electroplated and reflowed tin that was then aged for four days at 135°C is approximately 2.4 x 10^{-4} cm.[4] The value of f for this example is 2 x 10^{-4}. No data on D_{vol} or D_{gb} exist for the copper-tin intermetallic phases, but D_{gb} has been measured for tin in copper.[64] This value can be used as an estimate of D_{gb} in the intermetallic. D_{gb} (cm^2/s) for tin in copper is given by

$$D_{gb} = 0.1\exp\left[\frac{75\text{ kJ}}{RT}\right] \tag{3.16}$$

For T=135°C, the diffusion coefficient along the grain boundary is 2.5 x 10^{-11} cm^2/s. fD_{gb} would then equal 5 x 10^{-15} cm^2/s. The observed diffusion coefficient for the copper-tin intermetallic for this temperature can be read from Figure 2.11 to be about 10^{-12} cm^2/s. Thus, for this case, grain boundary diffusion is not significant.

Another grain size measurement was taken from a micrograph of the intermetallic layer resulting from aging a couple comprised of copper and electroplated tin for 25 days at 135°C.[63] This grain size was determined to be 4.7 x 10^{-4} cm. f for this case would be 1.1 x 10^{-4}, about the same as it was in the previous case. Since the temperature is the same as for the above example, the same values of D_{gb} and D_{obs} apply. Again, the grain boundary contribution to the overall diffusion coefficient would be negligible. However, it was assumed that D_{gb} in copper is comparable to D_{gb} in the intermetallics, and this assumption may not be valid.

3.2.3 Interface structure

The interface between the growing intermetallic and the base metal is not necessarily planar. Numerous micrographs in the literature[3,4,63,65] illustrate this fact as shown in Figures 3.18 and 3.19. Often, diffusion coefficients reported for intermetallic compounds are calculated from intermetallic growth measurements. This analysis assumes that the intermetallic layers are planar. The roughness of the interface, then, could introduce error into the calculation of the diffusion coefficient. The surface area available for diffusion at a rough interface can be two or more times greater than that at a flat one as shown by the calculation in Appendix B.

An increase in area of the interface would have more of an effect on the growth rate of the intermetallic layer if the growth were interface controlled. Most researchers assume

3.2.1.3 Iron-tin system

There are two low temperature intermetallic phases in the iron-tin system, FeSn and $FeSn_2$. Both of these intermetallic phases are line compounds with no range of composition.

The FeSn intermetallic has the NiAs structure ($B8_1$).[58] Unlike Cu_6Sn_5 and Ni_3Sn_2 which also both have the NiAs structure, FeSn has no excess of either species and no range of composition over which it is stable. Thus, FeSn has the NiAs structure shown in Figure 3.15 without any atoms on the "red" interstitial sites. Without the effect of the interstitial atoms, the FeSn lattice remains more close packed than the Cu_6Sn_5 and Ni_3Sn_2 lattices do. Consequently, there will be less free space in the FeSn structure. Additionally, since this phase is stoichiometric, no defects would be inherent to the structure to enhance the diffusion.

The structure of the $FeSn_2$ intermetallic is of the $CuAl_2$ type (C16).[58] As this compound is also stoichiometric, no composition-induced defects are established in this structure either.

3.2.1.4 Application of crystal structure analysis

Consideration of the crystal structure can help in understanding fast diffusion in intermetallics. The open lattices and high defect concentrations that can result from the lattices' accommodation of the composition ranges of intermetallic phases, support the existence of fast diffusion. Observed diffusion rates can be partially explained through analysis of the crystal structure. For example, fast diffusion has been reported in the copper-tin intermetallics. Diffusion in the nickel-tin intermetallics is slower than that in the copper-tin ones, and diffusion in the iron-tin intermetallic is much slower than that in the nickel-tin intermetallics. Since the iron-tin intermetallics are stoichiometric and lack the inherent defect structure that the copper- and nickel-tin intermetallics have, slower diffusion would be expected in the iron-tin intermetallics. However, less distinction can be made between the copper- and nickel-tin intermetallics based on crystal structure. Both systems have intermetallics with open structures and inherent defects. Thus, evaluation of the crystal structures can explain why diffusion in the iron-tin system is slow but it cannot rationalize the difference between the copper- and nickel-tin intermetallic.

3.2.2 Grain boundary effects

Grain boundaries are high diffusivity paths because the mean jump frequency at the grain boundary is much higher than the jump frequency in the lattice.[42] The atoms have that the growth of intermetallic layers is diffusion controlled. However, it will be shown later in this work that for the copper-tin and nickel-tin systems, interface control is important. Thus, the area of the interface becomes a key parameter since the rate of an interface controlled reaction is proportional to the interfacial area.[66]

Figure 3.18: Aluminum-gold diffusion couple with intermetallic layers.[65] Aged at 400°C for 600 minutes, 750X. Note that the interface between the intermetallic and the gold is not planar. Reprinted from Solid-State Electronics, 13, E. Philofsky, "Intermetallic Formation in Gold-Aluminum Systems," Pages No. 1391-1399, Copyright 1970, with kind permission from Elsevier Science Ltd., The Boulevard, Langford Lane, Kidlington 0X5 1GB, UK.

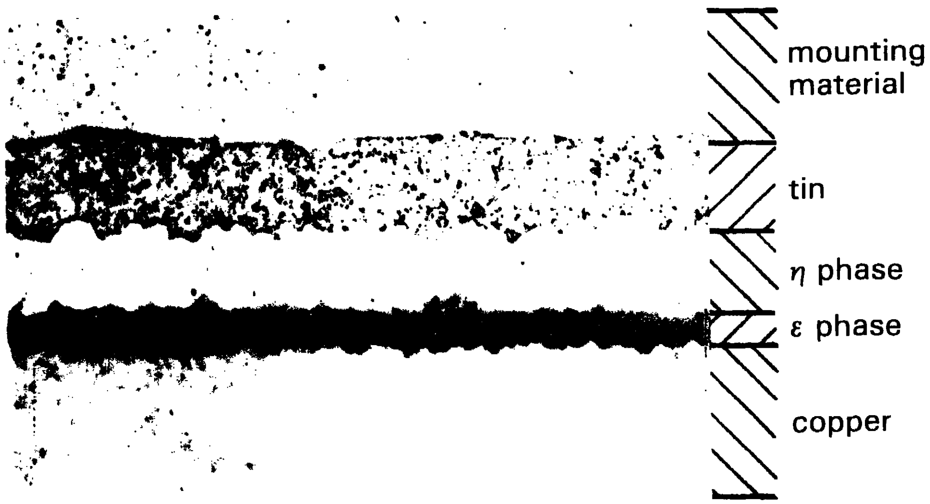

Figure 3.19: Intermetallic layers between copper and tin. Aged at 170°C for 4000 hours. Note the interfaces are not planar. Used with permission from ref. 63.

3.3 Discussion of fast diffusion

Several chemical and physical factors that affect diffusion in intermetallics have been discussed. These factors can be used to rationalize fast diffusion. For instance, all the systems that exhibit fast diffusion also have metallic bonding. Through analysis of the derivative of the chemical potential, the thermodynamic contributions can be removed from the diffusion coefficient to leave the mobility. Such an analysis was used to compare the mobilities in two copper-zinc intermetallics which exhibit fast diffusion to the mobility in FeAl which does not exhibit fast diffusion. The mobilities in the copper-zinc intermetallics are two to three orders of magnitudes larger than the mobility in FeAl. Analysis of the crystal structures of the iron-, nickel- and copper-tin intermetallics explained why the iron-tin intermetallics have the slowest diffusion rate. The contribution of grain boundary diffusion to the overall diffusion rate was investigated for two copper-tin examples and found to be negligible. However, no systematic method for combining all these factors has been developed. A comprehensive hypothesis for explaining fast diffusion cannot be based on one or two of these factors, and the interactions between the factors are too complex to allow a combined model.

4. Mei's model

Theoretical analysis of the flux possible through intermetallic phases may be able to determine the order of magnitude or relative magnitude of the diffusion coefficient in an intermetallic. However, concrete values for the diffusion coefficients in specific phases for specific situations are difficult to determine accurately from a purely theoretical study. To find precise values for the diffusion coefficient for an application, experimental data needs to be incorporated. Modeling intermetallic growth supplies the means to combine the theoretical aspects of growth and experimental data. A model can provide insight into the interplay of the controlling mechanisms of growth and the ability to predict intermetallic growth rates for practical situations.

Two existing models are evaluated and expanded upon in this work. The first, a model developed by Mei *et al.*[32], uses a series of moving boundaries to model intermetallic growth. This approach assumes that diffusion controls intermetallic growth. The development of Mei's modeling equations is described in Section 4.1. Then, in Section 4.2, the copper-tin system is evaluated with a model based on Mei's equations, and the results of these modeling efforts are discussed. The results found in this work do not agree with those reported by Mei. Much of the discussion of this model focuses on this discrepancy in the results. The conclusion is that, while Mei's model is comprehensive in terms of diffusion controlled growth, the model does not fully describe intermetallic growth in the copper-tin system because growth in this system is not purely diffusion controlled. Instead, the growth in the copper-tin system is a case of mixed diffusion and interface control at low temperatures.

Since Mei's diffusion control based model was found to be lacking for describing intermetallic formation in the copper-tin system, a theory developed by Philibert,[67,68] which includes both diffusion and interface reaction rates, is examined in Chapter 5. This theory had not yet been applied to specific systems. In this work, it is applied to the copper-tin and nickel-tin systems (Sections 5.2 and 5.3, respectively).

4.1 Derivation of Mei's model

Mei's model is developed for intermetallic growth in the copper-tin system.[32] As shown in the phase diagram in Figure 2.5, two intermetallic layers, the ε phase and the η phase, should form at the temperatures for which the model is designed, 190-220°C, in the copper-tin system.

The modeling approach assumes

1) equilibrium at the interfaces
2) constant diffusion coefficients in the layers
3) diffusion controlled growth
4) planar layers
5) semi-infinite base metals.

For growth in this temperature range, these assumptions should be generally valid though the layers may not be planar. Assuming planar layers is particularly questionable if, in the history of the diffusion couple, the tin was once liquid. When the intermetallic layers form between liquid tin and solid copper, the interface is much rougher and more hillocked than when both the tin and copper are solids.[8]

The copper concentration in the copper solid solution, in the ε phase, in the η phase, and in the tin solid solution is fit to the standard error function solution to Fick's Law:

$$c_i = A_i - B_i \operatorname{erf}\left(\frac{x}{2\sqrt{\tilde{D}_i t}}\right) \tag{4.1}$$

where c_i is the copper concentration in layer i, A_i and B_i are constants determined from the boundary conditions, and $\tilde{D}_i$ is the interdiffusion coefficient. The subscript i indicates the layer: copper solid solution = 1, ε = 2, η = 3, tin solid solution = 4. A sketch of the concentration profiles is given in Figure 4.1.

The boundary conditions are

$$\begin{aligned}
&c_1=c_o \text{ at } x=-\infty && c_3=c_{32} \text{ at } x=\zeta_{23}\\
&c_1=c_{12} \text{ at } x=\zeta_{12} && c_3=c_{34} \text{ at } x=\zeta_{34}\\
&c_2=c_{21} \text{ at } x=\zeta_{12} && c_4=c_{43} \text{ at } x=\zeta_{34}\\
&c_2=c_{23} \text{ at } x=\zeta_{23} && c_4=c_s \text{ at } x=\infty
\end{aligned} \tag{4.2}$$

The subscripts in the boundary conditions correlate with the labels in Figure 4.1. For a given temperature, the concentrations at the interfaces can be determined from the phase diagram because equilibrium at the interfaces is assumed. Thus, all the concentrations in

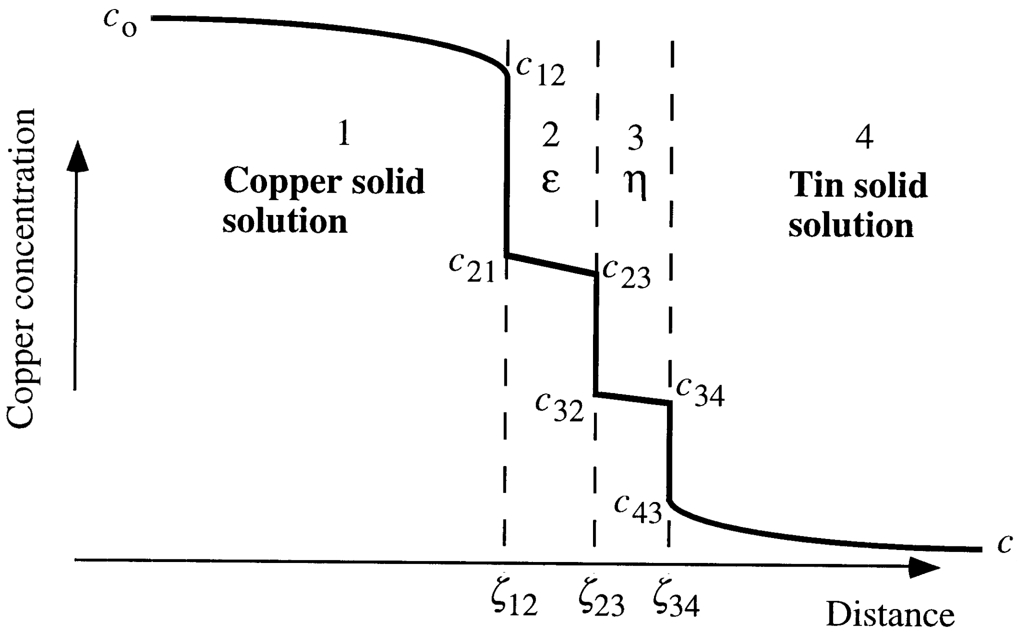

Figure 4.1: The concentration profiles and boundary conditions for a copper-tin diffusion couple at low temperatures. Adapted from ref. 32.

the boundary conditions, Equation 4.2 and Figure 4.1, can be determined once the temperature is specified.

These boundary conditions can be used to evaluate the constants A_i and B_i in Equation 4.1 for the copper concentration in each layer:[32]

$$c_{Cu} = c_1 = c_o - \frac{c_o - c_{12}}{1+\mathrm{erf}g_1}\left[1+\mathrm{erf}\frac{x}{2\sqrt{\tilde{D}_1 t}}\right] \tag{4.3}$$

$$c_\varepsilon = c_2 = c_{21} - \frac{c_{21} - c_{23}}{\mathrm{erf}g_2 - \mathrm{erf}\left(g_1\sqrt{r_{12}}\right)}\left[\mathrm{erf}\frac{x}{2\sqrt{\tilde{D}_2 t}} - \mathrm{erf}g_1\sqrt{r_{12}}\right] \tag{4.4}$$

$$c_\eta = c_3 = c_{32} - \frac{c_{32} - c_{34}}{\mathrm{erf}g_3 - \mathrm{erf}\left(g_2\sqrt{r_{23}}\right)}\left[\mathrm{erf}\frac{x}{2\sqrt{\tilde{D}_3 t}} - \mathrm{erf}g_2\sqrt{r_{23}}\right] \tag{4.5}$$

$$c_{Sn} = c_4 = c_s + \frac{c_{43} - c_s}{1-\mathrm{erf}\left(g_3\sqrt{r_{34}}\right)}\left[1-\mathrm{erf}\frac{x}{2\sqrt{\tilde{D}_4 t}}\right] \tag{4.6}$$

where

$$g_i = \frac{\zeta_{ij}}{2\sqrt{\tilde{D}_i t}} \tag{4.7}$$

and

$$r_{ij} = \tilde{D}_i \big/ \tilde{D}_j \tag{4.8}$$

The mass balance at each interface supplies the relationship that ties the concentration profiles to the interface movements.[32]

$$-\tilde{D}_i \frac{\partial c_i}{\partial x} + \tilde{D}_j \frac{\partial c_j}{\partial x} = \left(c_{ij} - c_{ji}\right)\frac{d\zeta_{ij}}{dt} \qquad (\text{for } i\text{=1 to 3}, j = i\text{+1}) \tag{4.9}$$

Substituting Equations 4.3-4.6 into Equation 4.9, results in three equations.[32]

$$\frac{(c_o - c_{12})\exp(-g_1^2)}{1 + \operatorname{erf} g_1} - \frac{(c_{21} - c_{23})\exp(-g_1^2 r_{12})}{\sqrt{r_{12}}\left[\operatorname{erf} g_2 - \operatorname{erf}\left(g_1\sqrt{r_{12}}\right)\right]} = g_1(c_{12} - c_{21})\sqrt{\pi} \tag{4.10}$$

$$\frac{(c_{21} - c_{23})\exp(-g_2^2)}{\operatorname{erf} g_2 - \operatorname{erf}\left(g_1\sqrt{r_{12}}\right)} - \frac{(c_{32} - c_{34})\exp(-g_2^2 r_{23})}{\sqrt{r_{23}}\left[\operatorname{erf} g_3 - \operatorname{erf}\left(g_2\sqrt{r_{23}}\right)\right]} = g_2(c_{23} - c_{32})\sqrt{\pi} \tag{4.11}$$

$$\frac{(c_{32} - c_{34})\exp(-g_3^2)}{\operatorname{erf} g_3 - \operatorname{erf}\left(g_2\sqrt{r_{23}}\right)} - \frac{(c_{43} - c_s)\exp(-g_3^2 r_{34})}{\sqrt{r_{34}}\left[1 - \operatorname{erf}\left(g_3\sqrt{r_{34}}\right)\right]} = g_3(c_{34} - c_{43})\sqrt{\pi} \tag{4.12}$$

These three equations, Equations 4.10-4.12, form the core of the model.[32] Recalling that r_{ij} is a function of the interdiffusion coefficients, $\tilde{D}_i$ and $\tilde{D}_j$, the unknowns and data necessary to solve these equation can be determined. The concentrations are determined from the phase diagram. Thus, there are seven unknowns in the above three equations: $\tilde{D}_1$, $\tilde{D}_2$, $\tilde{D}_3$, $\tilde{D}_4$, g_1, g_2, and g_3.

If the interdiffusion coefficients are known ($\tilde{D}_1$, $\tilde{D}_2$, $\tilde{D}_3$, and $\tilde{D}_4$), then g_1, g_2, and g_3 can be calculated. From the values of g_1, g_2, and g_3, the interface positions and layer thicknesses can be determined as a function of time. However, interdiffusion coefficients in most intermetallic phases are not well characterized. It is more common to have data in the form of layer thicknesses as a function of time.

When only layer thickness as a function of time is known, additional equations and additional data are required to solve the equations. Layer thickness data are typically in the form of thicknesses of the intermetallic layers, w_ε and w_η, as a function of time at a specific temperature. Since diffusion control is assumed, these data can be fit to the equations

$$w_\varepsilon = k_\varepsilon \sqrt{t} \qquad \text{and} \qquad w_\eta = k_\eta \sqrt{t} \tag{4.13}$$

where k_ε and k_η are constants for a given temperature. The intermetallic layer thicknesses are related to the interface positions which can also be written in terms of g_i:[32]

$$\begin{aligned} w_\varepsilon &= \zeta_{23} - \zeta_{12} = 2\left[g_2\sqrt{\tilde{D}_2 t_1} - g_1\sqrt{\tilde{D}_1 t}\right] \\ w_\eta &= \zeta_{34} - \zeta_{23} = 2\left[g_3\sqrt{\tilde{D}_3 t} - g_2\sqrt{\tilde{D}_2 t}\right] \end{aligned} \tag{4.14}$$

Comparing Equations 4.13 and 4.14, expressions for k_ε and k_η in terms of the g_i's and D_i's result: [32]

$$\begin{aligned} k_\varepsilon &= 2\left[g_2\sqrt{\tilde{D}_2} - g_1\sqrt{\tilde{D}_1}\right] \\ k_\eta &= 2\left[g_3\sqrt{\tilde{D}_3} - g_2\sqrt{\tilde{D}_2}\right] \end{aligned} \tag{4.15}$$

Now, with the original three equations (Equations 4.10-4.12), the two relations in Equation 4.15, and the thickness versus time data, there are five equations and still seven unknowns: $\tilde{D}_1$, $\tilde{D}_2$, $\tilde{D}_3$, $\tilde{D}_4$, g_1, g_2, and g_3. Two additional quantities, such as the interdiffusion coefficients in the solid solutions, $\tilde{D}_1$ and $\tilde{D}_4$, are necessary to solve the equations. These data are usually readily available in the literature.

However, the modeling equations are not straightforward to solve even with an equal number of equations and unknowns. An iterative technique must be used. Both in Mei's work and in this work, the Newton-Raphson method is employed.[69,70]

As described above, the model can be used to solve for either the interface positions or the interdiffusion coefficients. If one knows the interdiffusion coefficients, one may solve for the interface positions. Alternately, one may solve for the interdiffusion coefficients in the intermetallic layers if the relationship between intermetallic layer thicknesses and time and the interdiffusion coefficients in the solid solutions are known. This second method is the one applied to the copper-tin system in the next section and is the method Mei uses in his work. The analysis can be adapted to accommodate as many or as few layers as are predicted to form so that any system could be modeled; though the equations involved become increasingly complex as does the solution technique when the number of layers is increased.

4.2 Application of Mei's model

Mei developed his model for the copper-tin system. Utilizing other researchers' data, he solved the modeling equations to determine the diffusion coefficients in the two copper-tin intermetallic phases, ε and η. In this work, a model was developed based on Mei's equations and run with the same data that Mei used. The results of these modeling efforts did not match those reported by Mei. The difference is attributed to the development of a better solution technique. Additionally, analysis of the results presented here, along with observations from the literature, indicate that intermetallic formation in the copper-tin system is not purely diffusion controlled at low temperatures. Thus, this model, which is based only on diffusion control, is inadequate for predicting growth in the copper-tin system.

Mei uses Onishi's and Fujibuchi's[36] experimental data in his model to calculate the diffusion coefficients in the ε and η phases. The data are in the form of intermetallic layer thickness as a function of time which gives the k_ε and k_η values from Equation 4.13. Two other pieces of information are required to have enough data to solve the modeling equations. The diffusion coefficients in the copper and tin solid solutions are reasonably well known so they supply sufficient data. Using the values for k_ε, k_η, D_{Cu}, and D_{Sn}, Mei solves the equations (Equations 4.10-4.12 and 4.15) for g_1, g_2, and g_3. In turn, the values for g_1, g_2, and g_3 can be substituted back into Equation 4.15 to determine the diffusion coefficients in the intermetallics. Table 4.1 shows the data Mei used to solve the equations and Table 4.2 presents Mei's results.

Table 4.1: Data Mei uses to solve modeling equations[32]

Temperature (°C)	k_ε (cm/s$^{1/2}$)	k_η (cm/s$^{1/2}$)	D_{Cu} (cm^2/s)	D_{Sn} (cm^2/s)
190	5.21×10^{-7}	9.39×10^{-7}	3.08×10^{-21}	4.49×10^{-7}
200	6.19×10^{-7}	1.06×10^{-6}	8.13×10^{-21}	5.39×10^{-7}
210	7.88×10^{-7}	1.19×10^{-6}	2.07×10^{-20}	6.41×10^{-7}
220	8.60×10^{-7}	1.43×10^{-6}	5.07×10^{-20}	7.56×10^{-7}

Table 4.2: Results from Mei's modeling efforts[32]

Temperature (°C)	g_1	g_2	g_3	D_ε (cm^2/s)	D_η (cm^2/s)
190	-8648	-9.11 x 10^{-2}	5.80 x 10^{-2}	5.80 x 10^{-12}	1.86 x 10^{-11}
200	-6130	-8.64 x 10^{-2}	5.87 x 10^{-2}	7.94 x 10^{-12}	2.39 x 10^{-11}
210	-4555	-7.55 x 10^{-2}	6.00 x 10^{-2}	1.19 x 10^{-11}	3.10 x 10^{-11}
220	-3336	-8.30 x 10^{-2}	5.97 x 10^{-2}	1.50 x 10^{-11}	4.35 x 10^{-11}

There is some question as to how Mei got his results. The modeling equations were incorporated into a Mathematica®* program to try to reproduce Mei's results. This program is listed in Appendix C. It proved impossible to generate the same solutions Mei reported. The problem is in the first term of the first basic model equation (Equation 4.10, reprinted below):

$$\underbrace{\frac{(c_o - c_{12})\exp(-g_1^2)}{1+\mathrm{erf}g_1}}_{} - \frac{(c_{21} - c_{23})\exp(-g_1^2 r_{12})}{\sqrt{r_{12}}\left[\mathrm{erf}g_2 - \mathrm{erf}\left(g_1\sqrt{r_{12}}\right)\right]} = g_1(c_{12} - c_{21})\sqrt{\pi} \qquad (4.16)$$

The method used to attempt to solve the equations is an iterative approach necessitated by the fact that the equations are nonlinear. First, all the terms are moved to the left-hand side of the each equation such that the right-hand side is zero. Estimates are made for the values of g_1, g_2, and g_3. Then, the values for g_1, g_2, and g_3 are iterated until the left-hand sides of the three equations all approach zero. The Newton-Raphson[69,70] method, which uses the derivatives of the equations to adjust the g_i values, is used for the iteration.

All the values Mei calculated for g_1 are large and negative. However, g_1 cannot be a large negative number because this makes the first term of Equation 4.16 unstable. Specifically, the problem is with the error function in the denominator of the first term. The error function of a large negative number very nearly equals -1 which makes the denominator of the first term in Equation 4.16 equal to a very small number. Large is a relative term; in this case, the argument of the error function only has to be less than -6 for the error function to be functionally equal to -1. Thus, any value of g_1 that is less than -6 is

---

*© Wolfram Research, Inc., Champaign, IL, USA

large enough to make the first term indefinite. The physical quantities that make g_1 large and negative will be discussed later.

This problem prevents the system of three equations (Equations 4.10-4.12) from producing Mei's solutions because, whenever the iteration gets a large negative value for g_1, the equations become unstable. However, another set of solutions for each temperature was found in running the model. These solutions will be examined later; first, further efforts to reproduce Mei's results will be discussed.

The first step in evaluating Mei's solutions was to check the relative magnitudes of the numerator and denominator of the first term. Several series approximations for both the error function and the exponential were employed in order to determine if the term would converge and a limit could be found. In every case, the term approached infinity when the value for g_1 was a large negative number.

Mei was contacted and asked how he solved these equations when the first term in the first equation was clearly unstable for the solutions he reported. His answer was unsatisfactory both from the standpoint of mathematical propriety and for reproducing his results. He claimed to have divided through by the offending denominator to move it to the numerator. This action does solve the problem with the first term. However, it creates other mathematical difficulties and does not aid in reproducing Mei's solutions.

Looking at the first equation as Mei is to have modified it, the reasons for the problems are clear:

$$(c_o - c_{12})\exp(-g_1^2) - \frac{(c_{21} - c_{23})\exp(-g_1^2 r_{12})(1 + \mathrm{erf} g_1)}{\sqrt{r_{12}}\left[\mathrm{erf} g_2 - \mathrm{erf}\left(g_1\sqrt{r_{12}}\right)\right]} - g_1(c_{12} - c_{21})\sqrt{\pi}(1 + \mathrm{erf} g_1) = 0 \qquad (4.17)$$

Just as before, when g_1 is a large negative number, the expression ($1+\mathrm{erf} g_1$) approaches zero. Instead of being in the denominator of only the first term of the equation, this expression is now in the numerator of the second and third terms. So the second and third terms approach zero when g_1 is large and negative. Thus, the first equation becomes a function of g_1 alone and serves to determine the value for g_1:

$$(c_o - c_{12})\exp(-g_1^2) = 0 \qquad (4.18)$$

Any large value, positive or negative, will satisfy this equation. In this case, a large value is one with an absolute value greater than 26.

This problem was reflected in attempts to solve a model with the first equation modified as recommended by Mei. Whenever, through the course of the iteration, g_1 became a large negative number (less than -26), that value for g_1 was locked onto because it satisfied the first equation. Only the values of g_2 and g_3 were then adjusted by further iteration to make the second and third modeling equations balance. The result is an infinite set of solutions; for every large negative value of g_1, the values of g_2 and g_3 can be adjusted accordingly to form a solution to the equations.

Besides having a multitude of solutions, this method of moving the denominator of the first term is questionable mathematically. When multiplying through by an expression, as Mei does with the term $(1+\mathrm{erf} g_1)$, it is assumed that this expression does not equal zero. In this case, that expression can be zero so it should not be multiplied through. While this expression only truly equals zero when g_1 equals negative infinity, this expression is a very small number for any value of g_1 smaller than -6. A large round-off error is associated with the calculation of such a small number. By moving this expression to the numerator, that error is propagated.

In a further effort to try to reproduce Mei's numbers, it was found that Mei's solutions resulted from the modeling equations when the first term of the first equation was summarily removed leaving

$$\frac{(c_{21}-c_{23})\exp(-g_1^2 r_{12})}{\sqrt{r_{12}}\left[\mathrm{erf} g_2 - \mathrm{erf}\left(g_1\sqrt{r_{12}}\right)\right]} + g_1(c_{12}-c_{21})\sqrt{\pi} = 0 \qquad (4.19)$$

However, there are no grounds for eliminating the first term of this equation in this manner. Limit analyses done on the first term indicate that it goes to zero for large positive values of g_1, but that it goes to infinity for large negative values of g_1. For small values of g_1, either negative or positive, this term has a finite value. Since for negative values this term goes to infinity and negative values are what Mei gets as solutions, this term cannot be dismissed. Hence, no acceptable method was found for reproducing Mei's solutions.

As mentioned previously, valid solutions to the modeling equations were determined in this work. The basic modeling equation (Equation 4.10-12) were not altered in any way. Instead, the determination of the initial estimates of g_1, g_2, and g_3 for the first iteration was focused on. The model was run for a large matrix of initial g_1, g_2, and g_3 values. The set of solutions that resulted from these efforts do not match Mei's solutions even though the same data that Mei utilized was used to run the model. The set of solutions found in this work is shown in Table 4.3.

A sensitivity analysis of Mei's model was also done. The results and a brief discussion of this analysis are contained in Appendix D. The main conclusion is that the model results presented here are stable. The model is not overly sensitive to the values of the diffusion coefficients. Variation of the diffusion coefficients by up to a factor of ten does not change the predictions significantly.

The diffusion rates found here are similar to those found by Mei. A major difference, however, is in the sign of the g_i values. The interface position parameters are determined from the g_i values and have the same signs as the corresponding value of g_i. The interface position parameters for both Mei's solutions and the solutions presented in this work are shown in Table 4.4.

Table 4.3: Solutions found in this work to the modeling equations

Temperature (°C)	g_1	g_2	g_3	D_ε (cm^2/s)	D_η (cm^2/s)
190	2755	-0.2085	0.0226	3.93×10^{-12}	6.17×10^{-12}
200	1652	-0.2266	0.0247	4.10×10^{-12}	8.36×10^{-12}
210	685.6	-0.3054	0.0293	2.60×10^{-12}	1.22×10^{-11}
220	778.3	-0.2436	0.0276	6.17×10^{-12}	1.58×10^{-11}

Table 4.4: Interface position parameters for Mei's solutions[32] and for the solutions presented in this work

Temperature (°C)	$\lambda_{Cu\text{-}\varepsilon}$ (cm/s$^{1/2}$)	$\lambda_{\varepsilon\text{-}\eta}$ (cm/s$^{1/2}$)	$\lambda_{\eta\text{-}Sn}$ (cm/s$^{1/2}$)
	For Mei's solutions		
190	-9.60×10^{-7}	-4.39×10^{-7}	5.00×10^{-7}
200	-1.11×10^{-6}	-4.87×10^{-7}	5.73×10^{-7}
210	-1.31×10^{-6}	-5.21×10^{-7}	6.68×10^{-7}
220	-1.50×10^{-6}	-6.43×10^{-7}	7.88×10^{-7}
	For the solutions presented here		
190	3.06×10^{-7}	-8.27×10^{-7}	1.12×10^{-7}
200	2.98×10^{-7}	-9.17×10^{-7}	1.43×10^{-7}
210	1.97×10^{-7}	-9.85×10^{-7}	2.05×10^{-7}
220	3.51×10^{-7}	-1.21×10^{-6}	2.20×10^{-7}

Mei's results predict that both intermetallic layers grow and that the original interface between the copper and tin remains in the η phase layer. Mei's solutions indicate that the Cu-ε and the ε-η interfaces move in the negative direction while the η-Sn interface moves in the positive direction. These signs mean that the original interface between the copper and the tin stays in the η layer which is seen experimentally.[36] Additionally, the Cu-ε interface moves faster than the ε-η interface which allows for the formation of the ε layer. An example of the layer thicknesses resulting for Mei's solutions is given in Figure 4.2 for aging at 190°C for one day. Two initial conditions are compared. In Figure 4.2(a), the initial state has no intermetallic layers while in Figure 4.2(b) one micron thick layers of both the ε and η phases exist from a previous treatment.

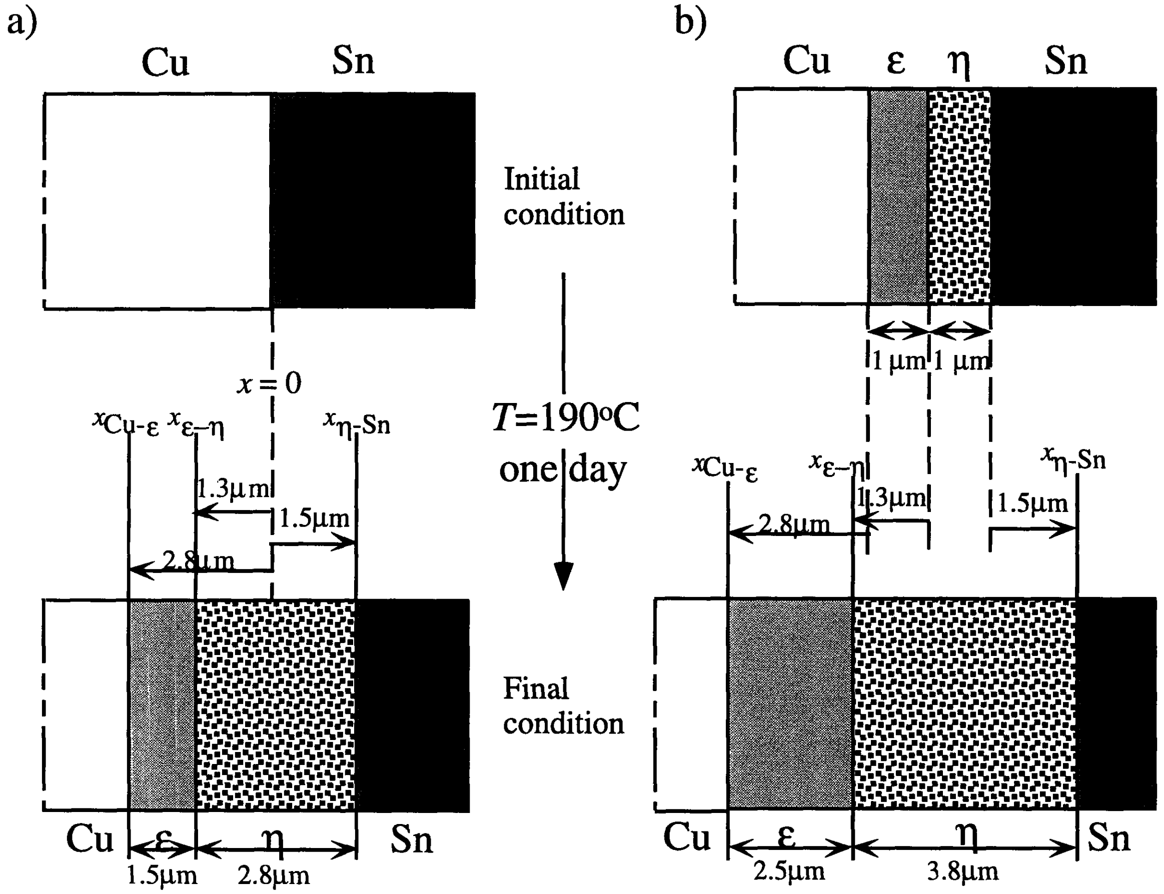

Figure 4.2: Growth of intermetallic layers in a copper-tin diffusion couple aged at 190°C for one day. Interface movements are calculated from Mei's interface position parameters (Table 4.4). In (a) the initial state contains no intermetallic layers while in (b) one micron layers of both the ε and η phase exist.

For the solutions presented here, the Cu-ε interface and the η-Sn interface both move in the positive direction and the ε-η interface moves in the negative direction. These results indicate that the ε phase should not form in this temperature range, and if it exists from a prior treatment, it should shrink. In Figure 4.3, the intermetallic layer thicknesses calculated from the solutions presented in this work for aging at 190°C for one day are shown. As in Figure 4.2, two initial conditions, one containing no intermetallics and one with pre-existing intermetallic layers, are compared in Figure 4.3.

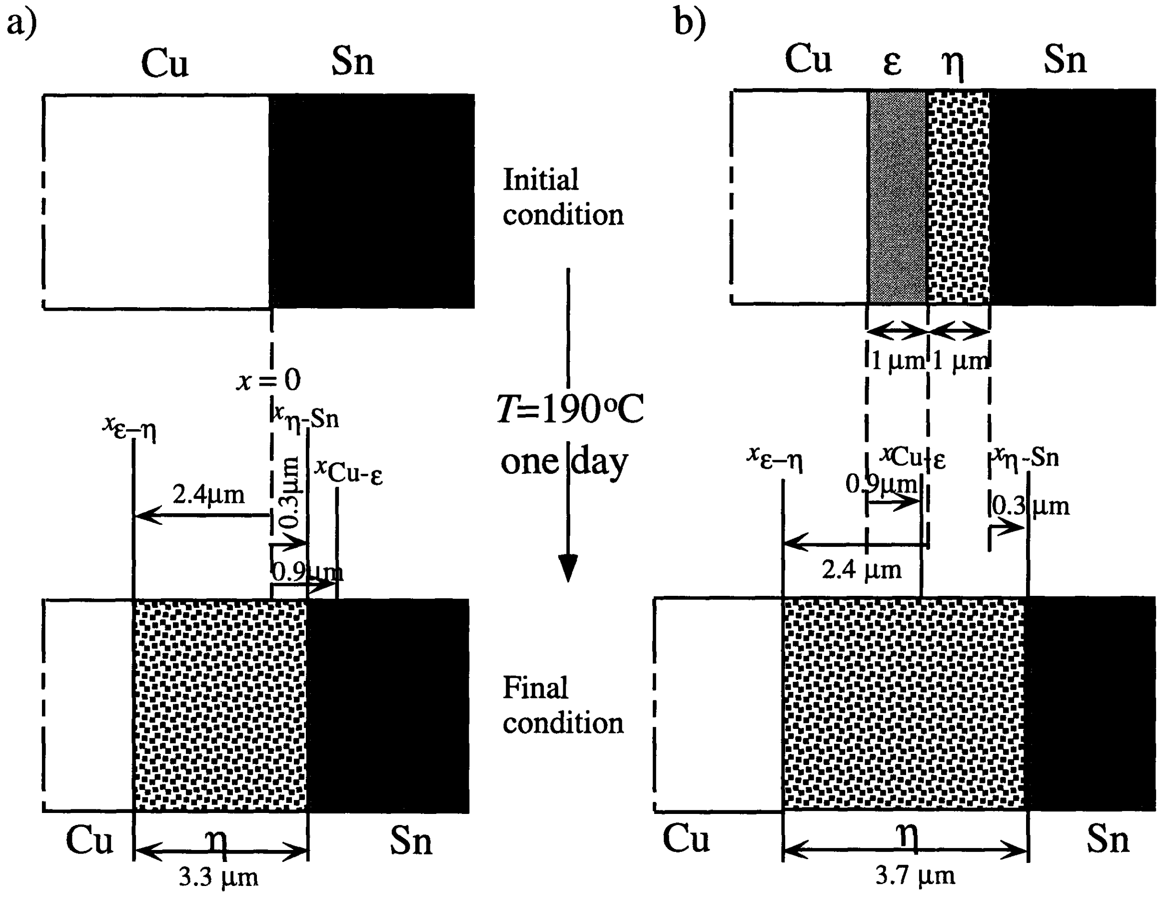

Figure 4.3: Growth of intermetallic layers in a copper-tin diffusion couple aged at 190°C for one day. Interface movements are calculated from the interface position parameters determined in this work (Table 4.4). In (a) the initial state contains no intermetallic layers while in (b) one micron layers of both the ε and η phase exist.

Mei's solutions seem reasonable when considered apart from the modeling equations. Mei's results predict the formation of both intermetallic layers and that the original interface remains in the η layer. Both of these phenomena are usually seen in experiments at these temperatures.[4,8,33,34,36,71-74] However, Mei's solutions do not satisfy the modeling equations. The solutions presented here do satisfy the model but do not predict the formation of both intermetallic layers which are usually seen at these temperatures.

Mei's solutions do not satisfy the model equations due to the large negative values he reports for g_I. These large negative values for g_I arise when the model tries to reconcile the diffusion rate in the copper, D_{Cu}, with the rates of the intermetallic growth, k_ε and k_η. g_I tends to be large because it is inversely proportional to the diffusion coefficient in the copper solid solution (refer to Equation 4.7). The diffusion coefficient in the copper solid solution is about nine orders of magnitude lower than the diffusion coefficient in the ε phase, the η phase, or the tin solid solution. The value for the diffusion coefficient in the copper used in the model is well documented[32,64,75] so it is likely to be accurate. g_I is negative because for the ε phase to grow, as indicated by the k_ε and k_η data, and for the original interface to stay in the η phase, the copper-ε interface must move in the negative direction. Experiments measuring the thickness of the intermetallic layers as a function of time are also well documented. As shown in Figure 4.4, the data Mei uses for intermetallic thickness is in general agreement with data from other researchers.[3,76,77]

However, these two pieces of data, the diffusion coefficient in copper and the layer growth rates, are not consistent. The diffusion rate for the copper is slow, and the intermetallic formation is fast. The diffusion based modeling equations try to reconcile these data and cannot do it satisfactorily. When the diffusion coefficient in the copper is set artificially high, the model produces solutions that agree with the intermetallic layer data indicating that both intermetallic layers form.

Perhaps the formation of the intermetallic in the copper-tin system is not purely diffusion controlled so the modeling equations, which assume diffusion control, do not fully describe the situation. Additionally, the model results presented here give kinetic criteria which overrule the thermodynamic prediction that both the ε and the η phases should form in copper-tin diffusion couples at low temperatures. There are published experimental data supporting both non-diffusion controlled growth of the intermetallic phases and selective phase growth in the copper-tin system.

Growth can generally be described by the equation

$$\Delta w = kt^n \qquad (4.20)$$

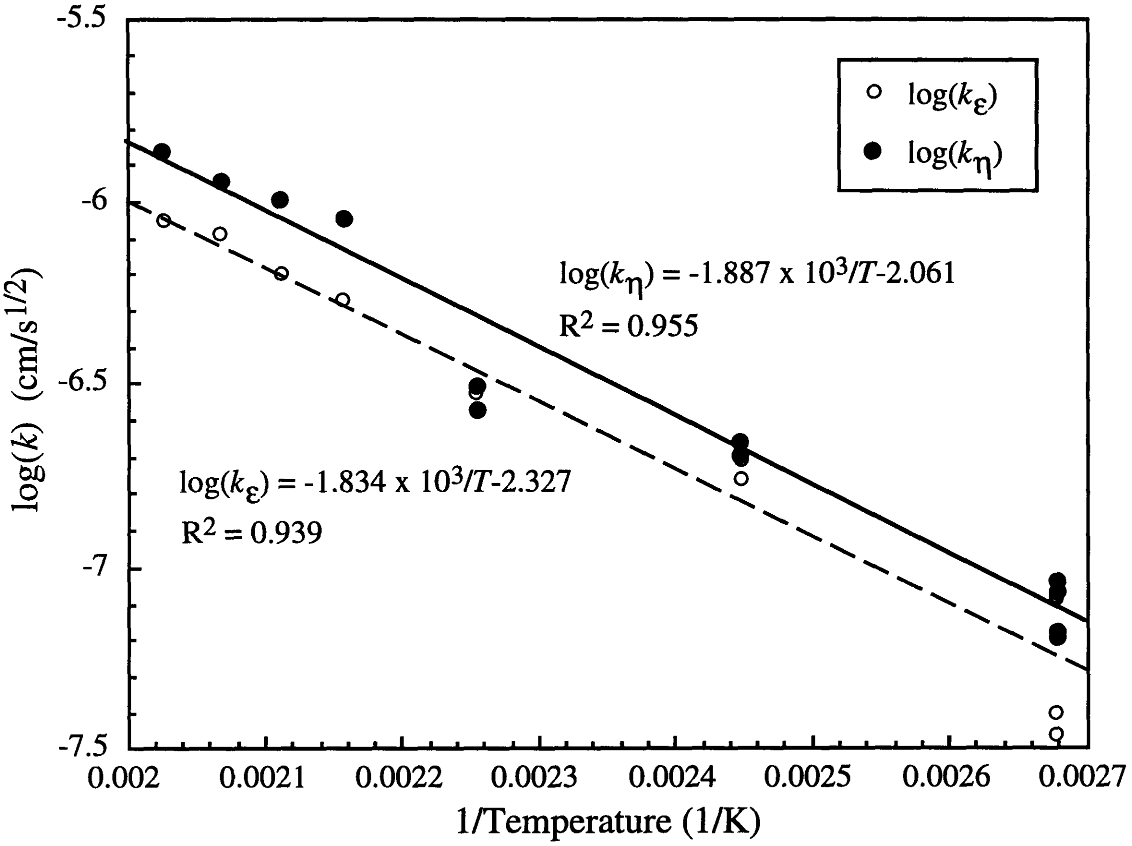

Figure 4.4: Several researchers' data[3,76,77] on the thickness constants, assuming parabolic growth, $\Delta w = kt^{1/2}$, for the copper-tin intermetallics plotted as a function of temperature. The data are quite consistent assuming an Arrhenius-type temperature dependence.

where Δw is the change in thickness of the growing layer, t is time, and k and n are constants. Diffusion controlled growth implies a parabolic relationship between layer thickness and time, meaning that the change in layer thickness is proportional to $t^{1/2}$, or n = 0.5.

Many researchers have found such a parabolic relationship to hold for the copper-tin intermetallics,[33,34,72,78] but several have indicated otherwise.[8,38,71,74,79] Cogan *et al.*[8] found that the thickness of the ε phase was proportional to $t^{1/2.53}$ and of the η phase to $t^{1/2.51}$. They conclude the variation of the exponent from ½ is due to the influence of grain boundary diffusion. Tu and Thompson[38] report that the growth of the ε phase is parabolic but that the growth of the η phase is linear with time, which would imply interface reaction control instead of any type of diffusion control. Kawakatsu *et al.*[74] also found that n =

0.53 for growth of the ε phase and $n = 0.38$ for the η phase. Conversely, Parent *et al.*[71] found that the ε phase grew linearly in time. Dehaven[79] studied the growth of the entire intermetallic layer, ε and η together, and concluded that for short times and low temperatures, intermetallic growth was interface reaction controlled, $n = 1$, but for long times or high temperatures, it was diffusion controlled, $n = 0.5$. These results are summarized in Table 4.5. Quite a range of values is reported for the growth exponent for the copper-tin intermetallic phases. This indicates that diffusion control may not be a good assumption.

In addition, several researchers have reported not seeing all the phases predicted by the phase diagram.[38,53,64,77,79-81] All the researchers observe the η phase initially, and then after long times or at higher temperatures, they see the ε phase. However, at temperatures below 50°C, the ε phase does not seem to form at all. Their observations are summarized in Table 4.6. Some attribute the lack of the ε phase to a barrier to nucleation which is more easily overcome at higher temperatures.[38,52]

Another reason that the η phase forms preferentially may relate to the differences in the diffusion rates of the copper and tin. Tin is the faster diffuser in this system. The supply of tin to the copper-intermetallic interface may overwhelm the supply of copper such that only the tin rich intermetallic will form. The η phase is richer in tin than the ε phase so only the η phase forms. A similar situation occurs in the nickel-tin system where the Ni_3Sn_4 phase, the intermetallic richest in tin in this system, forms preferentially.

The observations of non-parabolic growth and of selective formation of the η phase in the copper-tin system indicate that the diffusion is not the only mechanism affecting intermetallic growth. Thus, Mei's model, which is based on pure diffusion control, is not accurate for the copper-tin system at low temperatures. This assessment is also supported by the comparison of the results Mei reports with the ones presented in this work. Mei's solutions do not satisfy the diffusion based modeling equations but do predict the formation of both the ε and η phases which is seen experimentally in this temperature range, 190-220°C. The model solutions presented here do fulfill the requirements of the modeling equations but only predict the formation of the η phase intermetallic. At lower temperatures, it is true that the η phase forms preferentially, but in the temperature range for which this model was designed, both phases are seen experimentally.

Selective phase growth has been seen in other systems.[34,35,55,80] Efforts have been made to explain why some phases form before or without others and to predict in which systems and for what conditions it will happen. These efforts focus on the rates of the competing controlling mechanisms. Philibert's model,[67,68] which is presented in the next chapter, combines diffusion and interface control to model non-parabolic growth and to explain selective phase formation. This type of model, which combines the control mechanisms, should be better at describing the copper-tin system. In Section 5.2, Philibert's model is applied to the copper-tin system with promising results.

Table 4.5: Growth exponent for the low temperature copper-tin intermetallic phases

n for ε phase growth	*n* for η phase growth	Temperature range of experiments (°C)	Reference
0.395	0.398	220	Cogan *et al.*[8]
0.5	1	115-150 for ε, 25 for η	Tu and Thompson[38]
0.53	0.38	320-580	Kawakatsu *et al.*[74]
1	---	230-350	Parent *et al.*[71]
low temperatures and short times: 1 longer times or high temperatures: 0.5		200-300	Dehaven[79]

Table 4.6: Observations of selective growth of copper-tin intermetallics

Observation of intermetallic growth	Reference
η appears first, ε appears after 4 to 9 days at temperatures from 70-170°C	Unsworth and Mackay[77]
only η forms at room temperature	Halimi *et al.*[81]
η forms at all temperatures, ε only forms at temperatures above 60°C	Tu[53]
η forms at all temperatures, ε does not form at room temperature even after 84 days, ε will form at temperatures above 50°C	Tu and Thompson[38]
η seen after only 1 minute, both η and ε seen after 5 minutes at a temperature between 200 and 300°C	Dehaven[79]
ε seen in hot dipped samples and reflowed samples but not in electroplated samples all stored at room temperature	Kay and Mackay[80]
η only seen at 60 and 80°C, η and ε seen at 150°C	Bandyopadhyay and Sen[64]

5. Philibert's model

Whereas Mei's model, described in the last chapter, only considers diffusion as a factor in intermetallic growth, Philibert's model includes interface reaction rates as well as diffusion. Thus, Philibert's[67,68] model should give a more complete view of intermetallic growth. However, the inclusion of interface reaction rates increases the amount of experimental data required to model intermetallic growth. Little data exist on the interface reaction rates; Philibert refers to these data as "ad hoc parameters beyond experimental determination."[68] This lack of data limits the use of Philibert's theory for quantitative predictions of intermetallic growth. Qualitative insights are possible, though, by considering experimental observations of intermetallic growth in conjunction with the model. Comparison of the theory and experimental observations is done for both the copper-tin system and the nickel-tin system in this work (Sections 5.2 and 5.3, respectively).

5.1 Development of Philibert's model

Philibert[67,68] develops equations which combine the diffusion rate and the interface reaction rate to describe the growth of an intermediate phase. Then, he examines the limiting case of pure diffusion control and the case of mixed control. His theoretical work aims to support the following experimental results:[68]

1) the intermediate phases do not appear simultaneously, but sequentially,
2) a critical thickness of the first phase that forms must be reached in order that the second phase be allowed to grow,
3) no basic differences exist between these processes in thin films and in infinite specimens,
4) in general, no nucleation barrier exists for the formation of the first phase though a nucleation barrier is possible for a later forming phase.

He develops his model based on the kinetic guideline that for a process comprised of steps in series, the slowness of each step in the series is added to determine the overall slowness of the process. This guideline relates to the addition of resistances in series in an electrical circuit where the total resistance, R_T, is determined from

$$R_T = R_1 + R_2 + R_3 \cdots \tag{5.1}$$

with each R_i representing the resistance of the individual resistors in the circuit. For the growth of an intermetallic layer, the "resistances" relate to the diffusion coefficients, D, and the interface reaction rates, k. Both the diffusion coefficient and the interface reaction rate are conductances, meaning they are the reciprocal of resistances. Thus, the resistance to diffusion is proportional to the inverse of the diffusion coefficient, and the resistance to the interface reaction is related to the inverse of the interface reaction rate. Since diffusion and the interface reaction are series processes these resistances are additive,

$$R=\frac{w}{D}+\frac{1}{k} \tag{5.2}$$

where w is the thickness of the layer. The growth of the intermetallic layer is related to the conductance, the reciprocal of this composite resistance:

$$\frac{\mathrm{d}w}{\mathrm{d}t}=\frac{1}{\frac{w}{D}+\frac{1}{k}} \tag{5.3}$$

Philibert develops his model for a hypothetical A-B system which contains one intermetallic phase, AB. Figure 5.1 shows the governing factors for intermetallic growth in this system taking A as the faster diffusing species in this couple. The processes occurring during intermetallic growth in the A-B system can be described based on the information in Figure 5.1:

$$\mathrm{A}_{\text{through AB}}\left(J_A\right)+\mathrm{B}\xrightarrow{k}\mathrm{AB}$$

The reaction at the A-AB interface is not considered because A is the faster diffusing species. The reaction at the A-AB interface would be

$$\mathrm{B}_{\text{through AB}}\left(J_B\right)+\mathrm{A}\xrightarrow{k'}\mathrm{AB}$$

The flux of B through the intermetallic, J_B, is much smaller than the flux of A in the first reaction. Since these two reactions describe parallel processes, the faster reaction is the one that dominates. Thus, the reaction at the A-AB interface can be ignored.

The equation for the growth rate of the intermetallic phase can be obtained from the first reaction above keeping in mind the "resistance" argument:

$$\frac{\mathrm{d}w_A}{\mathrm{d}t}=\frac{1}{\frac{w_A}{D_A}+\frac{1}{k}} \tag{5.4}$$

This equation is similar to Equation 5.3.

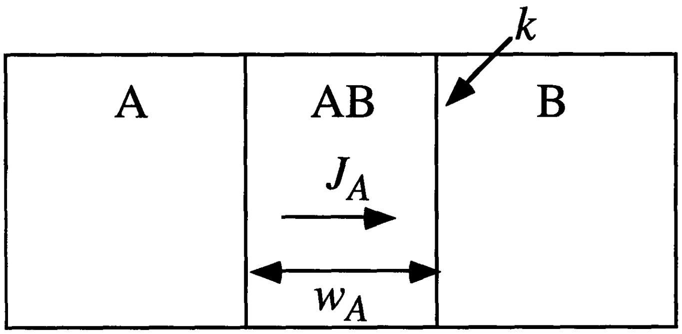

Figure 5.1: The governing factors for intermetallic growth in the hypothetical A-B system which contains one intermetallic phase, AB. A is taken as the faster diffusing species in this system. J_A is the flux of A through the intermetallic AB. w_A is the width of the intermetallic layer, and k is the reaction rate for the formation of AB at the interface.

For diffusion control, the interface reaction rate is considered to be very large compared to D_A: $k >> D_A$. Thus, Equation 5.4 would simplify to

$$\frac{\mathrm{d}w_A}{\mathrm{d}t} = \frac{D_A}{w_A} \tag{5.5}$$

The integration of Equation 5.5 results in the common diffusion controlled, parabolic growth law:

$$w_A^2 = D_A t \tag{5.6}$$

This model can be expanded to describe systems in which more than one intermetallic phase forms. This extension of the model is done for the copper-tin system which contains two low temperature intermetallic phases in Section 5.2 and for the nickel-tin system which has three low temperature intermetallics in Section 5.3. When there is more than one intermetallic layer in the system, the growth of one layer is coupled to the growth of the layers adjacent to it. The conductances related to growth of adjacent layers must be combined:

$$\frac{\mathrm{d}w_1}{\mathrm{d}t} = \frac{1}{\frac{w_1}{D_1}+\frac{1}{k_1}} - \frac{1}{\frac{w_2}{D_2}+\frac{1}{k_2}} \tag{5.7}$$

where

w_1 is the thickness of layer 1,
w_2 is the thickness of layer 2,
D_1 is the diffusion coefficient in layer 1,

D_2 is the diffusion coefficient in layer 2,

k_1 is the reaction rate for the formation of layer 1, and

k_2 is the reaction rate for the formation of layer 2.

The two terms in Equation 5.4 are subtracted because the formation of layer 2 is at the expense of layer 1. A similar equation can be written for the growth rate of layer 2. The full set of equations for a system containing two layers of intermetallic is derived in Section 5.2 when the copper-tin system is analyzed.

The resulting system of equations, one equation for the growth rate of each intermetallic layer, is useful in evaluating intermetallic formation. However, this evaluation is usually restricted to qualitative conclusions because there is little data on the interface reaction rates. Some insight can be gained from assessing the limiting cases of diffusion control and interface control. For diffusion control, the interface reaction rates would be very large such that the $1/k$ terms would be negligible, and for interface reaction control, the diffusion coefficients would be large so that the $1/D$ terms would be negligible. These assumptions greatly simply the growth rate equations as will be shown in the applications of this model in the following sections.

Additional insight is gained from looking at the bounds defined by setting the growth rates equal to zero. For example,

$$\frac{\mathrm{d}w_1}{\mathrm{d}t} = 0 = \frac{1}{\dfrac{w_1}{D_1} + \dfrac{1}{k_1}} - \frac{1}{\dfrac{w_2}{D_2} + \dfrac{1}{k_2}} \tag{5.8}$$

The right-hand side of Equation 5.5 defines a line in w_1-w_2 space. Examining the regions on either side of this line can explain the growth or lack of growth of a phase. On one side of the line the growth rate, $\mathrm{d}w_1/\mathrm{d}t$ is positive which would indicate a phase will grow, and on the other it is negative which indicates a phase would not grow. The analysis is applied to the copper-tin system in Section 5.2 and to the nickel-tin system in Section 5.3 and is the method Philibert uses to explain the experimental results cited at the beginning of this section.

5.2 Application to copper-tin system

Based on the experimental observations of non-parabolic growth and selective formation of the η phase in low temperature copper-tin couples, it was concluded that intermetallic growth in this system is not purely diffusion controlled at low temperatures. Thus, Mei's model, which assumes diffusion control, is not adequate for describing the copper-tin system. Philibert's model should be more accurate in predicting intermetallic growth in the copper-tin system because it includes both diffusion and interface control. Philibert's model has not previously been applied to a real system, however. Here, it is applied to the copper-tin system, and in the next section, it will be applied to the nickel-tin system.

To evaluate the copper-tin system in terms of Philibert's model, first, the processes taking place during the formation of the intermetallic layers must be considered. The copper-tin phase diagram is shown in Figure 2.5. Two intermetallic phases are stable in this system at low temperatures, the ε phase, Cu_3Sn, and the η phase, Cu_6Sn_5. Tin is the faster diffuser in this system[36,78,82,83] so the processes are determined with tin as the moving species. Several processes are occurring at once:

1) Tin is diffusing though the η phase.
2) The η phase is forming at the ε-η interface from the ε and the tin that just diffused through the η phase.
3) Tin is diffusing through the ε phase.
4) Copper and the tin that diffused through the ε phase combine to form more ε phase at the copper-ε interface.

These processes can be combined and written in the form of three reactions:

$$\mathrm{Sn}_{\text{though }\eta}(J_\eta) + \varepsilon \xrightarrow{k_1} \eta$$
$$\eta \xrightarrow{k_2} \varepsilon + \mathrm{Sn}_{\text{through }\varepsilon}(J_\varepsilon)$$
$$\mathrm{Sn}_{\text{through }\varepsilon}(J_\varepsilon) + \mathrm{Cu} \xrightarrow{k_3} \varepsilon$$

Figure 5.2 depicts the processes occurring between the tin and copper used to write these three reactions. No reactions at the tin-η phase interface are considered because the tin is the faster diffusing species in this system.

The growth of each intermetallic layer is governed by the rates of both the reactions and diffusion in the above processes and can be expressed by analogy to resistors in series in an electrical circuit as was described in the previous section:

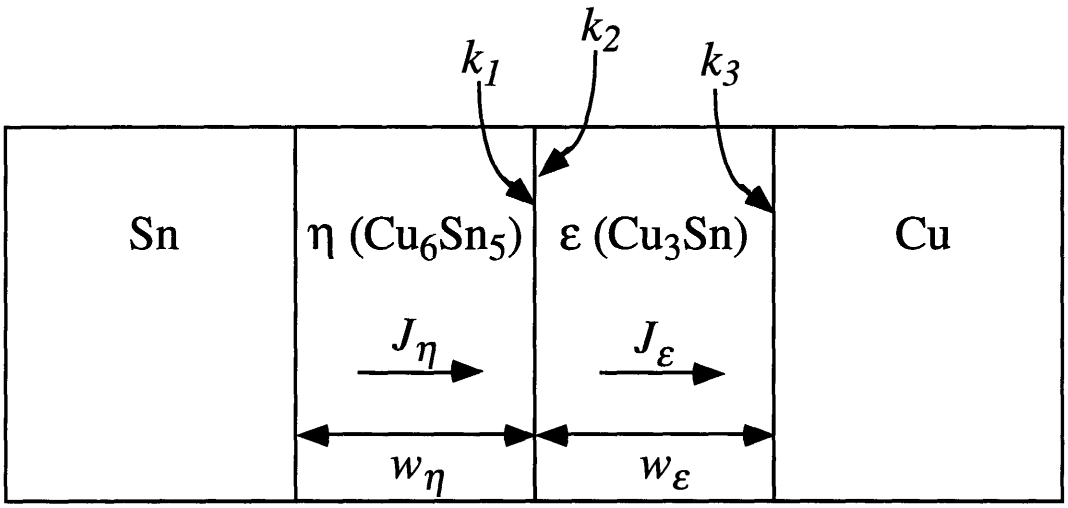

Figure 5.2: System used to determine the processes occurring during intermetallic formation between copper and tin. Tin is the faster diffusing atom. J_η and J_ε are the fluxes of tin through the η and ε intermetallic layers respectively. w_η and w_ε are the thicknesses of the layers, and k_1, k_2, and k_3 are the interfacial reaction rate constants.

$$\frac{\mathrm{d}w_\eta}{\mathrm{d}t} = \frac{1}{\frac{w_\eta}{D_\eta}+\frac{1}{k_1}} - \frac{1}{\frac{w_\varepsilon}{D_\varepsilon}+\frac{1}{k_2}} \tag{5.9}$$

$$\frac{\mathrm{d}w_\varepsilon}{\mathrm{d}t} = \frac{1}{\frac{w_\varepsilon}{D_\varepsilon}+\frac{1}{k_2}} + \frac{1}{\frac{w_\varepsilon}{D_\varepsilon}+\frac{1}{k_3}} - \frac{1}{\frac{w_\eta}{D_\eta}+\frac{1}{k_1}} \tag{5.10}$$

The variables in Equations 5.9 and 5.10 are defined Figure 5.2.

These equations define three regimes of growth in w_ε-w_η space demarcated by the lines determined by setting $\mathrm{d}w_\varepsilon/\mathrm{d}t$ and $\mathrm{d}w_\eta/\mathrm{d}t$ equal to zero:

$$\frac{\mathrm{d}w_\eta}{\mathrm{d}t} = 0 \Rightarrow w_\varepsilon = \frac{D_\varepsilon}{D_\eta} w_\eta + D_\varepsilon \left[\frac{1}{k_1} - \frac{1}{k_2}\right] \tag{5.11}$$

$$\frac{\mathrm{d}w_\varepsilon}{\mathrm{d}t} = 0 \Rightarrow \left(\frac{w_\varepsilon}{D_\varepsilon}\right)^2 - 2\frac{w_\varepsilon}{D_\varepsilon}\frac{w_\eta}{D_\eta} + E\frac{w_\varepsilon}{D_\varepsilon} + F\frac{w_\eta}{D_\eta} + G = 0 \tag{5.12}$$

where E, F, and G are constants:

$$E=\left[\frac{2}{k_1}-\frac{1}{k_2}-\frac{1}{k_3}\right] \tag{5.13}$$

$$F=-\left[\frac{1}{k_2}+\frac{1}{k_3}\right] \tag{5.14}$$

$$G=\left[\frac{1}{k_2k_3}-\frac{1}{k_1k_3}-\frac{1}{k_1k_2}\right] \tag{5.15}$$

For a first approximation, the interface reactions can be assumed to be non-rate limiting. For the reactions to be non-rate limiting, the reaction rates, k_1, k_2, and k_3, would be very large. Then, all the $1/k$ terms would approach zero, leaving the terms which only contain the diffusion coefficients:

$$\frac{\mathrm{d}w_\eta}{\mathrm{d}t}=0\Rightarrow w_\varepsilon=\frac{D_\varepsilon}{D_\eta}w_\eta \tag{5.16}$$

$$\frac{\mathrm{d}w_\varepsilon}{\mathrm{d}t}=0\Rightarrow w_\varepsilon=2\frac{D_\varepsilon}{D_\eta}w_\eta \tag{5.17}$$

As shown in Figure 5.3, these two equations, Equations 5.16 and 5.17, define nodal lines in w_ε-w_η space. These lines define three regions of intermetallic growth based on the signs of the derivatives on either side of each line. Equations 5.9 and 5.10 can be used to determine the signs of the derivatives in the various regions.[68] In region I in Figure 5.3, $\mathrm{d}w_\eta/\mathrm{d}t$ is negative and $\mathrm{d}w_\varepsilon/\mathrm{d}t$ is positive so the ε phase would grow while any existing η layer would be consumed. In region III, $\mathrm{d}w_\varepsilon/\mathrm{d}t$ is negative and $\mathrm{d}w_\eta/\mathrm{d}t$ is positive so the η phase would grow while any existing ε phase would be consumed. Only in region II, where both derivatives are positive, would both phases grow together.

For the copper-tin system, at low temperatures, it was concluded in the previous chapter that diffusion control alone could not accurately describe intermetallic growth. When both diffusion and the interface reactions are important, the lines defined by Equations 5.11 and 5.12 must be used to determine the growth of the layers. These lines are plotted in Figure 5.4. The only effect of including the interface reactions rates on the $\mathrm{d}w_\eta/\mathrm{d}t = 0$ line is translation of the intercept (compare Equation 5.16 to 5.11). The slope is still D_ε/D_η. Including the interface reaction rates makes the $\mathrm{d}w_\varepsilon/\mathrm{d}t = 0$ equation much more complex (compare Equation 5.17 to 5.12). However, the three regions described for the simpler case of diffusion control still exist.

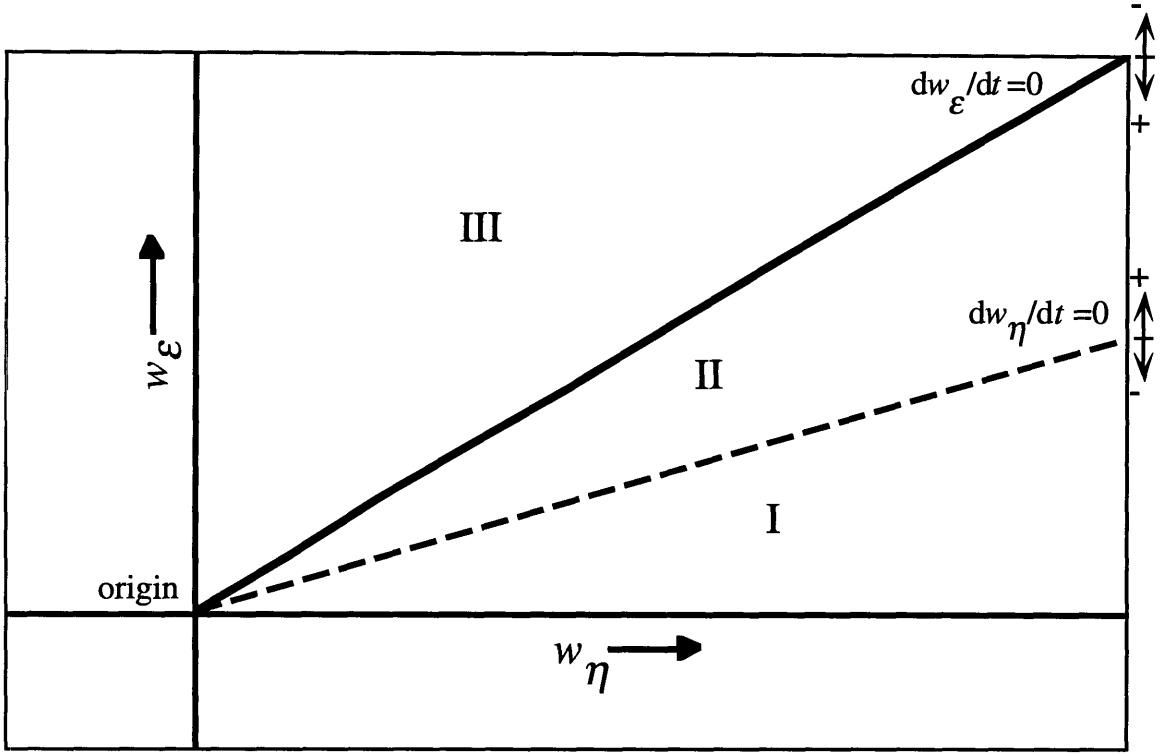

Figure 5.3: Regimes of intermetallic growth are defined by the nodal lines, $dw_\varepsilon/dt = 0$ and $dw_\eta/dt = 0$, in this plot. Diffusion control is assumed; the interface reactions are taken to be very fast. In region I, dw_η/dt is negative, so only the ε phase would grow, and any existing η phase would shrink. In region III, dw_ε/dt is negative so the η phase would grow and any existing ε layer would shrink. In region II, both phases would grow. Based on Philibert's model.[68]

The direction of the change in the intercept determines the order of phase growth. If the intercept of the $dw_\eta/dt = 0$ line is positive,

$$D_\varepsilon\left[\frac{1}{k_1}-\frac{1}{k_2}\right] > 0, \qquad (5.18)$$

then the origin will fall in region I and only the ε phase will form. If the intercept is negative, then the origin will fall in region II and both phases will form. This case is the one depicted in Figure 5.4. If the intercepts are shifted even farther into the negative range, the origin will fall in region III and only the η phase will form initially. Thus, the kinetics of the system, not the thermodynamic stability, determine which phase will form first.[68]

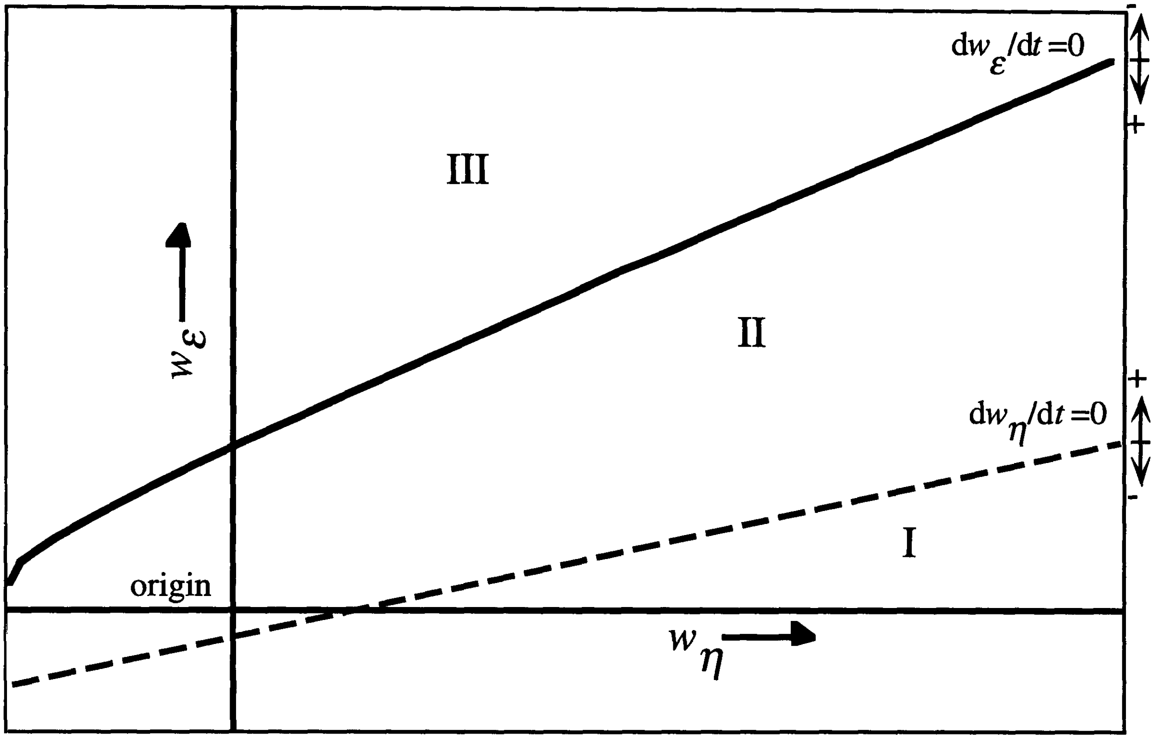

Figure 5.4: Regimes of intermetallic growth are defined by the lines, $\mathrm{d}w_\varepsilon/\mathrm{d}t$ = 0 and $\mathrm{d}w_\eta/\mathrm{d}t$ = 0. This plot illustrates the effect of combined interface and diffusion control. The interplay of the interface reaction rates determines intercepts of the nodal lines. In region I, $\mathrm{d}w_\eta/\mathrm{d}t$ is negative, so only the ε phase would grow, and any existing η phase would shrink. In region III, $\mathrm{d}w_\varepsilon/\mathrm{d}t$ is negative so the η phase would grow and any existing ε layer would shrink. In region II, both phases would grow.

Since little data on the interface reaction rates exists, experimental observations can be used to evaluate the model. At high temperatures, above 100°C, both the ε and the η phase are seen in copper-tin diffusion couples (refer to Table 4.6). This observation indicates the origin of the w_ε-w_η graph lies in region II as depicted in Figure 5.5. For this situation, no matter what the initial condition is, both intermetallic layers will appear in the couple upon aging. This is illustrated in Figure 5.5 by the progression of the three different starting conditions marked ①, ②, and ③. In each case both intermetallic phases are seen in the system immediately. However, both phases are not growing in each case.

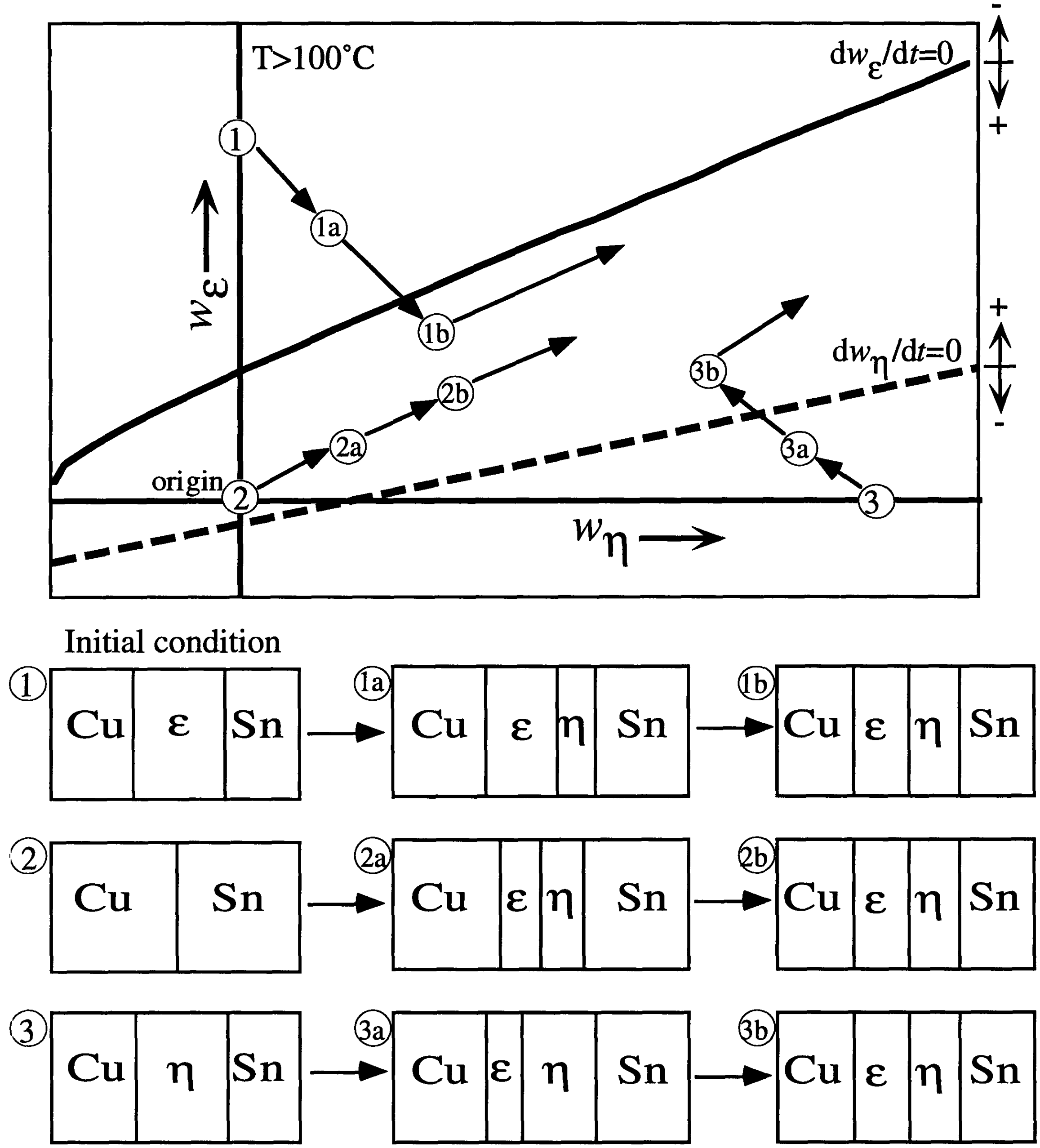

Figure 5.5: The various regimes of intermetallic growth in the copper-tin system for combined diffusion and interface control for temperatures greater than 100°C. The arrows indicate the progression of each couple over time. See the text for a full discussion of the progression from each initial condition; ①, ②, and ③.

For case ①, the ε phase already exists in the starting system. This point lies in region III which indicates that the η phase will from preferentially. Thus, the η phase grows while the ε phase shrinks. Both phases are seen in the couple, but only the η phase is growing initially. Eventually, the system crosses over into region II in which both intermetallic phases will grow. The progression for the initial condition marked ③ is similar except that it is the η phase that is present initially and the ε phase which forms preferentially until the system crosses into region II where both phases then grow. Only for case ②, which contains no intermetallic layers initially, do both intermetallic phases grow from the start.

At low temperatures, temperatures below 100 °C, only the η phase is seen initially in copper-tin couples. Observations of selective growth of the η phase were summarized in Table 4.6. These observations indicate that the origin is in region III as depicted in Figure 5.6. The main difference between this case and the previous shown in Figure 5.5 is for the starting condition without any intermetallic layers, represented by case ②. At high temperatures (Figure 5.5), both phases would grow in this couple, but at low temperatures (Figure 5.6), only the η phase grows at first. Thus, the arrow indicating the path this system takes follows the w_η axis until it reaches region II in which both phases will grow.

Comparing Figures 5.5 and 5.6, the shift in the lines with temperature can be seen. As the temperature increases, the lines shift upward such that the origin is moved from region III to region II. This shift reflects the preferential growth of the η phase at low temperatures, and the growth of both the ε and η phases at higher temperatures. However, this shift of the growth regions can not be extended to predict further shifting of the origin into region I where the ε phase would grow preferentially. At higher temperatures, other intermetallic phases exist in the copper-tin system (refer to the phase diagram in Figure 2.5). At 350°C, these other intermetallic phases start to appear and complicate the analysis. To accurately model higher temperature intermetallic growth in the copper-tin system, the model would have to include these intermetallics.

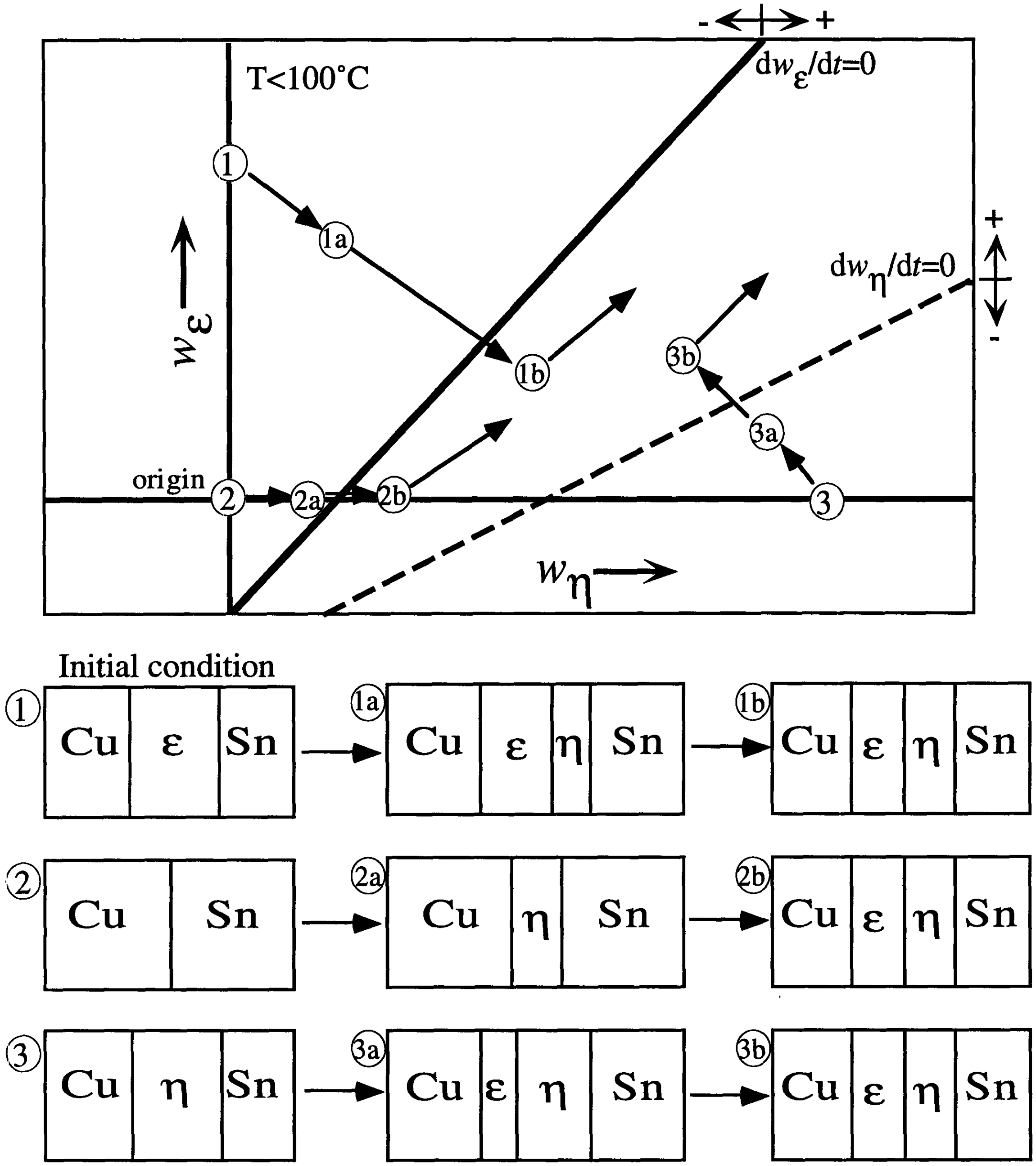

Figure 5.6: The various regimes of intermetallic growth in the copper-tin system for combined diffusion and interface control for temperatures less than 100°C. The arrows indicate the progression of each couple over time. See the text for a full discussion of the progression from each initial condition; ①, ②, and ③.

For the copper-tin system, the diffusion coefficients in the ε and η phase have been established for high temperatures (refer to Table 2.2 and Figure 2.11) but little work has been done on determining the interface reaction rates. From the experimental observations discussed previously, indicating that at low temperatures the η phase forms first and later the ε phase may form, qualitative statements can be made about the values of k_1, k_2, and k_3 at low temperatures.

Since initially only the η phase forms, region III is the one of interest. The origin must lie in this region so the nodal lines must be shifted down as shown in Figure 5.6. Thus,

$$D_\varepsilon\left[\frac{1}{k_1}-\frac{1}{k_2}\right]<0 \tag{5.19}$$

which means that $k_1 > k_2$. This result is logical looking back to the original reactions. The reaction which forms the η phase has the rate k_1, while the reaction which disassociates the η phase has the rate constant k_2. Since the η phase grows, one would expect k_1 to be greater than k_2.

The relative magnitude of k_3 can also be determined by looking at Equation 5.12. The w_ε intercept must be negative for the origin to be in region III. To determine the w_ε intercept, w_η can be set equal to zero in Equation 5.12. A quadratic equation in w_ε results. The quadratic formula can be used to find the two roots of this equation. Because the η phase forms first, the intercepts, which are given by the roots of the quadratic equation, must be negative.

The two roots of the equation are given by

$$w_\varepsilon=\frac{D_\varepsilon}{2}\left[\left[\frac{1}{k_3}+\frac{1}{k_2}-\frac{2}{k_1}\right]\pm\sqrt{\left(\frac{1}{k_3}-\frac{1}{k_2}\right)^2+\left(\frac{2}{k_1}\right)^2}\right] \tag{5.20}$$

The root which is physically significant, as shown in Appendix E, is the one with the plus sign in Equation 5.20. This root is negative when

$$\frac{2}{k_1}>\frac{1}{k_3}+\frac{1}{k_2}+\sqrt{\left(\frac{1}{k_3}-\frac{1}{k_2}\right)^2+\left(\frac{2}{k_1}\right)^2}\,. \tag{5.21}$$

Recalling that $k_1 > k_2$ it can be seen that $k_3 > k_1$. So the rank of the magnitudes of the interface reaction rates at low temperatures is

$$k_3>k_1>k_2 \tag{5.22}$$

Philibert's analysis ignores another reaction that occurs in intermediate phase formation. The omitted reaction is the one that occurs at the interface between the last intermetallic layer and the base metal that is not the fast diffusing species. Written in terms of the copper-tin system, that equation would be

$$\varepsilon \xrightarrow{k_4} (\mathrm{Cu}) + \mathrm{Sn}_{\mathrm{through\ (Cu)}}(J_{Cu})$$

where (Cu) indicates the copper solid solution and J_{Cu} is the flux of the tin in the copper solid solution. For the copper-tin system, this reaction is inconsequential because the diffusion coefficient of tin in copper is very small compared to that in the intermetallic phases. Thus, the flux J_{Cu} would be very small. Another indication that this reaction is not important is that several researchers have noted a lack of tin in the copper side of the diffusion couple. Kay and Mackay[76] observed little tin in the copper as well as no copper in the tin phase. Onishi and Fujibuchi[36] also noted that lack of the copper solid solution in their diffusion couples. These observations indicate that k_4 and J_{Cu} are both small and can be discounted, at least for the copper-tin system.

Analyzing intermetallic growth by examining the effects of both diffusion and interface reaction rates as outlined by Philibert[67,68] provides insight into the formation of the intermetallic layers. Particularly, it can explain why one phase will form before or in the absence of another phase despite the predicted thermodynamic stability of both phases. The analysis can be combined with experimental observations and applied to a specific system, as is done with the copper-tin system above, to provide qualitative estimates of the parameters and mechanisms involved in the intermetallic formation. In the next section this analysis is extended to a system with three intermetallic phases, the nickel-tin system. As in the copper-tin system, selective phase formation is observed experimentally in this system.

5.3 Application to nickel-tin system

The nickel-tin system was chosen for evaluation by Philibert's model for several reasons. The nickel-tin phase diagram, shown in Figure 2.1, indicates that three intermetallic phases, Ni_3Sn, Ni_3Sn_2, and Ni_3Sn_4, are thermodynamically stable at low temperatures. Thus, applying Philibert's model to this system requires extending the model to accommodate three intermetallic phases as compared to the two intermetallic phases modeled in the copper-tin system. Additionally, the nickel-tin system is a commonly studied system so ample experimental data exists for interpretation of Philibert's model.

However, the most significant reason for using Philibert's model to evaluate the nickel-tin is the observation of selective phase formation in nickel-tin couples. Selective phase formation in the nickel-tin system has been observed in aged samples in which tin was electroplated onto a nickel substrate[35,55,80] and in which nickel was dipped into molten tin.[35,76,84] Table 5.1 summarizes the experimental observations of selective phase growth in the nickel-tin system. The Ni_3Sn_4 intermetallic phase is usually the only phase seen in these samples. The only mention of all three phases forming is by Allen *et al.*[55] They found all three nickel-tin phases when the nickel substrate had been chemically or chemically-abrasively activated before the tin was electroplated onto the surface. When the nickel was not subject to any special treatment prior to plating with tin, only the Ni_3Sn_4 phase was observed. Based on these results, they conclude that it is a nucleation barrier that prevents the other nickel-tin intermetallics from forming. These observations of selective phase formation will be used later to interpret the model developed based on Philibert's theory.

To start, all the processes involved in intermetallic formation must be catalogued, as was done for the copper-tin system. Figure 5.7 shows the system and the processes involved. Taking the tin as the faster diffuser because tin has a much lower melting point than nickel, the processes occurring in this couple can be written:

$$\mathrm{Sn}_{\text{through Ni}_3\text{Sn}_4}(J_1)+\mathrm{Ni}_3\mathrm{Sn}_2 \xrightarrow{k_1} \mathrm{Ni}_3\mathrm{Sn}_4$$

$$\mathrm{Ni}_3\mathrm{Sn}_4 \xrightarrow{k_2} \mathrm{Sn}_{\text{through Ni}_3\text{Sn}_2}(J_2)+\mathrm{Ni}_3\mathrm{Sn}_2$$

$$\mathrm{Sn}_{\text{through Ni}_3\text{Sn}_2}(J_2)+\mathrm{Ni}_3\mathrm{Sn} \xrightarrow{k_3} \mathrm{Ni}_3\mathrm{Sn}_2$$

$$\mathrm{Ni}_3\mathrm{Sn}_2 \xrightarrow{k_4} \mathrm{Sn}_{\text{through Ni}_3\text{Sn}}(J_3)+\mathrm{Ni}_3\mathrm{Sn}$$

$$\mathrm{Sn}_{\text{through Ni}_3\text{Sn}}(J_3)+\mathrm{Ni} \xrightarrow{k_5} \mathrm{Ni}_3\mathrm{Sn}$$

The quantities in the reactions are defined in Figure 5.7.

Table 5.1: Observations of selective phase formation in the nickel-tin system

Application of tin	Temperature (°C)	Observations	Reference
plated	100 and 190	-only Ni_3Sn_4 for untreated nickel -all three phases when nickel surface activated prior to tin plating	Allen *et al.*[55]
dipped, plated	100-213	only Ni_3Sn_4	Olsen *et al.*[35]
plated	170	only Ni_3Sn_4	Kay and Mackay[80]
dipped	25-170	mainly Ni_3Sn_4 but a thin layer of an acicular phase not seen on the phase diagram	Kay and Mackay[76]
dipped	300-530	-Ni_3Sn_4 only for short times (< 30 seconds) -Ni_3Sn_2 and Ni_3Sn_4 for long times (>30 minutes)	Kang and Ramachandran[84]

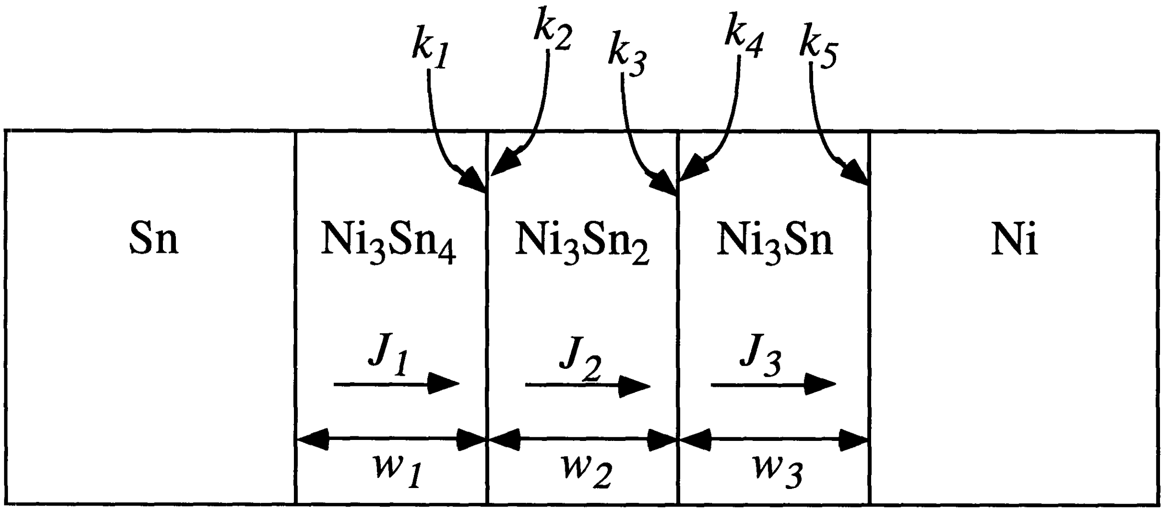

Figure 5.7: Processes occurring during intermetallic formation in the nickel-tin system. Tin is the faster diffusing atom. J_1, J_2, and J_3 are the fluxes of tin through each of the intermetallic layers. w_1, w_2, and w_3 are the thicknesses of the layers, and k_1, k_2, k_3, k_4, and k_5 are the interfacial reaction rate constants.

From these reactions, the equations governing the growth of each of the three intermetallic phases can be written:

$$\frac{dw_1}{dt}=\frac{1}{\frac{w_1}{D_1}+\frac{1}{k_1}}-\frac{1}{\frac{w_2}{D_2}+\frac{1}{k_2}} \tag{5.23}$$

$$\frac{dw_2}{dt}=\frac{1}{\frac{w_2}{D_2}+\frac{1}{k_2}}+\frac{1}{\frac{w_2}{D_2}+\frac{1}{k_3}}-\frac{1}{\frac{w_1}{D_1}+\frac{1}{k_1}}-\frac{1}{\frac{w_3}{D_3}+\frac{1}{k_4}} \tag{5.24}$$

$$\frac{dw_3}{dt}=\frac{1}{\frac{w_3}{D_3}+\frac{1}{k_4}}+\frac{1}{\frac{w_3}{D_3}+\frac{1}{k_5}}-\frac{1}{\frac{w_2}{D_2}+\frac{1}{k_3}} \tag{5.25}$$

In the above equations, the growth rate of an intermetallic layer is only a function of the processes in the layers adjacent to it. For instance, the width of the first layer and the diffusion coefficient in the first layer do not directly enter into the growth equation for the third layer. The growth of the first layer only indirectly affects the growth rate of the third layer through the growth rate of the second layer.

The bounds of the growth regimes can be found by setting each time derivative to zero. Since there are three intermetallic layers, three dimensions need to be considered: w_1, w_2, and w_3. The bounds of the growth regimes, then, are planes, not lines as they were in the two dimensional copper-tin case. The equations including both the interface reaction rates and the diffusion coefficients are quite complex. It is illustrative to look at the limiting case of diffusion control. If diffusion control is assumed, it implies that the interface reaction rates are fast. Thus, the k values are large and the $1/k$ terms all go to zero. The resulting equations for the limiting planes are

$$\frac{dw_1}{dt}=0\Rightarrow\frac{w_2}{D_2}=\frac{w_1}{D_1} \tag{5.26}$$

$$\frac{dw_2}{dt}=0\Rightarrow\frac{w_2}{D_2}=\frac{2\frac{w_1}{D_1}\frac{w_3}{D_3}}{\frac{w_1}{D_1}+\frac{w_3}{D_3}} \tag{5.27}$$

$$\frac{dw_3}{dt}=0\Rightarrow\frac{w_3}{D_3}=\frac{2w_2}{D_2} \tag{5.28}$$

These equations are each plotted separately in Figure 5.8. To determine the regimes of intermetallic growth, the bounds defined by the three planes must be overlaid to determine the growth regimes. Figure 5.9 shows all three planes graphed together.

The different volumes defined by the intersection of the planes each represent a different growth region just as the different areas in the two dimensional plot for the copper-tin system defined growth regimes. The signs of the derivatives indicate which phase or phases will grow in a given region. Equations 5.23-5.25 can be used to determine the sign of the derivatives on each side of the planes:

- dw_1/dt is positive above and negative below its zero plane.
- dw_2/dt is positive below and negative above its zero plane.
- dw_3/dt is positive above and negative below its zero plane.

The sign of the derivative is indicated for each plane by the arrows on the right in Figure 5.8.

From the signs of the derivatives, the volumes corresponding to the different growth regimes can be identified. For example, all three intermetallic layers grow in the volume in which all three derivatives are positive. This volume is the one above the dw_1/dt plane, below the dw_2/dt plane, and above the dw_3/dt plane. The various growth regions are summarized in Table 5.2.

Table 5.2: Various growth regions for the nickel-tin system.

Phases that grow in region defined by →	Direction from dw_1/dt zero plane	Direction from dw_2/dt zero plane	Direction from dw_3/dt zero plane
Ni_3Sn_4, Ni_3Sn_2, and Ni_3Sn	above	below	above
only Ni_3Sn_4	above	above	below
only Ni_3Sn_2	below	below	below
only Ni_3Sn	below	above	above
Ni_3Sn_4 and Ni_3Sn_2	above	below	below
Ni_3Sn_4 and Ni_3Sn	above	above	above
Ni_3Sn_2 and Ni_3Sn	below	below	above

a) $dw_1/dt = 0$

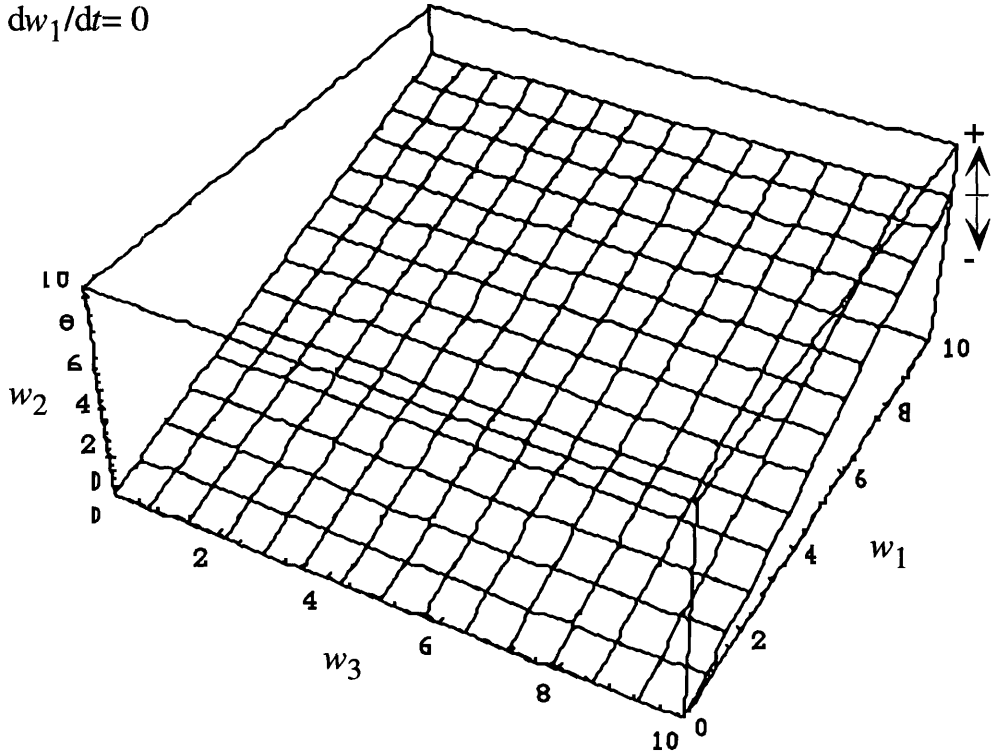

b) $dw_2/dt = 0$

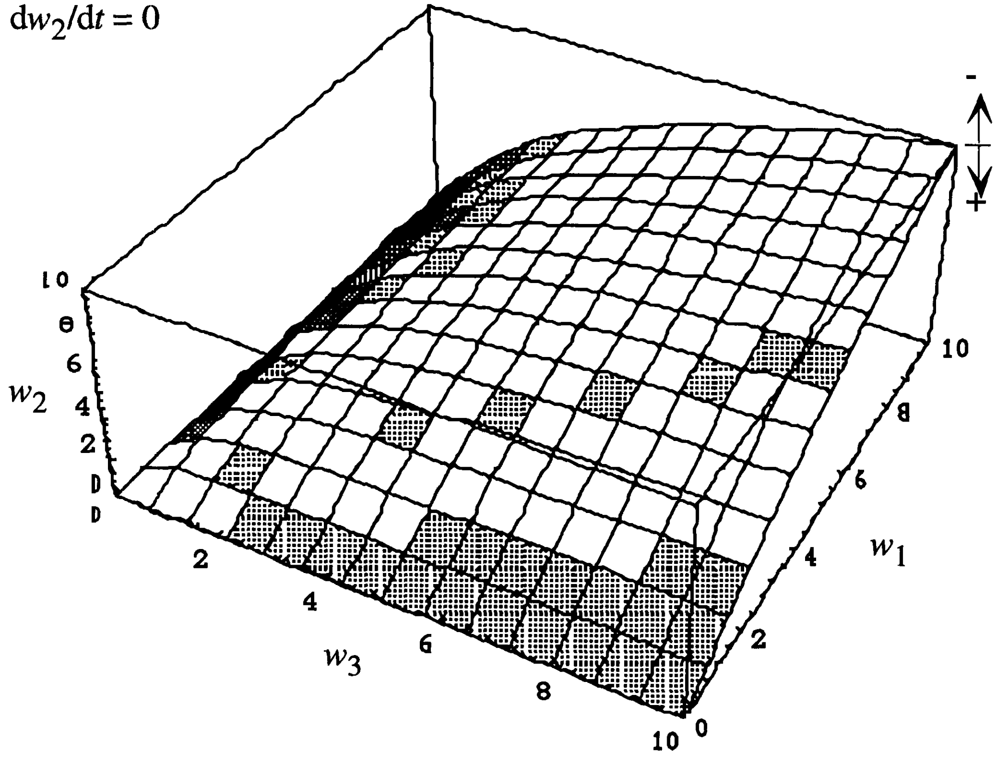

c) dw_3/dt = 0

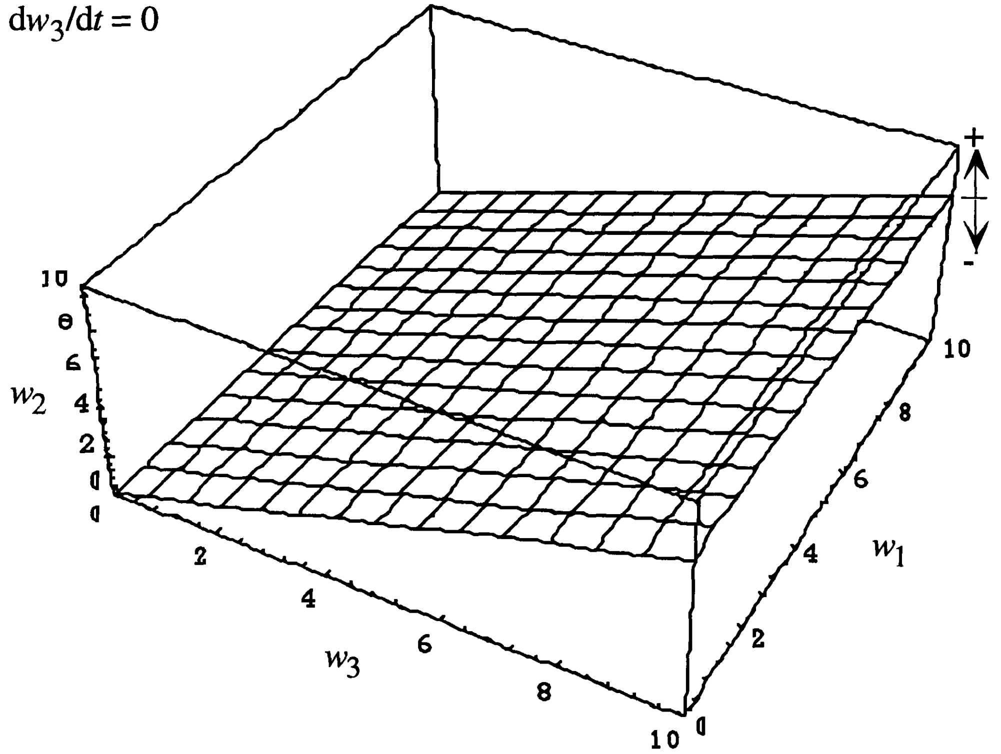

Figure 5.8: The three limiting planes for the diffusion controlled case of intermetallic formation in the nickel-tin system. The intersections of these planes define the various regimes of intermetallic growth. The signs of the derivatives in each region determine whether a phase grows or not. (a) dw_1/dt = 0 (Equation 5.26), (b) dw_2/dt = 0 (Equation 5.27), and (c) dw_3/dt = 0 (Equation 5.28).

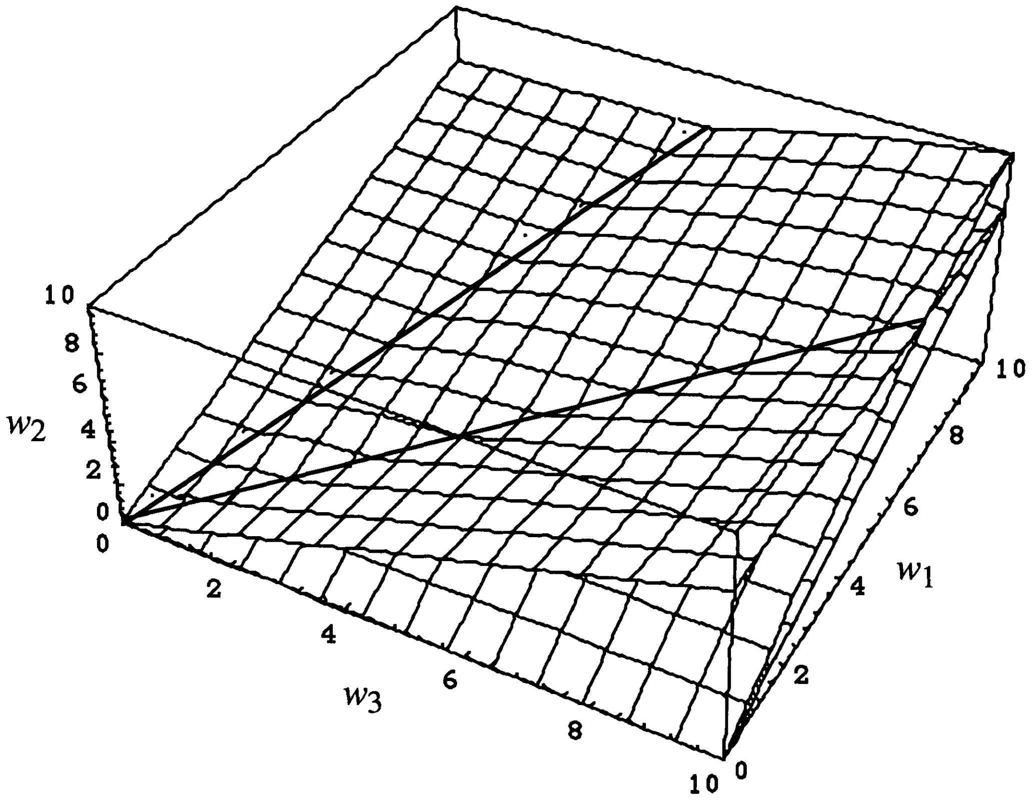

Figure 5.9: Overlay of the three limiting planes for the case of diffusion control. The volumes partitioned by the planes and their intersections define the various growth regimes of the nickel-tin intermetallics.

Since selective phase formation is seen in the nickel-tin system, diffusion alone will not completely describe intermetallic growth. The full equations which incorporate the interface reactions rates must be used. Including the interface reaction rates in the equations for the boundary planes only shifts the planes for $dw_1/dt = 0$ and for $dw_3/dt = 0$. The effect on the $dw_2/dt = 0$ plane is more complex as can be seen in Equation 5.24. An example of how the planes can be shifted by the reaction rates is shown in Figure 5.10. The three planes are overlaid in Figure 5.11.

The growth regions are defined in the same way they were for the diffusion controlled case. The sign of a derivative above its zero plane is the same as in the diffusion control case so the volumes defined in Table 5.2 hold for these planes as well.

The origin can be placed in the correct growth region by considering the experimental data on intermetallic growth in the nickel-tin system. The Ni_3Sn_4 phase is the first phase and usually the only phase that is seen in nickel-tin couples as was discussed at the beginning of this chapter and is summarized in Table 5.1. This observation indicates that the origin is in the region where only Ni_3Sn_4 forms, the volume above the dw_1/dt plane, above the dw_2/dt plane and below the dw_3/dt plane. This region is indicated in Figure 5.11.

Additionally, Kang and Ramachandran[84] found both Ni_3Sn_4 and Ni_3Sn_2 in their nickel-tin couples after long times(refer to Table 5.1). The experiments are the highest temperature experiments listed for the nickel-tin system. Based on these observations, it can be inferred that as the temperature increases, the planes shift such that the origin moves towards the volume in which both of these phases grow, the volume above the dw_1/dt plane, below the dw_2/dt plane and below the dw_3/dt plane.

Philibert's model is valuable because it provides a context for evaluating mixed diffusion and interface control of intermetallic formation. Selective phase growth can be explained with this model as was illustrated with both the copper-tin system and the nickel-tin system. The mathematical manipulation required in Philibert's model is limited to algebra. This makes the model much simpler to evaluate than Mei's model which requires some calculus to solve the non-linear system of equations. The results of applications of Philibert's model can be easily graphed if less than three intermetallic phases are involved. The model can be applied to systems with more than three intermetallic layers. However graphical interpretation in four or more dimensional space is difficult though not out of the question.

a) dw_1/dt = 0

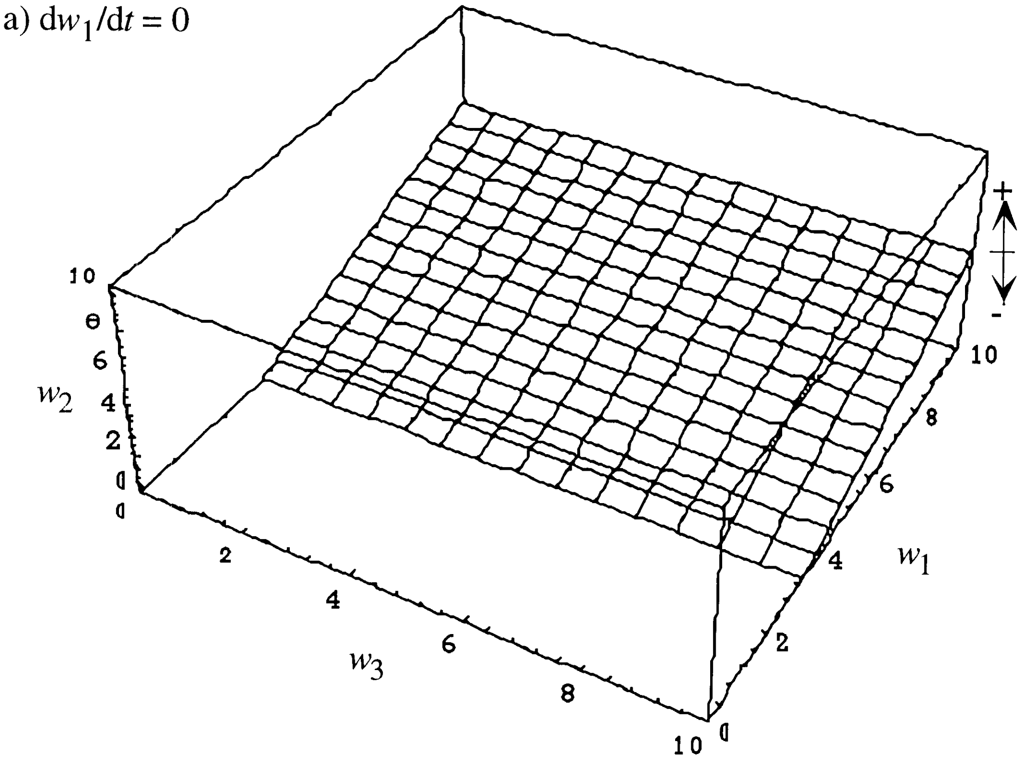

b) dw_2/dt = 0

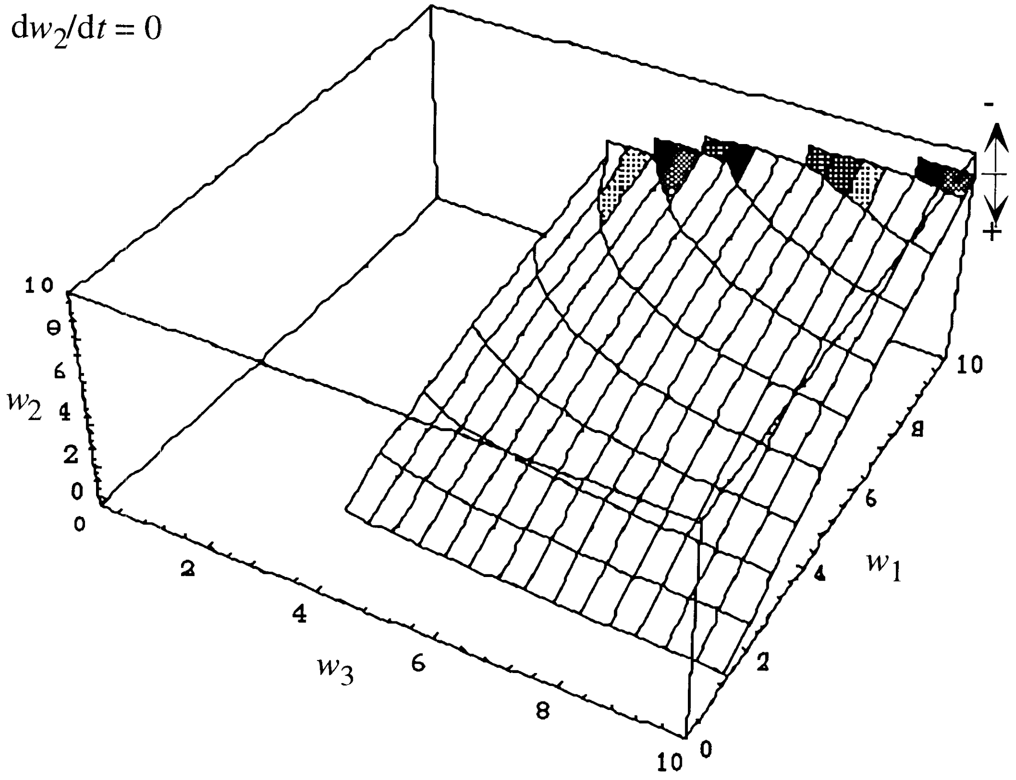

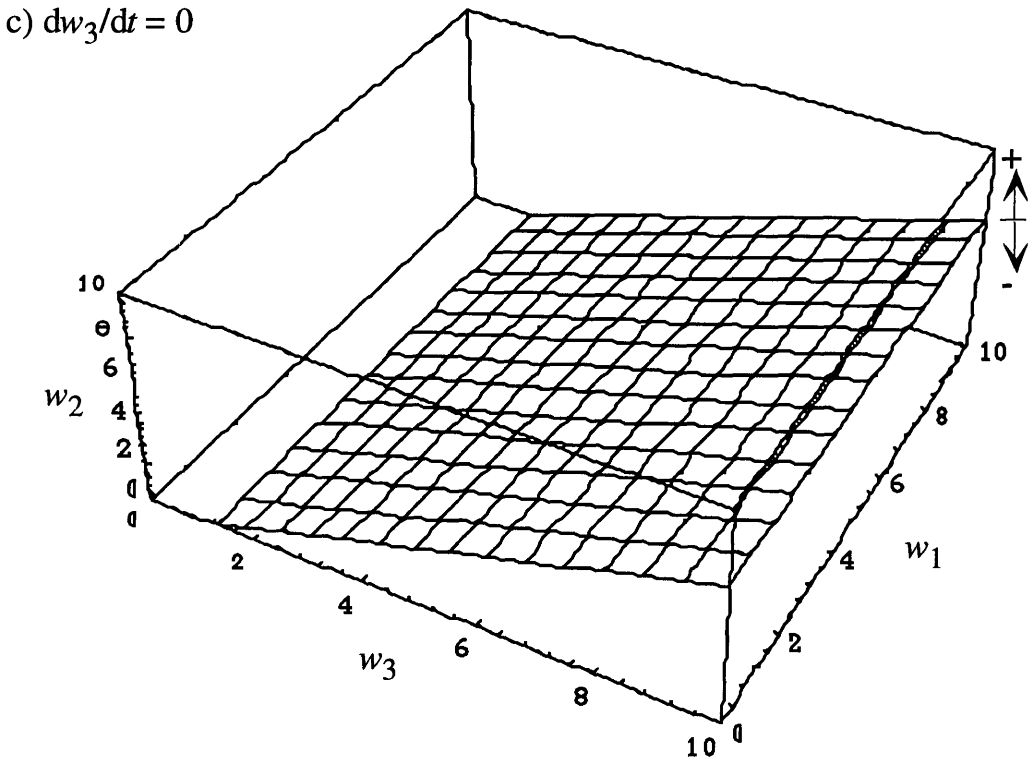

Figure 5.10: The three limiting planes for the case of mixed diffusion and interface control of intermetallic formation in the nickel-tin system. The volumes partitioned by the planes and their intersections define the various regimes of intermetallic growth. The signs of the derivatives in each region determine whether a phase grows or not. (a) $dw_1/dt = 0$ (Equation 5.23), (b) $dw_2/dt = 0$ (Equation 5.24), and (c) $dw_3/dt = 0$ (Equation 5.25).

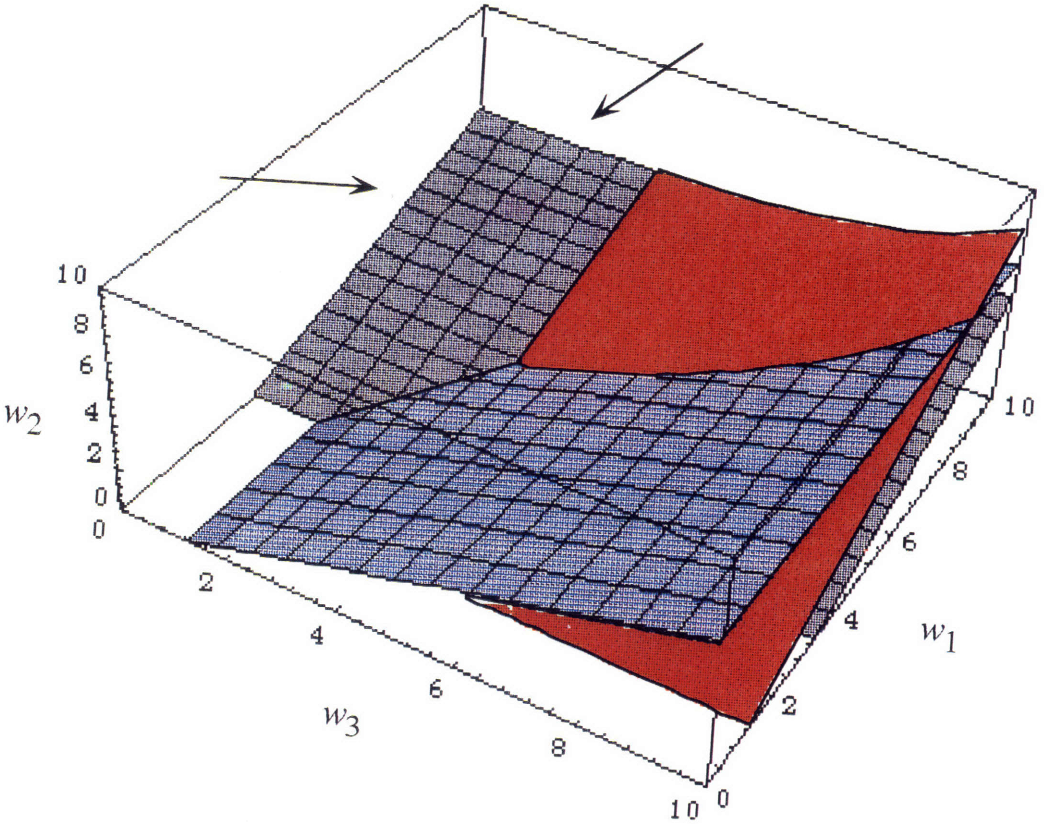

Figure 5.11: Overlay of the three limiting planes for the case of mixed diffusion and interface control. The volumes partitioned by the planes and their intersections define the various growth regimes for the nickel-tin intermetallic phases. The volume in which the origin should lie for low temperatures is indicated by the arrows. This volume is under the gray plane and above the red and blue planes.

6. Summary and Conclusions

6.1 Summary

6.1.1 Diffusion in intermetallic phases

Two sets of factors, chemical and physical, that affect diffusion were discussed as they apply to intermetallic phases. The chemical factors examined were bond character and chemical potential. Bond character in an intermetallic can be inferred from a combination of heat of formation, electronegativity difference, and size difference. A correlation between metallic bonding and fast diffusion was shown to exist.

Chemical potential gradient is the true driving force for diffusion. The diffusion coefficient is the product of the derivative of the chemical potential with respect to concentration and the mobility. The derivative of the chemical potential can be calculated from the activity data and then, coupled with data on the diffusion coefficient, the mobility can be determined. The mobility was calculated in the this manner for two copper-zinc intermetallics which exhibit fast diffusion and for an iron-aluminum intermetallic which does not exhibit fast diffusion. The differences seen in the mobilities cannot be explained with bonding and structural arguments since all three systems are very similar in these respects. This method allows for separation of the diffusion coefficient into a thermodynamic component, represented by the derivative of the chemical potential, and a physical component, represented by the mobility.

The physical factors that were evaluated were crystal structure, grain boundaries and interface structure. Crystal structures of intermetallics often have a significant amount of free space which implies the energetic barrier to migration of the atoms is lower than in close packed structures. Intermetallics often have defects that are inherent to their structures because the structures have to accommodate a range of compositions. These defects can help to enhance diffusion. An analysis of the copper-, nickel-, and iron-tin intermetallics based on crystal structures was able to rationalize the slow diffusion seen in the iron-tin system, but it could not differentiate between diffusion in the copper-tin system and the nickel-tin system though diffusion in the copper-tin system is faster than that in the nickel-tin system.

Grain boundary diffusion is faster than diffusion through the bulk material. The density of grain boundaries is a factor in determining the degree to which grain boundary diffusion contributes to the overall diffusion rate. Temperature and the magnitude of D_{gb} also influence the impact of grain boundary diffusion. The contribution of grain boundary diffusion to the observed diffusion rate was calculated for two copper-tin cases. In both, the contribution of grain boundary diffusion was found to be negligible.

The interface between the intermetallic and the base metal is not always planar. Rough interfaces can have two or more times as much surface area as flat ones. The larger area can influence diffusion to some degree. However, the area of the interface has more effect on the rate of an interface reaction. Since interface reaction rates were shown to be important to intermetallic growth in the copper-tin and nickel-tin systems, the roughness of the interface cannot be ignored.

All of these factors that affect diffusion are interdependent. No one factor can be separated from the others and used to explain diffusion rates in intermetallics. Since the nature of the interactions of these factors is still unknown, a comprehensive hypothesis cannot be developed. Hypotheses based on only certain aspects of diffusion are not unique or encompassing. Another hypothesis based on a different set of characteristics may be just as accurate and predictive.

6.1.2 Models of intermetallic growth

Two existing models of intermetallic growth were discussed and expanded upon. Mei's model, a diffusion-based model, was shown to be inadequate for describing low temperature growth of intermetallics in the copper-tin system. Mei's results could not be reproduced. Instead, another set of solutions to the basic modeling equations were determined in this work. The solutions developed here fulfill the modeling equations but do not correlate with experimental observations at the same temperatures. Mei's solutions do match experimental observations but do not satisfy the modeling equations. It was concluded that the model is unstable because intermetallic growth in the copper-tin system is not controlled purely by diffusion. This model would be useful for evaluating intermetallic growth that is purely diffusion controlled because it is very complete and quantitative, though complex to solve.

Philibert's model was introduced because it includes both diffusion and interface control. Applications of this model to the copper-tin and nickel-tin systems were able to explain the selective phase formation seen in both systems and account for non-parabolic growth in the copper-tin system. Quantitative use of Philibert's model is limited by the lack of data on interface reaction rates. Qualitative understanding of the results is possible with graphical methods and limit analysis.

6.2 Conclusions

Four conclusions can be drawn from this work:

- The observed kinetics of intermetallic growth in the copper-tin and nickel-tin systems at low temperature are inconsistent with pure diffusion control. Growth in these systems must involve mixed diffusion and interface control.

- Fast diffusion in certain intermetallic phases can be rationalized by considering basic factors such as bonding and crystal structure. It is not helpful to postulate complex mechanisms to explain fast diffusion since the interactions of the factors that influence diffusion are not understood well enough to differentiate between hypotheses.

- The predictive capability of two existing models of intermetallic growth evaluated here is limited. Mei's model is adequate for systems in which diffusion is the only controlling mechanism, but intermetallic formation at low temperatures is not purely diffusion controlled. Philibert's model is more complete in that it includes both diffusion and interface control, but quantitative predictions cannot be made due to the lack of the availability of data on the intermetallic systems.

- Accurate predictions of intermetallic growth rates must be based on empirical data. Too many factors influence the growth of intermetallic phases to be combined into a general predictive model.

7. Future work

Several areas of further work are suggested by the conclusions presented here. For one, all the diffusion coefficients reported for the copper-tin intermetallics are based on intermetallic layer growth measurements. Since intermetallic growth is not purely diffusion controlled, calculation of the diffusion coefficients based on the assumption that growth is diffusion controlled may be incorrect. A better method for determining the diffusion coefficients would be the more traditional tracer diffusion experiment. Schaefer *et al.*[85] have perfected a process for producing bulk samples of copper-tin intermetallic compounds. These bulk samples could be plated with a radioactive tracer, heat treated, and sectioned accordingly to determine the true diffusion coefficient in the intermetallic. The diffusion coefficients would then be more likely to represent diffusion through the intermetallic and could be used to provide insight into intermetallic growth and to develop more accurate models. Additionally, experimental determination of the grain boundary diffusion coefficient and the volumetric diffusion coefficient in these intermetallic samples would be useful in assessing the effect of grain boundaries on intermetallic growth.

Several researchers[3,8] have noted that the morphology of the intermetallic that forms at a liquid-solid interface is different than that of the intermetallic that forms from solid state diffusion. The majority of research on intermetallic growth has been done on solid state growth. A better understanding of how intermetallic formation is different at a liquid-solid interface is essential for applications such as TLP bonding and brazing.

Since Mei's model is comprehensive in describing diffusion controlled growth, adapting it for a system in which intermetallic growth is diffusion controlled would be useful. Mei's model could also be expanded to other diffusion controlled, multiple layer growth problems, not strictly intermetallic growth. Oxidation and carburization would be two areas where Mei's model could be useful. Since Mei's model includes equations for the concentration profiles in the base metal, the effects of a surface treatment on the base metal of a coated piece could be determined.

The interface reaction rates for intermetallic formation need to be determined for a system so a more rigorous evaluation of Philibert's[67,68] approach could be carried out. This approach shows promise for developing a predictive model of intermetallic growth, but more experimental data is necessary to assess the possibilities quantitatively. However, interface reaction rates are usually thought to be "beyond experimental determination."[68]

The development of a model for intermetallic growth would have several practical applications. Much use could be made of a model such as Mei's, which could determine the interdiffusion coefficients from layer thickness measurements as a function of time.

With only a few experiments to measure the thickness of the intermetallic layers as a function of time at a certain temperature, the interdiffusion coefficients could be determined for the intermetallic layers. These interdiffusion coefficients could then be used in the model to predict intermetallic growth at that temperature for many different situations. If the intermetallic thickness experiments are conducted at several different temperatures, then the temperature dependence of the interdiffusion coefficient could be determined, and the model could be used for a range of temperatures, including temperatures which were not specifically tested.

The ability to predict intermetallic layer thickness would be useful in evaluating the aging of pre-tinned components since the growth of intermetallic layers can effect the wettability of the solder.[3,4] The growth of intermetallic layers in joints that are thermally cycled, such as those found in a computer chip or an aircraft engine, could also be modeled. Coupled with knowledge of the effect of the intermetallic layer on the mechanical strength of the joint, intermetallic growth predictions could be used to design inspection and replacement schedules.

An intermetallic growth model could also be used to predict bonding time for TLP joints. Looking at the joint as two symmetrical halves, the joint solidifies when the advancing layers meet at the midpoint of the original interlayer. Even dissimilar material joints could be modeled in this manner by calculating the rate of advance of the solidification front for each side of the joint. Then, a balance of the two rates could be done to see when and where the solidification fronts would meet.

Appendix A

Linear approximation of activity as a function of composition

For most intermetallic compounds data on the activity only exists for the phase boundaries. With only these two points, the only reasonable approximation one could make would be a linear one. However, there would be no way of knowing if a linear fit was a sound assessment.

For a few compounds, activity data through the intermetallic phases exist. The data on these compounds can be used to indicate whether or not a linear fit is generally appropriate for fitting the activity data as a function of composition in an intermetallic phase. Table A.1 lists the intermetallic compounds for which data on the activity of the components in the intermetallic exist. All the activity data are from *Selected Values of the Thermodynamic Properties of Binary Alloys*.[49] The activity data for these compounds have been fit to a line. The correlation coefficient, R^2, which indicates the closeness of the fit, $R^2 = 1$ being a perfect fit, for this linear fit of the activity as a function of composition is also reported in Table A.1. Since most of the R^2 values are close to one, a linear fit of the activity data is acceptable.

Table A.1: Correlation coefficient, R^2, for a linear fit of the activity data in several intermetallic phases.

Intermetallic	Temperature	Element	R^2 for a linear fit
β-FeAl	900°C	Fe	0.9730
		Al	0.8854
β'-AlNi	1000°C	Al	0.6464
		Ni	0.9275
β-$MgCu_2$	477°C	Mg	0.9775
		Cu	0.9621
β-CuZn	500°C	Cu	0.9994
		Zn	0.9957
γ-Cu_5Zn_8	500°C	Cu	0.9361
		Zn	0.9669
ε-(CuZn)*	500°C	Cu	0.9457
		Zn	0.9960

---

* No formula is used to describe the ε-(CuZn) phase. The composition of this phase at 500°C ranges from 23.9 to 15.3 atomic percent copper.

The two R^2 values that are very low compared to the others, the correlation coefficient for Al in AlNi and for Al in FeAl, can be attributed to the fact that the activity for these components gets very small in the intermetallic phase. For example, the activity of Al in the AlNi intermetallic goes from 0.0775 to 0.0000433 across the intermetallic phase. As the activity approaches zero, it tends to flatten out in an exponential fashion. Refer to Figure 3.8 where the activities of Al and Ni in the AlNi intermetallic are shown. This flattening of the activity throws off the linear curve fit for these phases.

Appendix B

Comparison of the area of a flat and a rough interface

The surface area of a rough interface is greater than that of a flat one. By assuming a simple geometry for the rough interface, the amount of increase in the surface area can be determined. The ratio, R, that describes the increase in area is

$$R = \frac{A_r}{A_f} \tag{B.1}$$

where A_r is the surface area of a rough interface and A_f is the area of the corresponding flat interface.

Several different geometries could be assumed for the shape of the rough interface. The simplest is one based on hemispherical caps. A cross-sectional view of this interface is shown in Figure B.1.

To determine the ratio of the areas the top view of the interface is helpful. The top view of the interface is shown in Figure B.2. The area of the rough interface outlined by the dark square can be calculated and compared to the area of the flat interface.

The area of the flat interface for this case is equal to the area of the square. The length of the side of the square is $2r$, where r is the radius of the hemispherical caps of the rough interface model. Thus,

$$A_{f1} = (2r)^2 = 4r^2 \tag{B.2}$$

The area of the rough interface in this square has two components. One part is the four quarters of the hemispherical caps, and the other is the space between the caps. The area of the four quarters of the cap is just one half the surface area of a sphere, $\frac{1}{2}(4\pi r^2)$. The area of the space between the caps is equal to the area of the square, $4r^2$, minus the area of the circle defined by the cap, πr^2. The equation of the area of the rough interface is then

$$A_{r1} = \frac{1}{2}\left(4\pi r^2\right) + \left[4r^2 - \pi r^2\right] \tag{B.3}$$

Figure B.1: Cross-section of the geometry assumed for a rough interface. The radius of the hemispherical caps that are used to model the rough interface is denoted r.

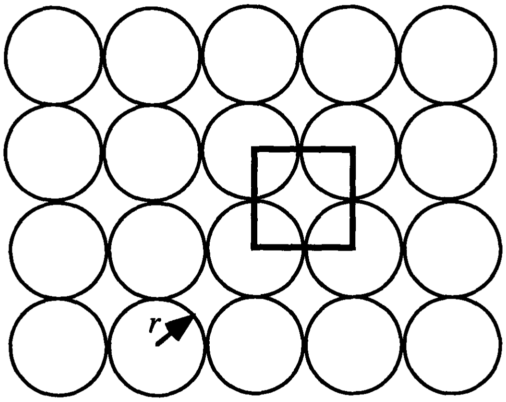

Figure B.2: Top view of the rough interface. The dark box outlines the region for which the area of the interface is calculated.

From Equation B.2 and B.3, the ratio of the two areas can easily be determined:

$$R_1 = \frac{A_{r1}}{A_{f1}} = \frac{\pi + 4}{4} \approx 1.8 \qquad \text{(B.4)}$$

Another packing scheme is possible for the hemispherical caps. This arrangement is shown in Figure B.3. The area of the flat interface for this case is equal to the area of the rhombus outlined in Figure B.3. The area of a rhombus is equal to the base times the height. The base of the rhombus is $2r$. Determining the height requires some elementary trigonometry. The acute angle of the rhombus is 60°. Thus, the height of the rhombus is one leg of a 30°-60°-90° triangle shown in Figure B.3. This height is equal to $r\sqrt{3}$. The area of the flat interface for this case is

$$A_{f2} = b \cdot h = 2r \cdot r\sqrt{3} = 2r^2\sqrt{3} \qquad \text{(B.5)}$$

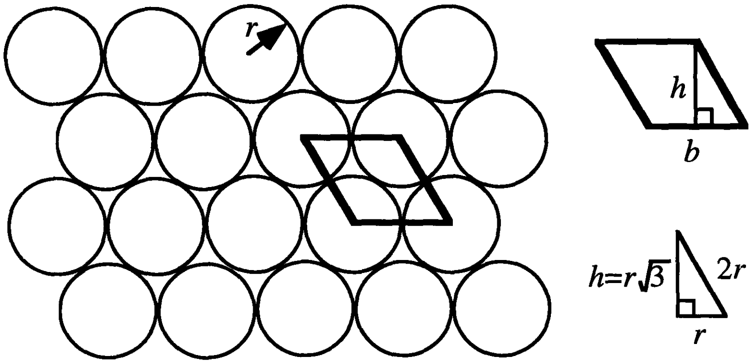

Figure B.3: Alternate top view of the rough interface. The dark box outlines the region for which the area of the interface is calculated.

The area of the rough interface contained in the dark box is similar to that calculated above. As before, there is one complete hemispherical cap in the box and then some area in between the caps. The area in between the caps can be determined from subtracting the area of the circle cut by the cap from the area of the rhombus. Thus, the area of the rough interface is

$$A_{r2} = \frac{1}{2}\left(4\pi r^2\right) + \left[2r^2\sqrt{3} - \pi r^2\right] \tag{B.6}$$

and the ratio of the two areas is

$$R_2 = \frac{A_{r2}}{A_{f2}} = \frac{\pi + 2\sqrt{3}}{2\sqrt{3}} \approx 1.9 \tag{B.7}$$

So for both cases the area of the rough interface was about twice the area of the corresponding flat interface. This is an average calculation though. The rough interface could be much flatter or much rougher as shown by the cross sections of interfaces in Figure B.4.

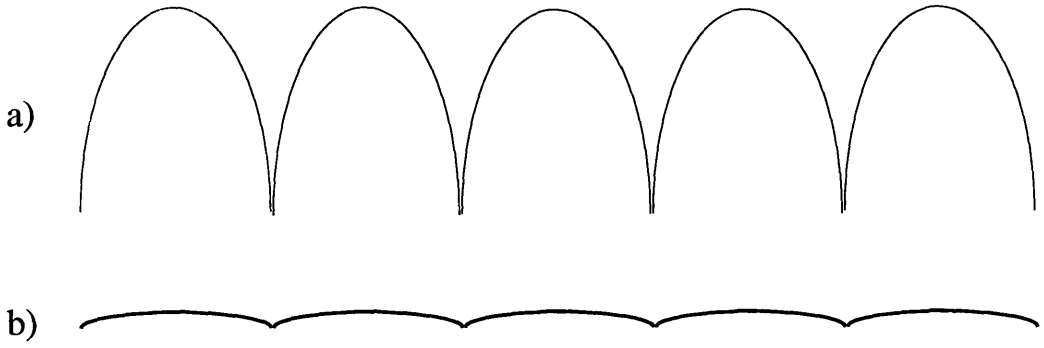

Figure B.4: (a) A rough interface that would have much more than twice the area of a flat interface and (b) a rough interface that would have only slightly more area than a flat one.

Appendix C

Model developed based on Mei's modeling equations[32] written in Mathematica

```
(* Mei's modeling equations for diffusion couple of Cu-Sn.
Results are shown in itallics *)

(* T= 190C, all in cm ,s, g, C *)
(* initial conditions and resetting of variables *)
r12 =.
ren =.
rns =.
g[1]=.
g[2]=.
g[3]=.
dn =.
de =.
co = 1.00;
co1 = 0.993;
ce1 = 0.765;
ce2 = 0.755;
cn2 = 0.549;
cn3 = 0.541;
cs3 = 0.00006;
cs = 0;
ke = 5.21 10^-7;
kn = 9.39 10^-7;
dcu = 3.08 10^-21;
de = ((ke/2 + g[1] Sqrt[dcu])/g[2])^2;
dn = ((kn/2 + g[2] Sqrt[de])/g[3])^2;
ds = 4.49 10^-7;
r12 = dcu/de;
ren = de/dn;
rns = dn/ds;


y[1] = (Exp[-g[1]^2] (co-co1))/(1+Erf[g[1]])
     -((ce1-ce2) Exp[-g[1]^2 r12]/(Erf[g[2]]-Erf[g[1]
Sqrt[r12]])) (1/Sqrt[r12])
     - g[1] Sqrt[N[Pi, 10]] (co1-ce1)


y[2]= Exp[-g[2]^2] (ce1-ce2) / (Erf[g[2]]-Erf[g[1]
Sqrt[r12]])
     - ((cn2-cn3) Exp[-g[2]^2 ren] / (Erf[g[3]]-Erf[g[2]
Sqrt[ren]])) (1/Sqrt[ren])
     - g[2] Sqrt[N[Pi, 10]] (ce2-cn2)


y[3]=Exp[-g[3]^2] (cn2-cn3) / (Erf[g[3]]-Erf[g[2] Sqrt[ren]])
     - ((cs3-cs) Exp[-g[3]^2 rns])/(Sqrt[rns] (1-Erf[g[3]
Sqrt[rns]]))
```

```
     - g[3] Sqrt[N[Pi, 10]] (cn3-cs3)


Do[dy[i,j]=D[y[i], g[j]], {i, 1, 3}, {j, 1, 3}]
(* calculates derivatives for use in
Newton-Raphson iteration *)


(* initial guesses to start iteration *)
g[1] = 2000;
g[2] = -0.2;
g[3] = 0.02;


Do[
dg1=.;
dg2=.;
dg3=.;
mat1 = dy[1,1] dg1 + dy[1,2] dg2 + dy[1,3] dg3;
mat2 = dy[2,1] dg1 + dy[2,2] dg2 + dy[2,3] dg3;
mat3 = dy[3,1] dg1 + dy[3,2] dg2 + dy[3,3] dg3;

ans=Solve[{mat1 == -y[1], mat2 == -y[2], mat3 == -y[3]},
{dg1, dg2, dg3}];

a = dg1 /.ans;
b = dg2 /.ans;
c = dg3 /.ans;

g[1]= g[1] + a;

g[2] = g[2] + b;

g[3] = g[3] + c;

Print["y1", y[1], "dg1", dg1 /.ans,"g", g[1], g[2], g[3]];

Print[$$$$$];

(* repeat to solve iteration *), {10}]


Print[ans]
Print[g[1], g[2], g[3]]
Print[y[1], y[2], y[3]]

                   -23                    -16                    -20
{{dg3->1.76665 10    , dg1->-5.15124 10    , dg2->-1.58385 10
}}
{2755.99}{-0.208549}{0.0225566}
                  -20             -20
{0.}{-8.80914 10    }{4.74338 10    }
```

```
N[de,4]
N[dn,4]
(* calculates and prints the diffusion coefficients *)

        -12
{3.93 10    }
         -12
{6.174 10    }



xst1=N[2 g[1] Sqrt[dcu]]
xst2=N[2 g[2] Sqrt[de]]
xst3=N[2 g[3] Sqrt[dn]]
(* gives distances in cm/sqrt(s) - not layer thicknesses but
interface movements *)

            -7
{3.05903 10   }
             -7
{-8.26903 10   }
            -7
{1.12097 10   }
```

Appendix D

Sensitivity analysis of Mei's model

The sensitivity of the interface position predictions derived from Mei's model to the values of the diffusion coefficients was evaluated. The diffusion coefficients were varied from $0.01D_i$ to $100D_i$ using the diffusion coefficients in the copper-tin system at 190°C as a baseline. The baseline diffusion coefficients, D_{Cu}, D_{ε}, D_{η}, and D_{Sn}, are shown in Table D.1. These diffusion coefficients were multiplied by factors of a, b, c, and d respectively, where a, b, c, and d ranged from 0.01 to 100. The model was run with each set of adjusted diffusion coefficients to determine the interface position parameters. The results are shown in Table D.2.

Table D.1: Baseline diffusion coefficients (cm^2/s) used for the sensitivity analysis.

D_{Cu}	D_{ε}	D_{η}	D_{Sn}
3×10^{-21}	5×10^{-12}	1×10^{-11}	5×10^{-7}

The interface position parameters indicate which phase or phases would form. As can be seen in the Results column of Table D.2, Mei's model never predicts the formation of both intermetallic phases. It only predicts the formation of one intermetallic phase or neither intermetallic phase. For the values of the diffusion coefficients that correspond to the copper-tin system over a wide range of temperatures, the model predicts the formation of only the η phase even if the diffusion coefficients are varied by an order of magnitude. Thus, the model is not overly sensitive to the values of the diffusion coefficients.

The model results do vary but in a predictable and stable way. For example, the rows that are shaded in Table D.2 illustrate how the model predictions change gradually and reliably with changes in the diffusion coefficients. As the relative magnitude of D_{Sn} increases (as d increases), less and less of the η phase forms. At first, the two interfaces of the η phase, $\lambda_{\varepsilon\text{-}\eta}$ and $\lambda_{\eta\text{-}Sn}$, are moving in different directions but the $\lambda_{\eta\text{-}Sn}$ interface slows down and then reverses direction, eventually overtaking the $\lambda_{\varepsilon\text{-}\eta}$ interface so that no intermetallic would form. Other similar examples can be found in the sensitivity results.

The ratios of the diffusion coefficients that would produce the different results according to Mei's model can be determined from the results in Table D.2. For no intermetallic layers to form, D_{ε}/D_{η} must be less than 5 and D_{ε}/D_{Sn} must be greater that

2.5×10^5. For only the ε phase to form, D_{Cu}/D_ε must be greater than 10^{-4}. For most other cases, only the η phase will form.

Table D.2: Conditions and results for the sensitivity analysis of Mei's model.

a	*b*	*c*	*d*	$\lambda_{Cu\text{-}\varepsilon}$ (cm/s$^{1/2}$)	$\lambda_{\varepsilon\text{-}\eta}$ (cm/s$^{1/2}$)	$\lambda_{\eta\text{-}Sn}$ (cm/s$^{1/2}$)	Result
1	0.01	0.01	0.01	3.31×10^{-8}	-1.00×10^{-7}	1.66×10^{-8}	η only
1	0.01	0.01	0.1	7.34×10^{-8}	1.46×10^{-8}	-6.49×10^{-8}	none
1	0.01	0.01	1	6.45×10^{-8}	-2.60×10^{-9}	-1.14×10^{-7}	none
1	0.01	0.01	10	5.34×10^{-8}	-2.78×10^{-8}	-2.90×10^{-7}	none
1	0.01	0.01	100	4.92×10^{-8}	-3.91×10^{-8}	-8.86×10^{-7}	none
1	0.01	0.1	0.01	1.80×10^{-8}	-2.48×10^{-7}	8.12×10^{-8}	η only
1	0.01	0.1	0.1	1.77×10^{-8}	-2.55×10^{-7}	6.49×10^{-8}	η only
1	0.01	0.1	1	1.67×10^{-8}	-2.77×10^{-7}	1.39×10^{-8}	η only
1	0.01	0.1	10	1.07×10^{-7}	6.62×10^{-8}	-3.49×10^{-7}	none
1	0.01	0.1	100	7.08×10^{-8}	9.74×10^{-9}	-9.13×10^{-7}	none
1	0.01	1	0.01	1.10×10^{-8}	-7.49×10^{-7}	2.79×10^{-7}	η only
1	0.01	1	0.1	1.09×10^{-8}	-7.55×10^{-7}	2.63×10^{-7}	η only
1	0.01	1	1	1.09×10^{-8}	-7.77×10^{-7}	2.12×10^{-7}	η only
1	0.01	1	10	1.08×10^{-8}	-8.51×10^{-7}	5.01×10^{-8}	η only
1	0.01	1	100	1.08×10^{-8}	-1.12×10^{-6}	-4.45×10^{-7}	η only
1	0.01	10	0.01	1.08×10^{-8}	-2.36×10^{-6}	9.00×10^{-7}	η only
1	0.01	10	0.1	1.08×10^{-8}	-2.37×10^{-6}	8.84×10^{-7}	η only
1	0.01	10	1	1.08×10^{-8}	-2.39×10^{-6}	8.32×10^{-7}	η only
1	0.01	10	10	1.08×10^{-8}	-2.46×10^{-6}	6.69×10^{-7}	η only
1	0.01	10	100	1.08×10^{-8}	-2.69×10^{-6}	1.59×10^{-7}	η only
1	0.01	100	0.01	1.08×10^{-8}	-7.45×10^{-6}	2.86×10^{-6}	η only
1	0.01	100	0.1	1.08×10^{-8}	-7.46×10^{-6}	2.85×10^{-6}	η only
1	0.01	100	1	1.08×10^{-8}	-7.48×10^{-6}	2.79×10^{-6}	η only
1	0.01	100	10	1.08×10^{-8}	-7.55×10^{-6}	2.63×10^{-6}	η only
1	0.01	100	100	1.08×10^{-8}	-7.77×10^{-6}	2.12×10^{-6}	η only
1	0.1	0.01	0.01	1.36×10^{-7}	-1.87×10^{-7}	6.86×10^{-9}	η only

1	0.1	0.01	0.1	1.87 x 10^{-7}	-4.38 x 10^{-8}	-9.06 x 10^{-8}	none
1	0.1	0.01	1	1.75 x 10^{-7}	-7.16 x 10^{-8}	-1.35 x 10^{-7}	none
1	0.1	0.01	10	1.56 x 10^{-7}	-1.24 x 10^{-7}	-2.95 x 10^{-7}	none
1	0.1	0.01	100	1.48 x 10^{-7}	-1.45 x 10^{-7}	-8.86 x 10^{-7}	none
1	0.1	0.1	0.01	1.06 x 10^{-7}	-3.12 x 10^{-7}	6.91 x 10^{-8}	η only
1	0.1	0.1	0.1	1.05 x 10^{-7}	-3.17 x 10^{-7}	5.25 x 10^{-8}	η only
1	0.1	0.1	1	2.32 x 10^{-7}	4.61 x 10^{-8}	-2.05 x 10^{-7}	none
1	0.1	0.1	10	2.04 x 10^{-7}	-8.22 x 10^{-9}	-3.62 x10^{-7}	none
1	0.1	0.1	100	1.69 x 10^{-7}	-8.80 x10^{-8}	-9.16 x 10^{-7}	none
1	0.1	1	0.01	5.74 x 10^{-8}	-7.78 x 10^{-7}	2.73 x 10^{-7}	η only
1	0.1	1	0.1	5.70 x 10^{-8}	-7.84 x 10^{-7}	2.57 x 10^{-7}	η only
1	0.1	1	1	5.60 x 10^{-8}	-8.05 x 10^{-7}	2.05 x 10^{-7}	η only
1	0.1	1	10	5.29 x 10^{-8}	-8.75 x 10^{-7}	4.41 x 10^{-8}	η only
1	0.1	1	100	3.37 x 10^{-7}	2.09 x 10^{-7}	-1.11 x 10^{-6}	none
1	0.1	10	0.01	3.46 x 10^{-8}	-2.36 x 10^{-6}	9.00 x 10^{-7}	η only
1	0.1	10	0.1	3.46 x 10^{-8}	-2.37 x 10^{-6}	8.83 x 10^{-7}	η only
1	0.1	10	1	3.46 x 10^{-8}	-2.39 x 10^{-6}	8.32 x 10^{-7}	η only
1	0.1	10	10	3.45 x 10^{-8}	-2.46 x 10^{-6}	6.69 x10^{-7}	η only
1	0.1	10	100	3.43 x 10^{-8}	-2.69 x 10^{-6}	1.58 x 10^{-7}	η only
1	0.1	100	0.01	3.4 x 10^{-8}	-7.45 x 10^{-6}	2.86 x 10^{-6}	η only
1	0.1	100	0.1	3.40 x 10^{-8}	-7.46 x 10^{-6}	2.85 x 10^{-6}	η only
1	0.1	100	1	3.40 x 10^{-8}	-7.48 x 10^{-6}	2.79 x 10^{-6}	η only
1	0.1	100	10	3.40 x 10^{-8}	-7.55 x 10^{-6}	2.63 x 10^{-6}	η only
1	0.1	100	100	3.40 x 10^{-8}	-7.77 x 10^{-6}	2.16 x 10^{-6}	η only
1	1	0.01	0.01	4.53 x 10^{-7}	-5.10 x 10^{-7}	-1.74 x 10^{-9}	η only
1	1	0.01	0.1	4.53 x 10^{-7}	-5.10 x 10^{-7}	-2.06 x 10^{-8}	η only
1	1	0.01	1	4.42 x 10^{-7}	5.12 x 10^{-7}	-7.99 x 10^{-8}	η only
1	1	0.01	10	4.50 x 10^{-7}	-5.19 x 10^{-7}	-2.65 x 10^{-7}	η only
1	1	0.01	100	4.63 x 10^{-7}	-4.79 x 10^{-7}	-8.88 x 10^{-7}	none
1	1	0.1	0.01	4.29 x 10^{-7}	-5.88 x 10^{-7}	3.98 x 10^{-8}	η only
1	1	0.1	0.1	4.29 x 10^{-7}	-5.90 x 10^{-7}	2.17 x 10^{-8}	η only
1	1	0.1	1	4.26 x 10^{-7}	-5.98 x 10^{-7}	-3.44 x 10^{-8}	η only
1	1	0.1	10	4.17 x 10^{-7}	-6.31 x 10^{-7}	-2.07 x 10^{-7}	η only
1	1	0.1	100	4.92 x 10^{-7}	-3.92 x 10^{-7}	-9.34 x 10^{-7}	none

1	1	1	0.01	3.35 x 10^{-7}	-9.82 x 10^{-7}	2.35 x 10^{-7}	η only
1	1	1	0.1	3.34 x 10^{-7}	-9.87 x 10^{-7}	2.19 x 10^{-7}	η only
1	1	1	1	3.31 x 10^{-7}	-1.00 x 10^{-6}	1.66 x 10^{-7}	η only
1	1	1	10	3.21 x 10^{-7}	-1.06 x 10^{-6}	1.94 x 10^{-9}	η only
1	1	1	100	2.86 x 10^{-7}	-1.27 x 10^{-6}	-4.98 x 10^{-7}	η only
1	1	10	0.01	1.82 x 10^{-7}	-2.45 x 10^{-6}	8.80 x 10^{-7}	η only
1	1	10	0.1	1.81 x 10^{-7}	-2.46 x 10^{-6}	8.64 x 10^{-7}	η only
1	1	10	1	1.80 x 10^{-7}	-2.48 x 10^{-6}	8.12 x 10^{-7}	η only
1	1	10	10	1.77 x 10^{-7}	-2.55 x 10^{-6}	6.49 x 10^{-7}	η only
1	1	10	100	1.67 x 10^{-7}	-2.77 x 10^{-6}	1.39 x 10^{-7}	η only
1	1	100	0.01	1.10 x 10^{-7}	-7.46 x 10^{-6}	2.86 x 10^{-6}	η only
1	1	100	0.1	1.10 x 10^{-7}	-7.46 x 10^{-6}	2.85 x 10^{-6}	η only
1	1	100	1	1.10 x 10^{-7}	-7.49 x 10^{-6}	2.79 x 10^{-6}	η only
1	1	100	10	1.09 x 10^{-7}	-7.55 x 10^{-6}	2.63 x 10^{-6}	η only
1	1	100	100	1.09 x 10^{-7}	-7.77 x 10^{-6}	2.11 x 10^{-6}	η only
1	10	0.01	0.01	1.44 x 10^{-6}	-1.59 x 10^{-6}	-3.54 x 10^{-9}	η only
1	10	0.01	0.1	1.44 x 10^{-6}	-1.59 x 10^{-6}	-2.25 x 10^{-8}	η only
1	10	0.01	1	1.80 x 10^{-6}	-6.10 x 10^{-7}	-6.16 x 10^{-7}	none
1	10	0.01	10	1.44 x 10^{-6}	-1.59 x 10^{-6}	-2.72 x 10^{-7}	η only
1	10	0.01	100	1.44 x 10^{-6}	-1.59 x 10^{-6}	-8.69 x 10^{-7}	η only
1	10	0.1	0.01	1.43 x 10^{-6}	-1.61 x 10^{-6}	1.33 x 10^{-8}	η only
1	10	0.1	0.1	1.43 x 10^{-6}	1.61 x 10^{-6}	-5.51 x 10^{-9}	η only
1	10	0.1	1	1.81 x 10^{-6}	-5.80 x10^{-7}	-6.34 x 10^{-7}	none
1	10	0.1	10	1.76 x 10^{-6}	-6.96 x 10^{-7}	-7.57 x 10^{-7}	none
1	10	0.1	100	1.62 x 10^{-6}	-1.05 x 10^{-6}	-1.16 x 10^{-6}	none
1	10	1	0.01	1.36 x 10^{-6}	-1.86 x 10^{-6}	1.43 x 10^{-8}	η only
1	10	1	0.1	1.36 x 10^{-6}	-1.86 x 10^{-6}	1.25 x 10^{-7}	η only
1	10	1	1	1.36 x 10^{-6}	-1.87 x 10^{-6}	6.86 x 10^{-8}	η only
1	10	1	10	1.87 x 10^{-6}	-4.38 x 10^{-7}	-9.06 x 10^{-7}	none
1	10	1	100	1.75 x 10^{-6}	-7.16 x 10^{-7}	-1.35 x 10^{-6}	none
1	10	10	0.01	1.06 x 10^{-6}	-3.10 x 10^{-6}	7.61 x 10^{-7}	η only
1	10	10	0.1	1.06 x 10^{-6}	-3.11 x 10^{-6}	7.44 x 10^{-7}	η only
1	10	10	1	1.06 x 10^{-6}	-3.12 x 10^{-6}	6.91 x 10^{-7}	η only
1	10	10	10	1.05 x 10^{-6}	-3.17 x 10^{-6}	5.25 x 10^{-7}	η only

1	10	10	100	1.02 x 10^{-6}	-3.34 x 10^{-6}	6.13 x 10^{-9}	η only
1	10	100	0.01	5.75 x 10^{-7}	-7.75 x 10^{-6}	2.80 x 10^{-6}	η only
1	10	100	0.1	5.75 x 10^{-7}	-7.76 x 10^{-6}	2.78 x 10^{-6}	η only
1	10	100	1	5.74 x 10^{-7}	-7.78 x 10^{-6}	2.73 x 10^{-6}	η only
1	10	100	10	5.70 x 10^{-7}	-7.84 x 10^{-6}	2.57 x 10^{-6}	η only
1	10	100	100	5.6 x 10^{-7}	-8.05 x 10^{-6}	2.05 x 10^{-6}	η only
1	100	0.01	0.01	4.55 x 10^{-6}	-5.03 x 10^{-6}	-3.54 x 10^{-9}	η only
1	100	0.01	0.1	4.55 x 10^{-6}	-5.03 x 10^{-6}	-2.25 x 10^{-8}	η only
1	100	0.01	1	4.55 x 10^{-6}	-5.03 x 10^{-6}	-8.24 x 10^{-8}	η only
1	100	0.01	10	4.55 x 10^{-6}	-5.03 x 10^{-6}	-2.72 x 10^{-7}	η only
1	100	0.01	100	4.55 x 10^{-6}	-5.03 x 10^{-6}	-8.70 x 10^{-7}	η only
1	100	0.1	0.01	4.55 x 10^{-6}	-5.03 x 10^{-6}	7.77 x 10^{-9}	η only
1	100	0.1	0.1	4.55 x 10^{-6}	-5.03 x 10^{-6}	-1.12 x 10^{-8}	η only
1	100	0.1	1	4.55 x 10^{-6}	-5.03 x 10^{-6}	-7.11 x 10^{-8}	η only
1	100	0.1	10	4.55 x 10^{-6}	-5.03 x 10^{-6}	-2.61 x 10^{-7}	η only
1	100	0.1	100	4.55 x 10^{-6}	-5.03 x 10^{-6}	-8.59 x 10^{-7}	η only
1	100	1	0.01	4.53 x 10^{-6}	-5.09 x 10^{-6}	6.09 x 10^{-8}	η only
1	100	1	0.1	4.53 x 10^{-6}	-5.09 x 10^{-6}	4.21 x 10^{-8}	η only
1	100	1	1	4.53 x 10^{-6}	-5.10 x 10^{-6}	-1.74 x 10^{-8}	η only
1	100	1	10	4.53 x 10^{-6}	-5.10 x 10^{-6}	-2.06 x 10^{-7}	η only
1	100	1	100	4.53 x 10^{-6}	-5.11 x 10^{-6}	-7.99 x 10^{-7}	η only
1	100	10	0.01	4.30 x 10^{-6}	-5.87 x 10^{-6}	4.70 x 10^{-7}	η only
1	100	10	0.1	4.29 x 10^{-6}	-5.87 x 10^{-6}	4.52 x 10^{-7}	η only
1	100	10	1	4.29 x 10^{-6}	-5.88 x 10^{-6}	3.95 x 10^{-7}	η only
1	100	10	10	4.29 x 10^{-6}	5.80 x 10^{-6}	2.17 x 10^{-7}	η only
1	100	10	100	4.26 x 10^{-6}	-5.98 x 10^{-6}	-3.44 x 10^{-7}	η only
1	100	100	0.01	3.36 x 10^{-6}	-9.80 x 10^{-6}	2.42 x 10^{-6}	η only
1	100	100	0.1	3.35 x 10^{-6}	-9.81 x 10^{-6}	2.41 x 10^{-6}	η only
1	100	100	1	3.35 x 10^{-6}	-9.82 x 10^{-6}	2.35 x 10^{-6}	η only
1	100	100	10	3.34 x 10^{-6}	-9.87 x 10^{-6}	2.19 x 10^{-6}	η only
1	100	100	100	3.31 x 10^{-6}	-1.11 x 10^{-5}	1.66 x 10^{-6}	η only
0.01	1	1	1	3.31 x 10^{-7}	-1.00 x 10^{-6}	1.66 x 10^{-7}	η only
0.1	1	1	1	3.31 x 10^{-7}	-1.00 x 10^{-6}	1.66 x 10^{-7}	η only
10	1	1	1	3.31 x 10^{-7}	-1.00 x 10^{-6}	1.66 x 10^{-7}	η only

100	1	1	1	3.31 x 10^{-7}	-1.00 x 10^{-6}	1.66 x 10^{-7}	η only
1000	1	1	1	3.31 x 10^{-7}	-1.00 x 10^{-6}	1.66 x 10^{-7}	η only
10000	1	1	1	3.31 x 10^{-7}	-1.00 x 10^{-6}	1.66 x 10^{-7}	η only
1E+05	1	1	1	3.31 x 10^{-7}	-1.00 x 10^{-6}	1.66 x 10^{-7}	η only
1E+06	1	1	1	3.31 x 10^{-7}	-1.00 x 10^{-6}	1.66 x 10^{-7}	η only
1E+06	1	1	1	-3.31 x 10^{-7}	9.60 x 10^{-7}	-3.20 x 10^{-7}	ε only
1E+09	1	1	1	3.75 x 10^{-7}	-9.97 x 10^{-7}	1.67 x 10^{-7}	η only
1E+09	1	1	1	-2.87 x 10^{-7}	9.67 x 10^{-7}	-3.19 x 10^{-7}	ε only
1E+10	1	1	1	4.80 x 10^{-7}	-9.83 x 10^{-7}	1.70 x 10^{-7}	η only
1E+10	1	1	1	-1.86 x 10^{-7}	9.86 x 10^{-7}	-3.16 x 10^{-7}	ε only
1E+12	1	1	1	2.10 x 10^{-6}	5.10 x 10^{-7}	-4.09 x 10^{-7}	none
1E+12	1	1	1	1.99 x 10^{-6}	-8.84 x 10^{-7}	1.89 x 10^{-7}	η only
1E-06	1	1	1	3.31 x 10^{-7}	-1.00 x 10^{-6}	1.66 x 10^{-7}	η only

Appendix E

Determination of the physically significant intercept

Equation 5.12 defines the curve corresponding to d $w_\varepsilon / dt = 0$:

$$\left(\frac{w_\varepsilon}{D_\varepsilon}\right)^2 - 2\frac{w_\varepsilon}{D_\varepsilon}\frac{w_\eta}{D_\eta} + E\frac{w_\varepsilon}{D_\varepsilon} + F\frac{w_\eta}{D_\eta} + G = 0 \qquad \text{(E.1)}$$

This equation is graphed for both positive and negative values of w_ε and w_η in Figure E.1. Since w_ε and w_η are thicknesses of the intermetallic layers, only the first quadrant, where both w_ε and w_η are positive, is significant. Negative thicknesses have no physical meaning. The upper curve, which crosses the first quadrant, is the one relevant to the model. Note that the intercept of this curve is always larger than the intercept of the lower curve.

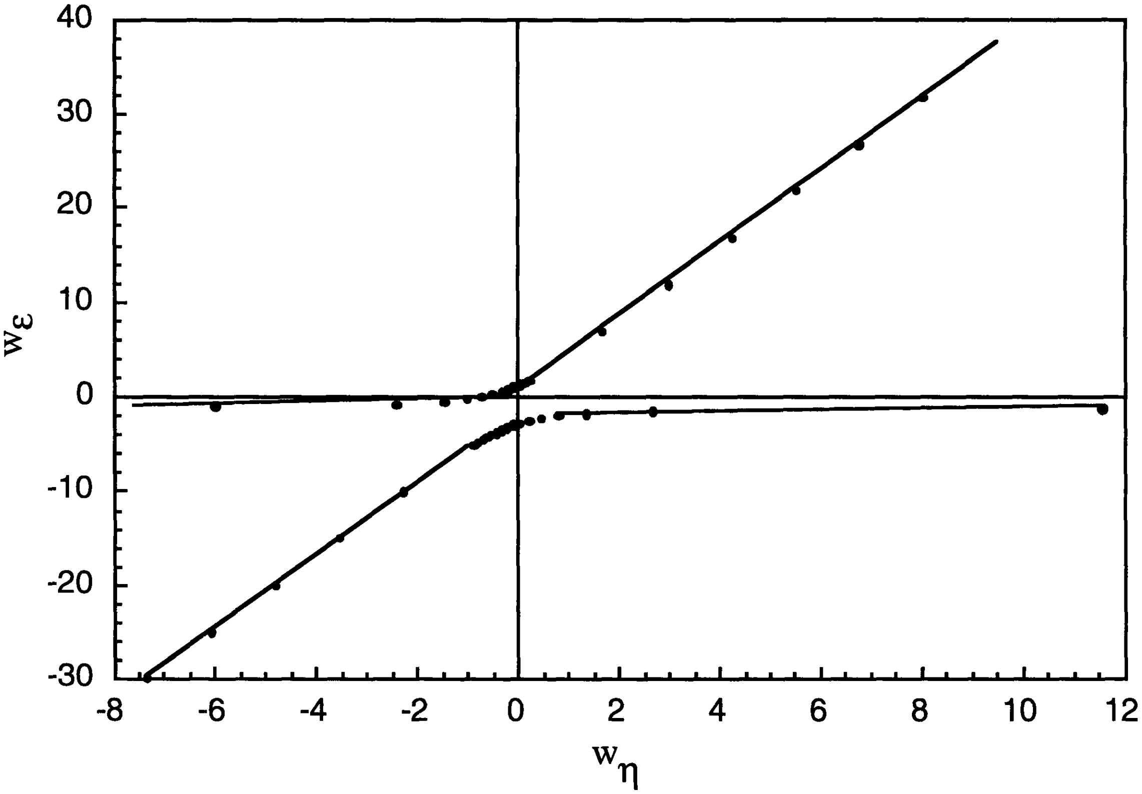

Figure E.1: Graph of Equation E.1 (Equation 5.12) for both negative and positive values of w_ε and w_η.

Equation 5.20 defines the intercepts of these two curves:

$$w_\varepsilon = \frac{D_\varepsilon}{2}\left[\left[\frac{1}{k_3}+\frac{1}{k_2}-\frac{2}{k_1}\right] \pm \sqrt{\left(\frac{1}{k_3}-\frac{1}{k_2}\right)^2+\left(\frac{2}{k_1}\right)^2}\,\right] \qquad \text{(E.2)}$$

The root given by Equation E.2 with the plus sign is always greater the root with the negative sign because the second term is always positive. Thus, the root with the plus sign is the intercept of the upper curve and the one that is pertinent to the model.

Bibliography

1. P. D. Genereux and D. F. Paulonis, "Nickel Base Superalloy Articles and Method for Making," United States Patent #4574015, March 4, 1986.

2. E. H. Van Der Molen, J. M. Oblak, and O. H. Kriege, "Control of γ' Particle Size and Volume Fraction in the High Temperature Superalloy Udimet 700," Metallurgical Transactions, 2, 1627-1633, 1971.

3. P. E. Davis, M. E. Warwick, and S. J. Muckett, "Intermetallic Compound Growth and Solderability of Reflowed Tin and Tin-Lead Coatings," Plating and Surface Finishing, 70(8), 49-53, 1983.

4. P. E. Davis, M. E. Warwick, and P. J. Kay, "Intermetallic Compound Growth and Solderability," Plating and Surface Finishing, 69(9), 72-76, 1982.

5. *Encyclopedia Americana-International ed.*, vol. 9, Grolier Inc., Connecticut, p. 398, 1994.

6. *Metals Handbook, 8th ed. vol. 1: Properties and Selection of Metals*, American Society of Metals, Metals Park, OH, p.21, 48-49, 1961.

7. R. J. Fields and S. R. Low III, "Physical and Mechanical Properties of Intermetallic Compounds Commonly Found in Solder Joints," *The Metal Science of Joining*, M. J. Cieslak, J. H. Perepezko, S. Kang and M. E. Glicksman, eds., The Minerals, Metals and Materials Society, pp. 165-173, 1992.

8. S. F. Cogan, S. Kwon, J. D. Klein, and R. M. Rose, "Diffusion in the CuSn binary system: Application to Nb_3Sn Composites," Journal of Materials Science, 19, 497-500, 1984.

9. T. B. Massalski, *Binary Alloy Phase Diagrams 2nd ed.,* ASM International, Materials Park, OH, 1990, p. 29 Ag-Cu, p. 1425 Cu-In, p. 1482 Cu-Sn, p. 2296 In-Sn, and p. 2864 Ni-Sn. Phase diagrams reprinted with permission from ASM International.

10. P. M. Robinson and M. B. Bever, "Thermodynamic Properties," in *Intermetallic Compounds*, J. H. Westbrook, ed., John Wiley, New York, 1967.

11. *The NBS Tables of Chemical Thermodynamic Properties*, Journal of Physical and Chemical Reference Data, vol. 11, Supplement No. 2, National Bureau of Standards, 1982.

12. T. B. Massalski and H. Pops, "Intermediate Phases in Metallic Phase Diagrams," in *Phase Diagrams: Materials Science and Technology, vol. 6-II,* A. A. Alper, ed., Academic Press, New York, 1970.

13. *Metals Handbook, 10th ed. vol. 2: Properties and Selection: Nonferrous Alloys and Special-Purpose Materials*, ASM International, Materials Park, OH, p.910, 1990.

14. A. P. Boresi, and O. M. Sidebottom, *Advanced Mechanics of Materials, 4th ed.*, John Wiley and Sons, New York, p. 134, 1985.

15. F. N. Rhines, *Phase Diagrams in Metallurgy: Their Development and Application*, New York: McGraw-Hill Book Company, p. 78-82, 1956.

16. J. W. Roman, "An Investigation of Low Temperature Transient Liquid Phase Bonding of Silver, Gold and Copper," SM Thesis, Department of Material Science and Engineering, MIT, 1991.

17. W. D. MacDonald and T. W. Eagar, "Transient Liquid Phase Bonding Processes," *The Metal Science of Joining*, M. J. Cieslak, J. H. Perepezko, S. Kang and M. E. Glicksman, eds., The Minerals, Metals and Materials Society, pp. 93-100, 1992.

18. D. S. Duvall, W. A. Owczarski, and D. F. Paulonis, "TLP Bonding: a New Method for Joining Heat Resistant Alloys," Welding Journal, 53, 203-214, 1974.

19. W. F. Gale and E. R. Wallach, "Microstructural Development in Transient Liquid-Phase Bonding", Metallurgical Transactions, 22A, 2451-57, 1991.

20. H. Kokawa, C. H. Lee, and T. H. North, "Effect of Grain Boundaries on Isothermal Solidification during Transient Liquid Phase Brazing," Metallurgical Transactions A, 22A(7), 1627-1631, 1991.

21. A. Sakamoto, C. Fujiwara, T. Hattori, and S. Sakai, "Optimizing Processing Variables in High-Temperature Brazing with Nickel-Based Filler Metals," Welding Journal, 68(3), 63-71, 1989.

22. A. LeBlanc and R. Mevrel, "Diffusion Brazing Study of DS247/BNi-3/Astroloy," *High Temperature Materials for Power Engineering 1990, part II,* Kluwer, Dordrecht, 1451-1460, 1990.

23. R. R. Wells, "Microstructural Control of Thin-Film Diffusion-Brazed Titanium," Welding Journal, Research Supplement, 55, 20s-27s, 1976.

24. T. Takemoto and I. Okamoto, "Intermetallic Compounds formed during Brazing of Titanium with Aluminum Filler Metals," Journal of Materials Science, 23(4), 1301-1308, 1988.

25. J. T. Niemann and R. A. Garrett, "Eutectic Bonding of Boron-Aluminum Structural Components," Welding Journal, Research Supplement, 53(4), 175s-184s, 1974.

26. M. M. Hou and T. W. Eagar, "Low Temperature Transient Liquid Phase (LTTLP) Bonding for Au/Cu and Cu/Cu Interconnections," Journal of Electronic Packaging, 114, 443-447, 1992.

27. J. W. Roman and T. W. Eagar, "Low Stress Die Attach by Low Temperature Transient Liquid Phase Bonding," Symposium Proceedings of the International Society for Hybrid Microelectronics (ISHM), 1992.

28. I. Tuah-Poku, M. Dollar, and T. B. Massalski, "A Study of the Transient Liquid Phase Bonding Process Applied to a Ag/Cu/Ag Sandwich Joint," Metallurgical Transactions A, 19A, 675-686, 1988.

29. Y. Zhou and T. H. North, "Kinetic Modeling of Diffusion-Controlled, Two-Phase Moving Interface Problems," Modelling Simulations in Materials Science and Engineering, 1, 505-516, 1993.

30. G. Lesoult, “Modeling of the Transient Liquid Phase Bonding Process I,” Center for the Joining of Materials Report, Carnegie-Mellon University, 1976.

31. W. D. MacDonald, “Kinetics of Transient Liquid Phase Bonding,” Ph.D. Thesis, Material Science and Engineering Department, MIT, 1993.

32. Z. Mei, A. J. Sunwoo, and J. W. Morris, Jr., “Analysis of Low-Temperature Intermetallic Growth in Copper-Tin Diffusion Couples,” Metallurgical Transactions A, 23A(3), 857-864, 1992.

33. D. S. Dunn, T. F. Marinis, W. M. Sherry, and C. J. Williams, “Dependence of Cu/Sn and Cu/60Sn40Pb Solder Joint Strength on Diffusion Controlled Growth of Cu_3Sn and Cu_6Sn_5,” *Electronic Packaging Materials Science*, E. A. Giess, K. N. Tu, and D. R. Uhlmann, eds., Materials Research Society, Pittsburgh, Pennsylvania, vol. 40, 129-138, 1985.

34. Z. Lubyovà, P. Fellner, and K. Matiasovsky, “Diffusion in the Systems Iron-Tin and Copper-Tin,” Zeitschrift für Metallkunde, 66(3), 179-182, 1975.

35. D. Olsen, R. Wright, and H. Berg, "Effects of Intermetallics on the Reliability of Tin Coated Cu, Ag, and Ni Parts," 13th Annual Proceedings of the IEEE International Reliability Physics Symposium, 80-86, 1975.

36. M. Onishi and H. Fujibuchi, “Reaction-Diffusion in the Cu-Sn System,” Transactions of the Japan Institute of Metals, 16(9), 539-547, 1975.

37. L. Zakraysek, “Intermetallic Growth in Tin-Rich solders,” Welding Journal, Research Supplement, 37, 536s-541s, 1972.

38. K. N. Tu and R. D. Thompson, “Kinetics of Interfacial Reaction in Bimetallic Cu-Sn Thin Films,” Acta Metallurgica, 30, 947-952, 1982.

39. E. Starke and H. Wever, “Diffusion und Kirkendall-Effekt in intermetallischen Phasen des Systems Kupfer-Zinn,” Zeitschrift für Metallkunde, 55(3), 107-116, 1964.

40. W. C. Hagel, “Diffusion” in *Intermetallic Compounds*, J. H. Westbrook, ed., John Wiley, New York, p.379-381, 1967.

41. G. H. Geiger and D. R. Poirier, *Transport Phenomena in Metallurgy*, Addison-Wesley Publishing Co., Massachusetts, p. 15, 1973.

42. P. G. Shewmon, *Diffusion in Solids*, The Minerals, Metals, and Materials Society, Ohio, p. 139, 155, and 189, 1989.

43. W. K. Warburton and D. Turnbull, “Fast Diffusion on Metals,” in *Diffusion in Solids: Recent Developments*, A. S. Novick and J. J. Burton, eds., Academic Press, New York, pp. 171-229, 1975.

44. Table of Periodic Properties of the Elements, Sargent-Welch Scientific Company, Illinois, 1980.

45. W. Gordy and W. J. Orville Thomas, "Electronegativities of the Elements," Journal of Chemical Physics, 24(2), 439-444, 1956.

46. L. S. Darken and R. W. Gurry, *Physical Chemistry of Metals*, McGraw-Hill, New York, p. 49-57,1953.

47. *CRC Handbook of Chemistry and Physics*, R. C. Weast, ed., CRC Press, Florida, 1982.

48. T. B. Massalski and H. Pops, "Intermediate Phases in Metallic Phase Diagrams," in *Phase Diagrams: Materials Science and Technology: The Use of Phase Diagrams in Metal, Refractory, Ceramic, and Cement Technology, vol. II*, Allen M. Alper, ed., Academic Press, New York, pp. 221-263, 1970.

49. R. Hultgren, P. D. Desai, D. T. Hawkins, M. Gleiser, K. K. Kelley, *Selected Values of the Thermodynamic Properties of Binary Alloys*, American Society for Metals, Ohio, 1973.

50. H. J. Beattie, Jr., "Close Packed Structures," in *Intermetallic Compounds*, J. H. Westbrook, ed., John Wiley, New York, p.159, 1967.

51. A. E. Dwight, "Body-Centered Cubic Derivative Structures," in *Intermetallic Compounds*, J. H. Westbrook, ed., John Wiley, New York, p.174, 1967.

52. A. J. Sunwoo, J. W. Morris, Jr., and G. K. Lucey, Jr., "The Growth of Cu-Sn Intermetallics at a Pretinned Copper-Solder Interface," Metallurgical Transactions A, 23A, 1323-1332, 1992.

53. K. N. Tu, "Interdiffusion and Reaction in Bimetallic Cu-Sn Thin Films," Acta Metallurgica, 21, 347-354, 1973.

54. W. D. Kingery, H. K. Bowen, and D. R. Uhlmann, *Introduction to Ceramics,* 2nd ed., John Wiley and Sons, New York, 1976.

55. C. W. Allen, M. R. Fulcher, A. S. Rai, G. A. Sargent, and A. E. Miller, "A Study of Intermetallic Compound Development in Nickel-Tin Interfacial Zones," *Electronic Packaging Materials Science*, E. A. Giess, K. N. Tu, and D. R. Uhlmann, eds., Materials Research Society, Pittsburgh, Pennsylvania, vol. 40, 139-144, 1985.

56. D. A. Porter and K. E. Easterling, *Phase Transformations in Metals and Alloys*, Chapman and Hall, New York, pp.66-68, 1981.

57. J. L. C. Daams, P. Villars, J. H. N. van Vucht, *Atlas of Crystal Structure Types for Intermetallic Phases*, ASM International, Ohio, 1991.

58. J. S. Kouvel, "Magnetic Properties," in *Intermetallic Compounds*, J. H. Westbrook, ed., John Wiley, New York, p.543-4, 1967.

59. M. V. Nevitt, "Miscellaneous Structures of Fixed Stoichiometry," in *Intermetallic Compounds*, J. H. Westbrook, ed., John Wiley, New York, p.226-7, 1967.

60. R. E. Reed-Hill, *Physical Metallurgy Principles, 2nd ed.*, PWS Engineering, Boston, pp. 419-421, 1973.

61. I. B. Borovskii, K. P. Gurov, I. D. Marchukova, and Yu. E'. Ugaste, *Interdiffusion in Alloys*, Amerind Publishing Co., New Delhi, pp. 194-195, 1986.

62. D. Grivas, D. Frear, L. Quan and J. W. Morris Jr., "The Formation of Cu_3Sn Intermetallic on the Reaction of Cu with 95Pb-5Sn Solder," Journal of Electronic Materials, 15(6), 355-359, 1986.

63. R. J. Klein Wassink, *Soldering in Electronics*, Electrochemical Publications, Scotland, pp. 155 and 157, 1989.

64. A. K. Bandyopadhyay and S. K. Sen, "A Study of Intermetallic Compound Formation in a Copper-Tin Bimetallic Couple," Journal of Applied Physics, 67(8), 3681-3688, 1990.

65. E. Philofesky, "Intermetallic Formation in Gold-Aluminum Systems," Solid-State Electronics, 13, 1391-1399, 1970.

66. J. Szekely and N. J. Themelis, *Rate Phenomena in Process Metallurgy*, Wiley-Interscience, New York, p. 617, 1971.

67. J. Philibert, "Reactive Diffusion in Thin Films," Applied Surface Science, 53, 74-81, 1991.

68. J. Philibert, "Reactive Interdiffusion," Materials Science Forum, 155-156, 15-30, 1994.

69. W. H. Press, B. P. Flannery, S. A. Teukolsky, and W. T. Vetterling, *Numerical Recipes: The Art of Scientific Computing*, Cambridge University Press, New York, pp. 254-259, 1986.

70. B. Carnahan and J. O. Wilkes, *Introduction to Algorithms and Numerical Methods*, University of Michigan, pp. 5.29b-5.29d, 1969.

71. J. O. G. Parent, D. D. L. Chung, I. M. Bernstein, "Effects of Intermetallic Formation at the Interface between Copper and Lead-Tin Solder," Journal of Materials Science, 23(7), 2564-2572, 1988.

72. E. K. Ohriner, "Intermetallic Formation in Soldered Copper-Based Alloys at 150° to 250°C," Welding Journal, Research Supplement, 66(7), 191s-202s, 1987.

73. K. W. Kirchner, G. K Lucey, and J. Geis, "Copper/Solder Intermetallic Growth Studies," Microscopy Research and Technique, 25, 503-508, 1993.

74. I. Kawakatsu, T. Osawa, and H. Yamaguchi, "On the Growth of Alloy Layer between Solid Copper and Liquid Tin," Transactions of the Japan Institute of Metals, 13, 436-443, 1972.

75. B. F. Dyson, T. R. Anthony, and D. Turnbull, "Interstitial Diffusion of Copper in Tin," Journal of Applied Physics, 38, 3408, 1967.

76. P. J. Kay and C. A. Mackay, "The Growth of Intermetallic Compounds of Common Basis Materials Coated with Tin and Tin-Lead Alloys," Transactions of the Institute of Metal Finishing, 54, 68-74, 1976.

77. D. A. Unsworth and C. A. Mackay, "A Preliminary Report on the Growth of Compound Layers on Various Metal Bases Plated with Tin and its Alloys," Transactions of the Institute of Metals Finishing, 51, 85-90, 1973.

78. Y. Wu, J. A. Sees, C. Pouraghabagher, L. A. Foster, J. L. Marshall, E. G. Jacobs, and R. F. Pinizzotto, "The Formation and Growth of Intermetallics in Composite Solder," Journal of Electronic Materials, 22(7), 769-777, 1993.

79. P. W. Dehaven, "The Reaction Kinetics of Liquid 60/40 Sn/Pb Solder with Copper and Nickel: a High Temperature X-ray Diffraction Study," *Electronic Packaging Materials Science*, E. A. Giess, K. N. Tu, and D. R. Uhlmann, eds., Materials Research Society, Pittsburgh, Pennsylvania, vol. 40, 123-128, 1985.

80. P. J. Kay and C. A. Mackay, "Barrier Layers Against Diffusion," Transactions of the Institute of Metal Finishing, 57(4), 169-174, 1979.

81. R. Halimi, E. M. Chpilevski, and D. A. Gorbatchevski, "Cinétique de Formation de Composés Intermétalliques dans les Couches Minces de Cu/Sn," Thin Solid Films, 148(1), 109-119, 1987.

82. H. C. Bhedwar, K. K. Ray, S. D. Kulkarni, V. Balasubramanian, "Kirkendall Effect Studies in Copper-Tin Diffusion Couples," Scripta Metallurgica, 6(10), 919-922, 1972.

83. K. Hoshino, Y. Iijima, and K. Hirano, "Interdiffusion and Kirkendall Effect in Cu-Sn Alloys," Transactions of the Japan Institute of Metals, 21(10), 674-682, 1980.

84. S. K. Kang and V. Ramachandran, "Growth Kinetics of Intermetallic Phases at the Liquid Sn and Solid Ni Interface," Scripta Metallurgica, 14, 421-424, 1980.

85. R. J. Schaefer, F. S. Biancaniello, and R. D. Jiggetts, "Preparation of Bulk Samples of Copper-Tin Intermetallic Compounds," *The Metal Science of Joining*, ed., M. J. Cieslak, J. H. Perepezko, S. Kang and M. E. Glicksman, The Minerals, Metals and Materials Society, pp. 175-181, 1992.

Biographical Note

Cheryl Ann Klepser

Education:	MS in Materials Engineering, Massachusetts Institute of Technology, 1992. BS in Materials Science and Engineering, Massachusetts Institute of Technology, 1991.
Internships:	Materials Research Laboratory, Pratt and Whitney, United Technologies, East Hartford, Connecticut, June 1991 - January 1992. Timken Research, The Timken Company, North Canton, Ohio, Summer 1989 and Summer 1990.
Other publications:	C. A. Klepser, "Effect of Continuous Cooling Rate on the Precipitation of Gamma Prime in Nickel-Based Superalloys," Scripta Metallurgica and Materialia, 33(4), 589-596, 1995. C. A. Klepser and T. W. Eagar, "Rate of Intermetallic Formation" presentation to be given during Alloy Design and Soldering Technologies for Lead-Free and Lead-Bearing Solders III session at ASM/TMS Materials Week, November 2, 1995, Cleveland, Ohio.
Earned:	Certified Engineer-in-Training. Member of Tau Beta Pi and Sigma Xi honor societies. Selected to Eastern Water Polo Association 1995 All Conference Team for New England North Region, Northern Division.
After MIT:	Metallurgical Engineering, Cummins Technical Center, Cummins Engine Company, Inc., Mail Code 50183, P. O. Box 3005, Columbus, IN 47202-3005.